PURDUE UNIVERSITY
GRADUATE SCHOOL
Thesis Acceptance

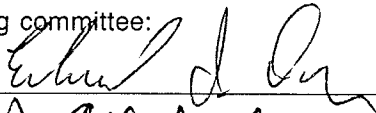This is to certify that the thesis prepared
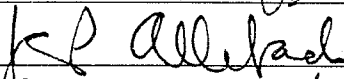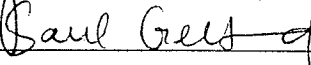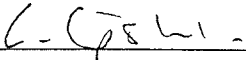
By _____ JISHENG SONG _____

Entitled

A Generalized Morphological Filter
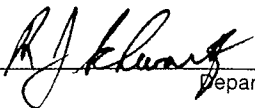
Complies with University regulations and meets the standards of the Graduate School for originality and quality

For the degree of _____ Doctor of Philosophy _____
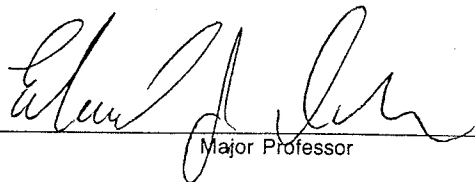
Signed by the final examining committee:

_____ , chair

_____

_____

_____

Approved by:

_____   7/29/91
                    Department Head   Date

☐ is
This thesis ☒ is not to be regarded as confidential

_____
                    Major Professor

A GENERALIZED MORPHOLOGICAL FILTER

A Thesis

Submitted to the Faculty

of

Purdue University

by

Jisheng Song

In Partial Fulfillment of the

Requirements for the Degree

of

Doctor of Philosophy

August 1991

ACKNOWLEDGMENTS

I wish to express my sincere thanks to my major Professor Edward J. Delp for his guidance and support academically and otherwise. I greatly appreciate his care and dedication in constructively criticizing my work during my graduate study, including this thesis. I have truly enjoyed and benefited from working with him.

I also wish to express thanks to the other members of my Advisory Committee: Professors Jan P. Allebach, Saul B. Gelfand, and Leonard M. Lipshitz for their support and interest in my work.

Special thanks to my wife Yuan Zheng, whose patience, understanding, and support have greatly aided in the successful completion of my graduate study.

This is dedicated

to my parents.

TABLE OF CONTENTS

LIST OF TABLES

LIST OF FIGURES

Figure   Page

ABSTRACT

Song, Jisheng. Ph.D., Purdue University, August 1991. A Generalized Morphological Filter. Major Professor: Edward J. Delp.

Mathematical morphology is an important class of image transformations that have been studied extensively in image processing and analysis. Mathematical morphology is a set algebra developed to deal with the geometrical structures of objects. Basic morphological transformations are performed using a set, known as the structuring element, which specifies a geometrical structure with certain shape and size properties. Morphological transformations can be used to extract information relative to the distribution of the geometrical structure specified by the structuring element. They can also be used to transform an image into another image which contains the specified geometrical structure.

One of the basic design requirements in image enhancement is to remove noise and minimize the blurring effect. A traditional morphological filter uses only one structuring element which is usually supported on a square or circular region. This filter can effectively remove impulsive noise with geometrical feature preservation if the image in consideration consists of large homogeneous regions. For an image that has fine details, the transformed image, resulting from the use of a single structuring element, has only the one geometrical structure specified by the structureing element in it and will not be visually pleasing. Morphological filters using multiple structuring elements are developed to address the difficulties of the traditional morphological filter. The goal is to preserve

within an image multiple basic geometrical structures, as defined by the structuring elements, that can form fine details and also maintain noise suppression. Motivated by exploiting the merits of linear filtering and morphological filtering techniques, we have developed a new filter structure which is known as the Generalized Morphological Filter (GMF). The output of the GMF is the linear combination of the ordered outputs of multiple morphological operators using different structuring elements. The deterministic and statistical properties of GMF have been investigated. Optimal coefficients in the linear part of the GMF combination have also been derived. The quantitative evaluation of the performance of the GMF has shown superior performance in comparison with other popular filters such as averaging and median filters.

CHAPTER 1

INTRODUCTION

1.1 The Necessity of Using Geometrical Structure Information

in Image Enhancement

The main objective of image enhancement is to process an image so that the result is more suitable either by being visually pleasing or for use in further processing, such as image analysis. Removing spurious content from an image is the goal of image enhancement. The spurious content of the original image is usually referred to as noise which is partly caused by image formation, acquisition, as well as transmission. For example, film-grain noise is formed in photographic film due to the randomness inherent in the silver grain deposition. In the case of photoelectronic systems, one process that is known to contribute noise in the acquired image is the random thermal noise sources in the circuits[1]. Recovering the noiseless image from the noisy one requires not only effective noise suppression, but also the preservation of the underlying geometrical structures in the image.

Many popular filtering techniques for suppressing noise in an image explore the algebraic information in an image, such as signal correlations, spectral content, and frequency response. Most of these techniques are direct extensions of one dimensional techniques to the two dimensional space. They, however, take into account little of the underlying geometrical structures in the image. This greatly affects their performance.

Image analysis is another area where geometrical structures of a scene are very important. In image analysis, shape, size, and orientation of the geometrical structures

are examined for feature extraction, shape description, pattern recognition, image segmentation, etc. Hence, developing appropriate mathematical tools to accomplish tasks related to processing geometrical structures in an image is very beneficial to both image processing and analysis.

1.2 Mathematical Tools

One set of mathematical tools that can be used in image processing that makes use of geometrical structure information is known as mathematical morphology. Developed to deal with geometrical structures of objects, mathematical morphology is a set algebra defined on a Euclidean space. It was first introduced in 1964 at the Paris School of Mines by two French mathematicians, G. Matheron and J. Serra. At that time they were asked to inspect and measure geometrical structures of microscopic images of mineral specimens and investigate their relationships with physical properties such as permeability and milling properties. Since then their work has resulted in a new branch of mathematics which opened an arena for theoretical research, and hardware development in image processing and analysis [2-4].

From Webster's Dictionary, the word morphology means "a study of structure or form". As its name suggests, mathematical morphology is the quantitative description of geometrical structures of objects. Matheron and Serra have written several books introducing mathematical methodology: *Random Sets and Integral Geometry* by Matheron [5] and *Image Analysis and Mathematical Morphology, volumes 1 and 2* by Serra [2, 3]. Mathematical morphology was initially developed to handle binary images. It was later extended to deal with gray scale images. Goetcherian introduced the extension of many binary image processing algorithms to gray scale images [6]. Sternberg and Preston used the umbra concept to extend morphological operations to gray scale images [7-10]. Among the hardware developments related to mathematical morphology, the first prototype of a texture analyzer was built at the Paris School of Mines by Serra and

his colleagues in 1965 [2]. Sternberg led the construction of a special purpose computer, known as the Cytocomputer, for morphological operations [8, 9, 11].

Basic morphological transformations involve set operations defined on an image and another set known as the structuring element[2, 12]. The structuring element acts like a probe to extract or preserve shape information in the image. By applying morphological operations, an image is transformed into another image that contains information describing the distribution of geometrical structures, represented by the structuring element, contained in the original image.

Due to the utilization of structure information, mathematical morphology has been successfully used in image processing and computer vision [4, 13]. A brief discussion of some applications is given below. Morphological filters have been extensively used in image enhancement[2, 3, 14, 15]. The relationship between a morphological filter and other nonlinear filters, such as rank order filters, has also been well established[14]. Morphological filters have been used to remove nonlinear variations in a signal due to background drift and signal dependent noise. Examples of this include removing streaks appearing in electrophoretic gel images, suppressing impulsive noise and background normalization of EKG signal, and enhancing infrared target images[9, 16-18]. Morphological techniques have also been used to remove speckle noise from radar imagery[19]. By designing a structuring element to describe a specific object, morphological operators can be used to detect the occurrences of this object in an image[20], e.g. determining the locations of protein spots in a gel image[16]. Using image functionals, one can define covariance functions, size distribution functions, and develop correlation type measurements using morphological operators to recognize objects[21, 22]. Edge detection algorithms using morphological operators have also been developed[6, 23, 24]. These edge operators have performance comparable with zero-crossing edge operators and are less computational expensive[23]. Morphological operations have also been used in the segmentation of ultrasound heart images corrupted by impulsive noise[25].

Morphological operators can be used to produce skeletons of an image which are suitable for image coding[26-28]. A digital morphological sampling theorem has also been developed[29]. In the following chapters, we will show how structure information can be used to improve the performance of a morphological filter used in image enhancement.

1.3 Contributions and Organization

Despite all the above work, it is still difficult to successfully use mathematical morphology in practical image processing and analysis. One reason for this difficulty is the lack of image models suitable for morphological operations. Another reason is the limitation of basic morphological operators in the description of geometrical structures represented by the structuring element. Although basic morphological operators can extract information relative to geometrical structure represented by the structuring element, this extraction is, however, quite restrictive in the sense that it does not allow variations. That is, it does not produce information about variations of the geometrical structure represented by the structuring element. In a real application, this places a limit on the performance of morphological operators.

In this thesis, we develop a new morphological filter known as the Generalized Morphological Filter (GMF) that uses multiple structuring elements. The outputs of the multiple morphological operators are linearly combined. Various versions of the GMF can be obtained to suppress different types of noise. Empirical studies have shown that the GMF has greatly improved the performance of morphological filters in image enhancement.

Another original development is the derivation of output probability distribution functions of morphological operators in terms of the input probability distribution function. There have been other efforts in this area [30, 31]. Indirect approaches were used

to obtain results, based on the threshold decomposition concept. Stevenson and Arce derived the output probability distribution functions of a cascade of opening and closing operators [30]. Although Neuvo, *et al.* derived the output probability distribution function of opening and closing operators, they did not address the difference between the one and two dimensional cases. Our derivation is directly based on the definition of gray scale morphological operators and can be easily verified.

An optimal design of the GMF is also developed in this thesis. The design is for a set of special structuring elements and is based on the minimum mean square error. The correlation matrix of the ordered outputs of the multiple morphological operators for the set of structuring elements is derived. Using the output probability distribution function and the correlation matrix, the optimal coefficients of the GMF are obtained. The results of the optimal design provide very valuable insights into how to design the GMF for any application.

The thesis is organized as the following. Following the introduction in this chapter, Chapter 2 contains a preliminary introduction to mathematical morphology. The statistical analysis of morphological operators is also presented in Chapter 2. As an example of the application of mathematical morphology in image analysis, Chapter 3 presents an geometrical inspection algorithm using mathematical morphology. Chapter 4 presents the structure of the GMF and some studies of the filter. In Chapter 5 we investigate the syntactic properties of the GMF. Some properties of morphological operators using multiple structuring elements are also developed in Chapter 5. They are used to prove the invariant properties of the GMF. The root signal structure of the GMF is also studied in Chapter 5. Chapter 6 introduces an optimal design of the GMF. In this chapter, the analytical derivation of the joint and marginal probability distribution functions of the outputs of several morphological operators is presented. They are then used in the computation of the optimal coefficients. In Chapter 7, we make some comments about possible future research in this field.

CHAPTER 2

MORPHOLOGICAL TRANSFORMATIONS AND FILTERS

In mathematical morphology, each image is viewed as a set in a Euclidean space. By using set operations, a morphological filter is used to transform an image. An image contains an unstructured wealth of information, most of which is of no use to us. From it we have to extract what interests us, obtaining a structure which is in fact a simplified sketch of the original image. This extraction involves a controlled loss of information, since we eliminate irrelevant features. Thus, the word "filter" used here implies the transformation of signals by "filtering out" or modifying some of their geometrical features. For example, in optical character recognition, one can simplify the recognition task by first transforming the binary image, representing the text, using a skeletonization technique, which reduces each connected component to a one-pixel thick skeleton. This discards all (useless) information relative to the thickness of the characters and makes further recognition steps quicker and easier.

To extract structural information, we first have to have a spatial or geometrical definition of the structure. This *a prior* spatial information is represented by a set known as the structuring element. A structuring element usually possesses a rather simpler shape and size. The structural information relevant to the defined structure is obtained by interactions between the structuring element and the original set. These interactions define various morphological operations.

Mathematical morphology was first developed for processing binary images by Matheron and Serra [2,5]. Its very basic operators are known as erosion and dilation,

which is also known as the hit or miss transforms [2]. Based on these two operators, two other basic morphological operators are constructed known as opening and closing. Opening and closing are often used to smooth contours in a binary image.

In this chapter, we will first review the basic binary and gray scale morphological operators and their properties. The statistical analysis of morphological operators, especially opening and closing are then presented.

2.1 Morphological Transformations

2.1.1 Binary Morphological Operators

Binary morphological operators are generic morphological operators that involve set operations. Morphological operators can be applied to sets of any dimensions. Since we are investigating the application of mathematical morphology in image processing, we will restrict our discussion to two dimensions. All the results presented here can be extended easily to higher dimensions. A binary image can be represented by a function that is defined on a two dimensional space and assumes only two values: one and zero. The binary image is considered as a set in mathematical morphology. The foreground of a binary image is represented by the set: $A = \{a : f(a) = 1\}$. The background of a binary image is the complement of the set A and defined as: $A^c = \{a : f(a) = 0\}$.

The primary set operation in binary mathematical morphology is set translation. By using set translation, the structuring element can interact with an image so that various morphological transformations can be performed. Let A be a set and p a vector in an Euclidean space. Then the translate of A by p can be expressed by the following:

$$A_p = \{a + p; \ a \in A\}. \tag{2.1.1}$$

Erosion of a set A by a structuring element K is defined as the locus of centers v of K_v included in the set A. The erosion operation is defined as the following:

$$A \ominus k = \left\{ v \; : \; K_v \subseteq A \right\} = \bigcap_{k \in K} A_{-k}. \tag{2.1.2}$$

Erosion is closely related to the classical Minkowski subtraction which is defined as [5]:

$$A \ominus K = \bigcap_{k \in K} A_k. \tag{2.1.3}$$

Hence the erosion can be described as a Minkowski subtraction by rotating the structuring element 180 degrees before the subtraction. The geometrical interpretation of the erosion operation is to extract the centers of the geometrical structures that are represented by the structuring element and contained in the original image. As a side effect, the erosion can also be used to shrink an object. An example of the erosion of a set A by a structuring element K is illustrated in Figure 2.1.

As a dual operation of erosion, dilation has the same geometrical interpretation as the erosion except that the object of the operation is the background of the image. The result of dilation is the locus of centers v of K_v contained in the background of A. Dilation is defined by the following expression:

$$A \oplus \overset{\cdot}{K} = \left\{ v \; : \; K_v \cap A \neq \varnothing \right\} = \bigcup_{k \in K} A_{-k}; \tag{2.1.4}$$

Dilation is the classical Minkowski addition obtained by rotating the structuring element 180 degrees. The Minkowski addition is expressed as [5]:

$$A \oplus K = \left\{ a + k \; : \; a \in A, \; k \in K \right\} = \bigcup_{k \in K} A_k; \tag{2.1.5}$$

From the above algebraic definition, another interpretation of dilation can be obtained which is more suitable for the implementation of the operation: the dilation is the locus of centers v of K_v which intersects the set A [2]. Figure 2.2 shows an example of dilation of a set A by a structuring element K.
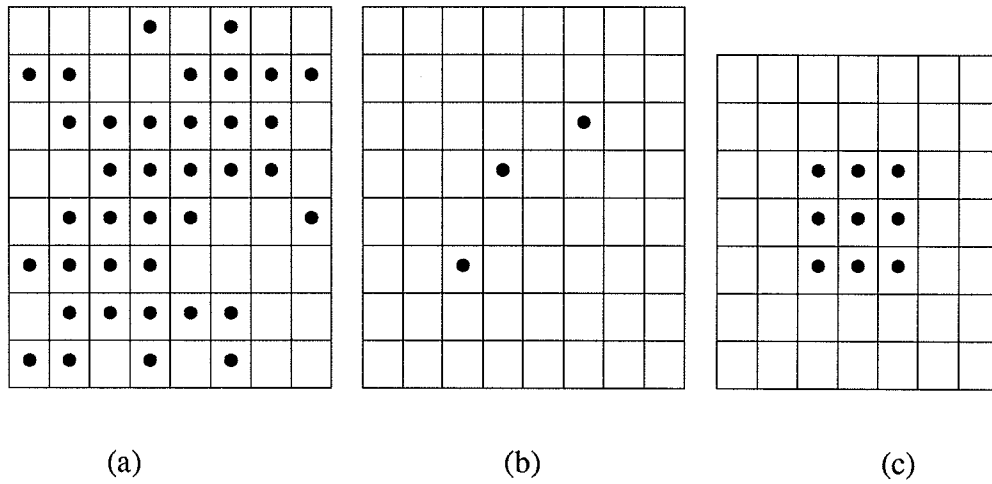
Figure 2.1. An example of the erosion operation: (a) the set A; (b) the erosion of A by K: $A \ominus K$; (c) the structuring element K.
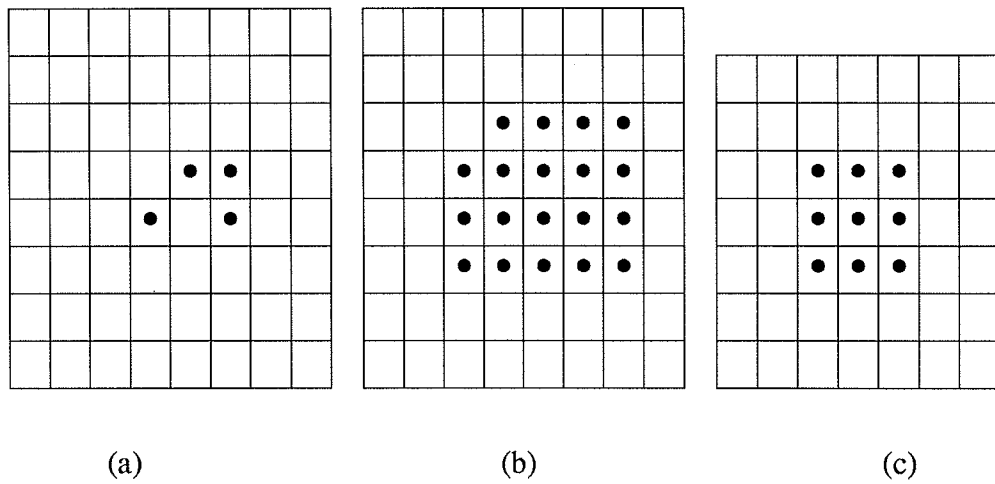
Figure 2.2.   An example of the dilation operation: (a) the set A; (b) the dilation of A by K: $A \oplus K$; (c) the structuring element K.

Erosion and dilation can be considered as operations which extract information relative to the distribution of geometrical structures in the original image that is represented by the structuring element. They are often used in the pattern recognition area to detect whether a structure, defined by the structuring element, is contained in the image.

Erosion and dilation are two nonlinear operations which are generally noninvertable. By "noninvertable", we mean that the original image is not recoverable from the results of the dilation and erosion since small details around the objects in the image are deleted. However, note that the erosion and dilation of an image by a point are just the translation of the image by the point. And the erosion and dilation of an image by the origin results in the image itself. Only in these two cases, can the original image be completely recovered from erosion and dilation.

Erosion and dilation have many interesting properties. The proofs of them can be found in[2, 12]:

(a) Only the dilation operation is commutative, i.e., for a binary image A and a structuring element K, we have $A \oplus K = K \oplus A$.

(b) Since the erosion is a shrinking operation and the dilation is an expanding operation, then it can be seen that if the structuring element contains the origin, then the erosion is anti-extensive and the dilation is extensive, i.e., $A \ominus K \subseteq A \subseteq A \oplus K$.

(c) Both dilation and erosion are increasing operations. Let $\Pi_K(A)$ denote the result when either operation is applied to the image A using structuring element K. Then we have

$$A \subseteq B \Rightarrow \Pi_K(A) \subseteq \Pi_K(B) \tag{2.1.6}$$

(d) Dilation distributes over set union and erosion distributes over set intersection. In addition, erosion by the union of two structuring elements is equivalent to the intersection of the two erosions by two structuring elements, respectively. These properties are

formulate by the following

$$(A \cup B) \oplus K = (A \oplus K) \cup (B \oplus K) \qquad (2.1.7a)$$

$$(A \cap B) \ominus K = (A \ominus K) \cap (B \ominus K) \qquad (2.1.7b)$$

$$A \oplus (K_1 \cup K_2) = (A \oplus K_1) \cup (A \oplus K_2) \qquad (2.1.7c)$$

$$A \ominus (K_1 \cup K_2) = (A \ominus K_1) \cap (A \ominus K_2) \qquad (2.1.7d)$$

These properties allow the dilation or erosion to be preformed using decomposition techniques.

(e) Dilation and erosion also have inclusion properties with set union and set intersection:

$$A \oplus (K_1 \cap K_2) \subset (A \oplus K_1) \cap (A \oplus K_2) \qquad (2.1.8a)$$

$$A \ominus (K_1 \cap K_2) \supset (A \ominus K_1) \cup (A \ominus K_2) \qquad (2.1.8b)$$

$$(A \cap B) \oplus K \subset (A \oplus K) \cap (B \oplus K) \qquad (2.1.8c)$$

$$(A \cup B) \ominus K \supset (A \ominus K) \cup (B \ominus K) \qquad (2.1.8d)$$

(f) The last property concerns the serial composition of dilation and erosion operations. They are defined by the following

$$(A \oplus K_1) \oplus K_2 = A \oplus (K_1 \oplus K_2) \qquad (2.1.9a)$$

$$(A \ominus K_1) \ominus K_2 = A \ominus (K_1 \oplus K_2) \qquad (2.1.9b)$$

The implication of the above is that it enables the users of morphological operators to decompose a given structuring element K into several simpler structuring elements K_i's. Then the morphological operations can be performed in the form of iterations of simpler operations. This approach is used in many applications. For example, sometimes the limitations of the computing hardware prohibits the use of large structuring elements, then an operation can be performed by iteration [32].

The other two basic morphological operators, opening and closing, are serial compositions of dilation and erosion operations. Opening and closing operations can be considered as a recovery operation from the dilation and erosion. They will not recover all the contents of the original image, since dilation and erosion are noninvertable operations, but rather they will recover the most essential parts of the image.

The opening of an image A by a structuring element K is defined as the union of all translates of K which are completely contained in the image A. The opening operation consists of an erosion followed by a dilation. The opening operation is defined as

$$A \circ K = (A \ominus K) \oplus K \qquad (2.1.10)$$

The output of the opening operator consists of all the geometrical structures that are represented by the structuring element and contained in the image A. Consequently, the fine details in the original image that are smaller in size than the given structuring element are removed by the opening operation. An example of the opening of a set A by structuring element K is shown in Figure 2.3.

The closing is the dual operation of the opening. Closing is formed by a dilation followed by an erosion. Closing of an image A by a structuring element K is defined as

$$A \bullet K = (A \oplus K) \ominus K. \qquad (2.1.11)$$

Closing of an image A by K can be considered as the collection of all translates of K which hit the image A. Figure 2.4 presents an example of the closing of a set A by a structuring element K.

The fine detail removal nature of the opening and closing contributes to the use of the two operators for contour smoothing of objects. However, the two operators perform smoothing in different ways. If we consider a binary image as a set of islands, then the opening operator smooths the contour of the islands by cutting narrow isthmuses, suppressing small islands and sharp capes, whereas the closing operator fills narrow
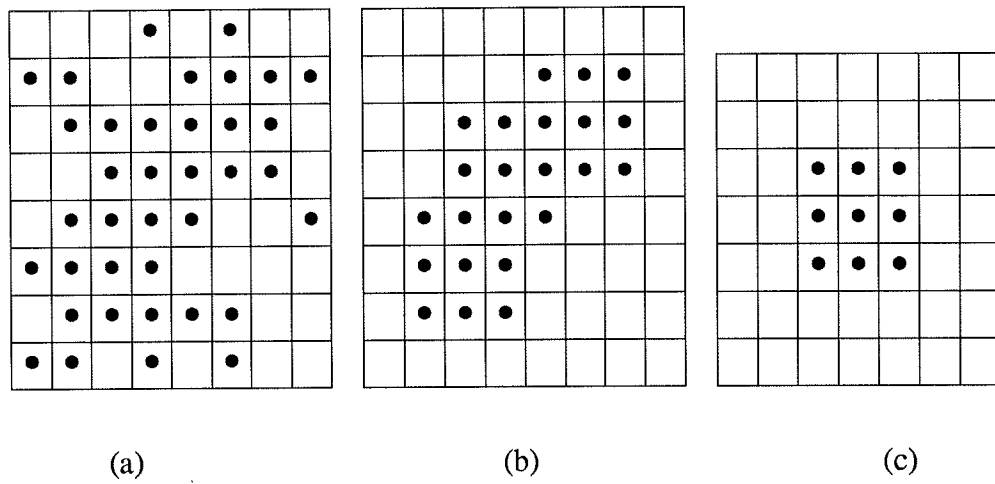
Figure 2.3.   An example of the opening operation: (a) the set A; (b) the opening of A
by K: $A \circ K$; (c) the structuring element K.

(a) (b) (c)
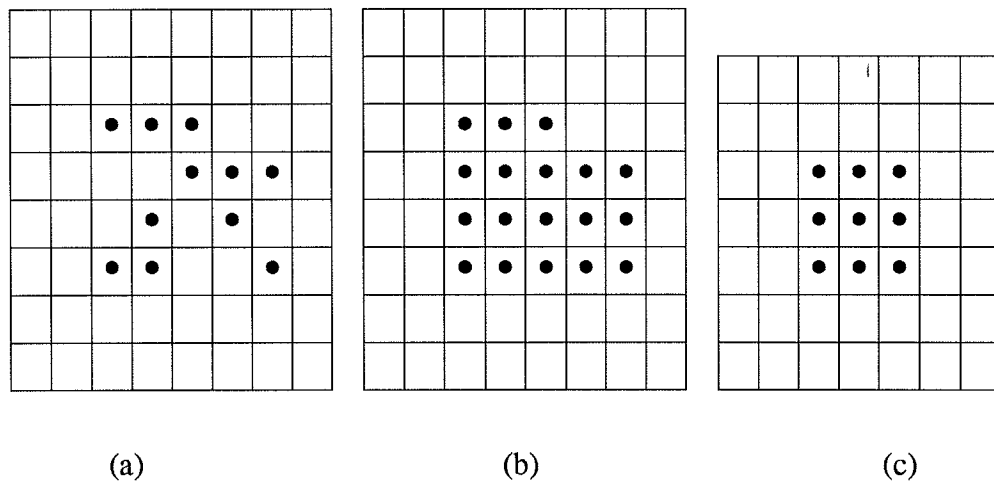
Figure 2.4.   An example of the closing operation: (a) the set A; (b) the closing of A
by K: $A \bullet K$; (c) the structuring element K.

channels, small lakes, and long thin gulfs. The smoothing effect of the opening and closing operators is also illustrated in Figures 2.3 and 2.4. Very often the two operators are applied in series order in order to achieve better smoothing.

One of the salient properties of the opening and closing operators is the idempotent property. By idempotent, we mean that the invariability of the result is achieved by a single application of the operator. That is, the result of the first application of the operator will remain invariant if the operator using the same structuring element is applied to the result again. The idempotent property of the opening and closing operators can be expressed as the following:

$$(A \circ K) \circ K = A \circ K, \quad \text{and} \quad (A \bullet K) \bullet K = A \bullet K. \tag{2.1.12}$$

Opening and closing operators are used to extract geometrical structures from the original image. The outputs of the two operators consists of structures represented by the structuring element. Therefore, the repeated applications of two operators using the same structuring element will produce the same structures and the idempotent property hence holds.

Opening and closing are both increasing operations. Opening is anti-extensive, whereas closing is extensive. That is

$$A \circ K \subseteq A \subseteq A \bullet K. \tag{2.1.13}$$

The extensiveness property of the opening and closing causes a bias effect when they are applied in series. This will be discussed later.

2.1.2 Gray Scale Morphological Operators

From above, mathematical morphology consists of set operations. Therefore, morphological transformations cannot be directly applied to functions. In order to extend morphological transformations to functions, it is necessary to define these set operations

in terms of algebraic operations. This is done by first assigning a special set structure to functions so that they can be treated as sets. This special set structure serves as a link between functions and sets. Morphological transformations involving algebraic operations are known as gray scale morphological transformations.

This special set structure is known as the umbra of the function f denoted by $U(f)$ [2, 9, 33]. For every function, there corresponds a unique umbra. The analytical definition of the umbra $U(f)$ of a function f is:

$$U(f) = \left\{ (x, t): f(x) \geq t \right\} \quad x \in I\!R^2, \quad -\infty < t < \infty. \qquad (2.1.14)$$

From the above definition, it is clear that the umbra $U(f)$ of a function f is the space under the profile of the function. Figure 2.5 illustrates an umbra $U(f)$ of a function f. The function f can also be uniquely reconstructed from its umbra by the following:

$$f(x) = \sup \left\{ t : (x, t) \in U(f) \right\}. \qquad (2.1.15)$$

Because of the uniqueness of a function and its umbra, the result of a morphological operator applied to the umbra of a function can be related to the operator applied to the image. The following two examples illustrate this: for functions f and k, k being the gray scale structuring element, we have:

$$f \oplus k \rightarrow U(f \oplus k) = U(f) \oplus U(k); \qquad (2.1.16)$$

$$f \ominus k \rightarrow U(f \ominus k) = U(f) \ominus U(k). \qquad (2.1.17)$$

Detailed proofs of this can be found in[2, 9, 33]. It is possible to define gray scale morphological operators as algebraic operations and avoid the umbra [2, 33].

The algebraic expressions for the dilation and erosion of a function f by a function k, as well as the opening and closing, are defined by the following:

$$\text{EROSION:} \quad (f \ominus k)(x) = \min_{z \in K} \left\{ f(x+z) - k(z) \right\} \qquad (2.1.18a)$$
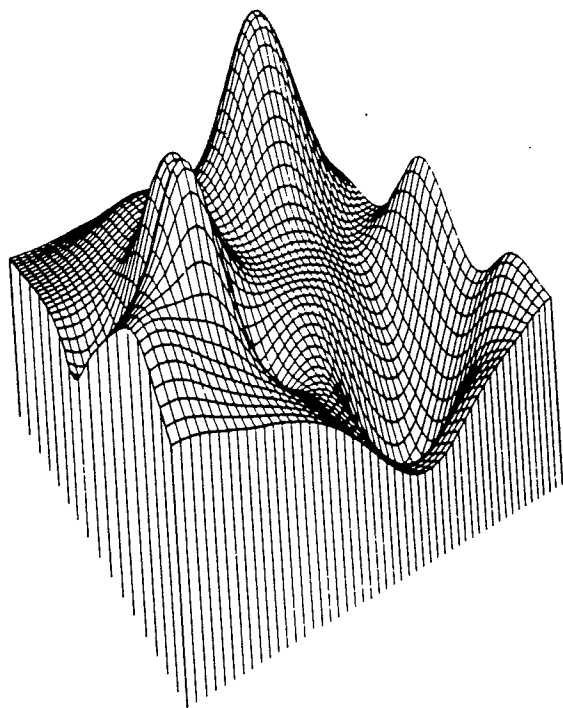
Figure 2.5.   An illustration of the umbra.

where K is the support region of the structuring element k;

$$\text{DILATION:} \quad (f \oplus k)(x) = \max_{z \in K} \left\{ f(x-z) + k(z) \right\}; \qquad (2.1.18b)$$

$$\text{OPENING:} \quad f \circ k = (f \ominus k) \oplus k; \qquad (2.1.18c)$$

$$\text{CLOSING:} \quad f \bullet k = (f \oplus k) \ominus k. \qquad (2.1.18d)$$

One dimensional examples of the above four operations are illustrated in Figure 2.6. The solid lines in the figure represent the original function and the dotted lines represent the results of gray scale morphological operators applied to the function. The structuring element used in these examples is a window of 3 samples. The shrinking and expanding effects of the erosion and dilation operators are exhibited. The examples of opening and closing operators also show their edge preservation as well as smoothing capabilities.

Gray scale morphological operators have properties similar to their binary counterparts. They are increasing operations, the results of the four operators have the following relationship:

$$f \ominus k \le f \circ k \le f \le f \bullet k \le f \oplus k . \qquad (2.1.19)$$

The following four properties describe the distributive properties of the morphological, max, and min operators.

$$\min \left\{ f, g \right\} \ominus k = \min \left\{ f \ominus k, g \ominus k \right\}. \qquad (2.1.20)$$

$$\max \left\{ f, g \right\} \ominus k \ge \max \left\{ f \ominus k, g \ominus k \right\}. \qquad (2.1.21)$$

$$\min \left\{ f, g \right\} \oplus k \le \min \left\{ f \oplus k, g \oplus k \right\}. \qquad (2.1.22)$$

$$\max \left\{ f, g \right\} \oplus k = \max \left\{ f \oplus k, g \oplus k \right\}. \qquad (2.1.23)$$
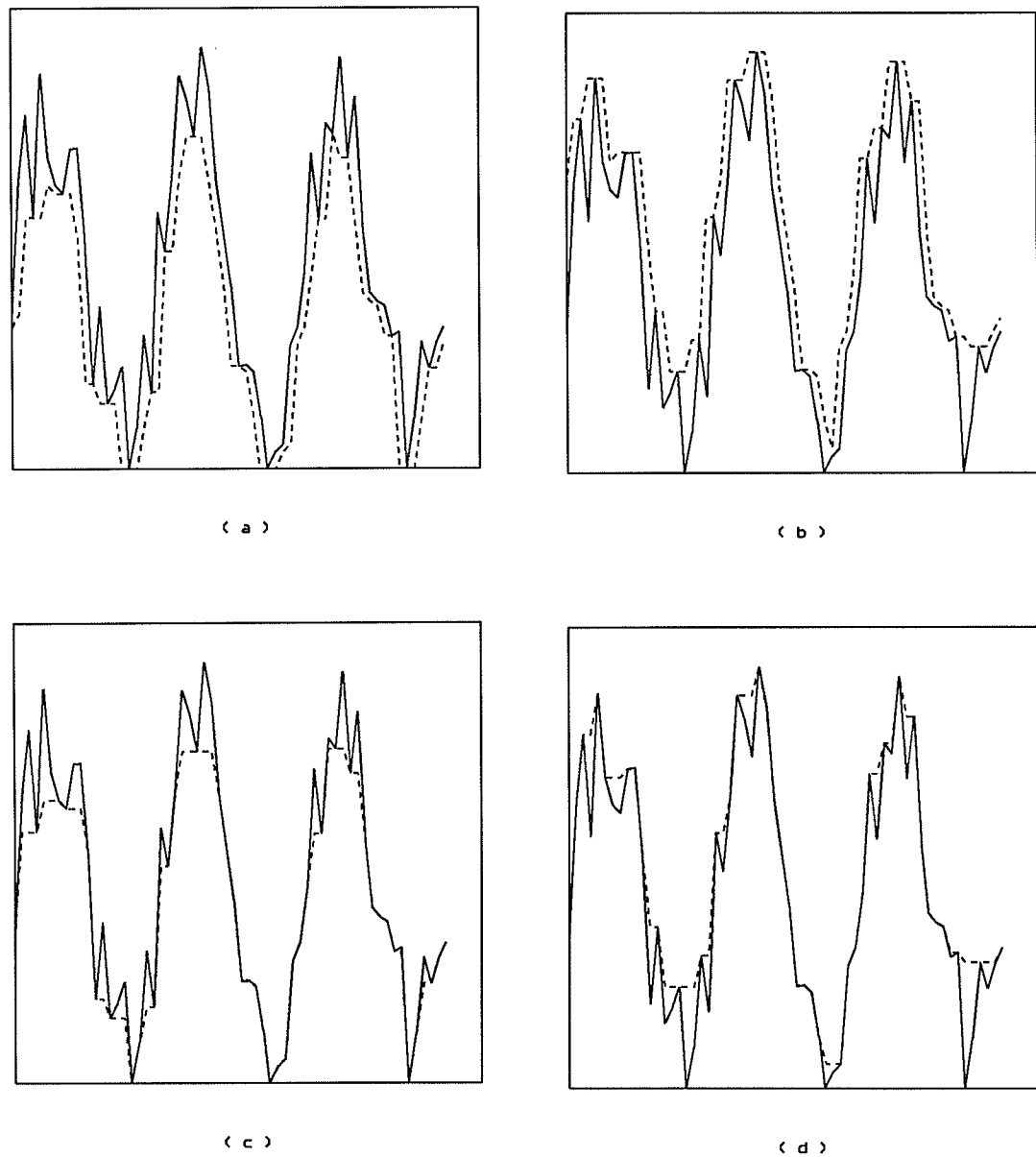
Figure 2.6. Examples of gray scale morphological operators. Solid lines represent the original functions, dotted lines represent the transformed functions The structuring element k used is defined as a window of three samples: { ⋅⋅⋅ }. (a) erosion of f by the structuring element k: $f \ominus k$; (b) dilation of f by the structuring element k: $f \oplus k$; (c) opening of f by the structuring element k: $f \circ k$; (d) closing of f by the structuring element k: $f \bullet k$.

Gray scale opening and closing are also idempotent.

$$\text{Let } g = f \circ k, \text{ then } g = g \circ k. \qquad (2.1.24)$$

$$\text{Let } g = f \bullet k, \text{ then } g = g \bullet k. \qquad (2.1.25)$$

Since they are nonlinear operations, gray scale morphological transformations do not have a superposition property. However, applying a morphological operation to a sum of a function and a constant is equivalent to the sum of the result of applying the morphological operation to the function and the constant. This property can be thought of as weak linearity of morphological operations [33]. Let c denote a constant. Then the property can be expressed as

$$\Psi(f + c) = \Psi(f) + c. \qquad (2.1.26)$$

Where $\Psi(\cdot)$ denotes a morphological operator. This property can easily be proved from the definitions of gray scale morphological operators. We use the gray scale erosion to illustrate the proof of the weak linearity.

Proof:

$$[(f + c) \ominus k](x) = \min_{z \in K} \left\{ f(x+z) - k(z) + c \right\} = \min_{z \in K} \left\{ f(x+z) - k(z) \right\} + c,$$

since the constant does not have any effect on the maximum operation.

Although gray scale structuring elements can be used in gray scale morphological transformations, flat structuring elements are most often used. By "flat structuring element", we mean that the structuring element has equal value at every location of its support region. For opening and closing operators, a flat structuring element can be treated as a set or a window in which the two morphological operations are applied. A very interesting property, known as threshold decomposition, holds for gray scale morphological transformations when flat structuring elements are used [2,33-35]. Threshold decomposition states that morphological transformations commute with the thresholding

operation. That is, thresholding at a gray level t the result of a gray scale morphological operator applied to an M-valued discrete function f is equivalent to applying the binary morphological operator to the cross section of the function f obtained by thresholding the function at the same level t. This can be expressed as

$$\Pi_t[\Psi_g(f)] = \Psi_b[\Pi_t(f)] = \Psi_b(F_t) \qquad (2.1.27)$$

where Π_t denotes the thresholding operation at gray level t, Ψ_g and Ψ_b gray scale and binary morphological operations, respectively, and F_t the cross section of the function f obtained by thresholding f at gray level t.

As a result of threshold decomposition, the output of a gray scale morphological operator applied to a function can be obtained by summing up all the outputs from the corresponding binary morphological operators applied to the cross sections of the function, respectively. This feature of morphological operations provides a very effective tool for analysis of morphological operations.

2.2 Statistical Analysis of Morphological Operators

In studying the performance of a morphological filter one is interested in two types of properties: syntactical and statistical. Syntactical properties include the ability of the morphological filter to preserve, extract, or delete structures in a signal. These include the root signal structure that results from repeated application of the filter[33, 36]. The type of statistical properties include the relationship between the output probability distribution function and the input noise probability distribution function. This is an indication of the ability of the filter to suppress noise. Other simple measures, such as variance reduction, have also been investigated [18, 36]. There have been some efforts in the development of the output probability distribution functions of morphological operators [30, 31, 37-39]. Indirect approaches, mainly based on the concept of threshold decomposition, were used. Stevenson and Arce derived the output probability

distribution function of a special filter consisting of a cascade of opening and closing operators [30]. Their approach was to examine the binary case first based on the ability of the filter to preserve structures in the input. They then generalized their results to gray scale operations. Using methods from the development of stack filters, Koskinen, *et al.* analyzed statistical properties of basic morphological operators [31]. This approach also started by addressing binary operations and then extending the results to gray scale operations.

Our development in this section will be different in that it is based exactly on the definition of one dimensional gray scale morphological operators. The output probability distribution functions will then be analytically derived. The results of our development also reveal some interesting statistical properties of morphological operators.

In this section, we will derive analytic forms for the univariate probability distribution functions for opening and closing operators using flat (constant) structuring elements. When a flat structuring element is used, the opening and closing operations are actually multiple level ordering operations. Hence our derivation will be based on order statistics.

2.2.1 One Dimensional Morphological Operators

First, an opening operation using a one dimensional structuring element is investigated. For a flat structuring element of width n samples, the opening operation applied to a sample x_i can be expressed as the following[33]:

$$y = \max \{\min\{x_{i-n+1}, \ldots, x_i\}, \min\{x_{i-n+2}, \ldots, x_i, x_{i+1}\}, \ldots,$$

$$\min\{x_i, \ldots, x_{i+n-1}\} \}. \tag{2.2.1}$$

Note that for a structuring element of n pixels long, there are $n - 1$ pixels at each side of x_i which are involved in the computation. In order to derive the output probability distribution function of the opening operator, we formulate the opening operation in a

slightly different way. This is done by removing x_i from all the min terms in (2.2.1):

$$y = \min\{ x_i, z \}, \tag{2.2.2}$$

where

$$z = \max \ \{\min\{x_{i-n+1}, \ldots, x_{i-1}\}, \min\{ x_{i-n+2}, \ldots, x_{i-1}, x_{i+1} \}, \ldots,$$

$$\min\{x_{i+1}, \ldots, x_{i+n-1}\} \ \}. \tag{2.2.3}$$

We will first derive the probability distribution function for z, and then use (2.2.2) to obtain the output probability distribution function of the opening operator.

For simplicity, we make a slight change in the indexing scheme in (2.2.3) and restate the problem. For $2m$, $m = 1, 2, 3, \ldots$, independent identically distributed random variables $\{x_1, x_2, \ldots, x_{2m}\}$ with univariate probability distribution function $F_x(\cdot)$, we desire to derive the output probability distribution function of the following operation:

$$z = \max \ \{\min\{x_1, x_2, \ldots, x_m\}, \min\{ x_2, x_3, \ldots, x_{m+1} \}, \ldots,$$

$$\min\{x_{m+1}, x_{m+2}, \ldots, x_{2m}\} \ \}. \tag{2.2.4}$$

Since (2.2.4) consists of ordering operations, the result consists of an element in the ordered sequence $\{x_{(i)}; 1 \le i \le 2m\}$ from the samples $\{x_i; 1 \le i \le 2m\}$, with $x_{(1)} \le x_{(2)} \le \cdots \le x_{(2m)}$. The following proposition describes the possible values of z in (2.2.4).

Proposition 2.2.1:

The possible values of z in (2.2.4) consist of elements with ranks from 2 to $m+1$ from the ordered sequence of the $2m$ elements. That is, $z = x_{(r)}, \ \ 2 \le r \le m+1$.

Proof:

The proof is begun by excluding elements in the order sequence that z cannot take. First, the smallest element, $x_{(1)}$, in the ordered sequence cannot be the output of the

operation. Note that no element in the sequence appears in every min term of (2.2.4). Therefore, while the smallest element will be the result of some min terms, there is at least one min term whose result is larger than $x_{(1)}$.

Next, we show that z cannot take on elements in the order sequence with ranks equal to or greater than $m+2$, that is, $x_{(m+2)} \leq \cdots \leq x_{(2m)}$. This is because every min term consists of m elements. There are only $m-1$ of elements in the order sequence with ranks greater than $m+1$. Therefore these elements cannot be the minimum of the elements in any min term.

Hence z takes elements that have ranks from 2 to $m+1$ from the ordered sequence of $\{x_i\}$.

Assuming that every sample in the ordered sequence is equally likely at sample positions 1 to $2m$, we first derive the probability that z is the *rth* element in the ordered sequence.

Proposition 2.2.2:

The probability that z is the *rth* element, $2 \leq r \leq m+1$, in the ordered sequence of the $2m$ samples is:

$$P\{\, z = x_{(r)}\,\} = \frac{\dfrac{(m+1)!}{(r-2)!\,(m-r+1)!}(r-1)!(2m-r)!}{(2m)!}, \qquad 2 \leq r \leq m+1. \quad (2.2.5)$$

Proof:

The only part in (2.2.5) that needs proof is the numerator. The numerator of (2.2.5) is actually the number of permutations of the $2m$ ordered elements with which the element with rank r is z. The proof is quite lengthy and is presented in the Appendix.

Using Proposition 2.2.2, the output probability distribution function of (2.2.4) can be obtained.

Proposition 2.2.3:

The probability distribution function of z in (2.2.4) is:

$$F_z(v) = P\{z \leq v\} = \sum_{r=2}^{m+1} P\{z = x_{(r)}\} P\{x_{(r)} \leq v\} \qquad (2.2.6)$$

The derivation of the probability distribution function $P\{x_{(r)} \leq v\}$ for an ordered sequence of i.i.d. random variables can be found in [40]. Consequently we have the following proposition.

Proposition 2.2.4:

The output probability distribution function for the opening operator using a one dimensional structuring element is:

$$F_y(v) = P\{\min(x_i, z) \leq v\} = 1 - [1 - F_x][1 - F_z] \qquad (2.2.7)$$

Table 2.1 shows several output probability distribution functions of a one dimensional opening operator using structuring elements of sizes ranging from 3 to 5 samples.

Given a Gaussian input probability distribution function $F_x(\cdot)$ with zero mean and unit variance, Figure 2.7 illustrates the corresponding probability density functions of the output. The means and variances of the output z are shown in Table 2.2. We can conclude from the figure and the table that the opening is a biased operation. The mean value of the output of an opening operator is always less than the input. The variance reduction capability of the opening operation is also shown in Table 2.2. Table 2.2 also shows that the larger the size of the structuring element, the greater the mean shift and the greater the variance reduction in the output.

The derivation for the closing operation is similar. For a one dimensional, flat structuring element of n samples, the closing operation can be formulated as:

$$y = \min \{\max\{x_{i-n+1}, \ldots, x_i\}, \max\{x_{i-n+2}, \ldots, x_i, x_{i+1}\}, \ldots,$$

$$\max\{x_i, \ldots, x_{i+n-1}\} \}. \qquad (2.2.8)$$

Table 2.1. Output probability distribution functions of the opening operator

Size of structuring element	Output Probability Distribution Function
3	$F_x + 3F_x{}^2 - 5F_x{}^3 + 2F_x{}^4$
4	$F_x + 6F_x{}^2 - 14F_x{}^3 + 21F_x{}^4 - 13F_x{}^5$
5	$F_x + 10F_x{}^2 - 30F_x{}^3 + 35F_x{}^4 - 19F_x{}^5 + 4F_x{}^6$

Table 2.2. Means and variances of the output distributions shown in Figure 2.7

Size of structuring element	Mean	Variance
3	-0.480	0.494
4	-0.629	0.411
5	-0.746	0.358
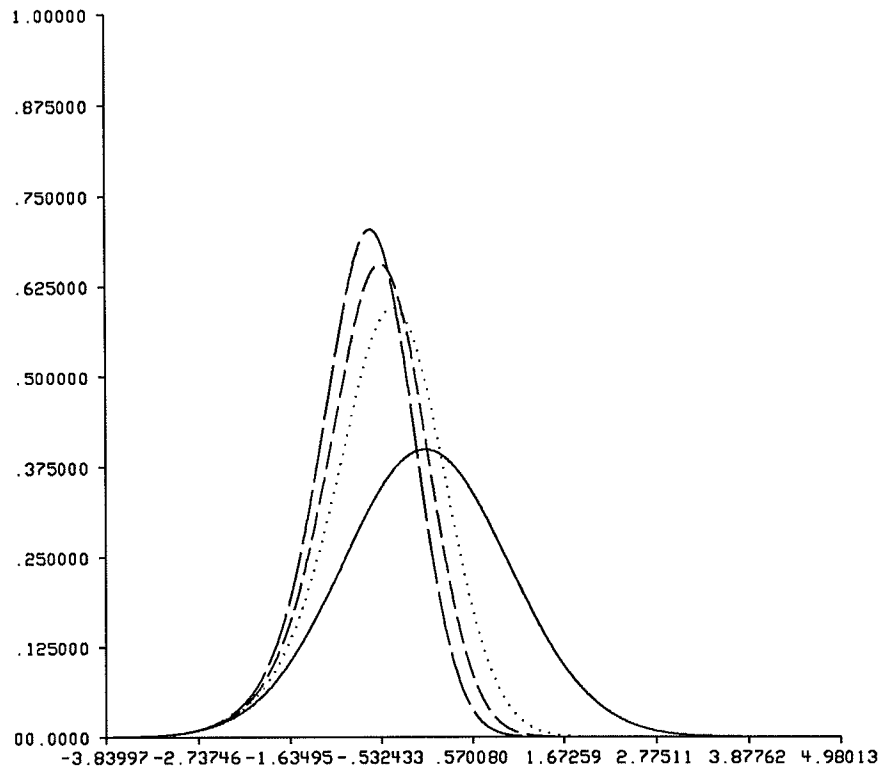
Figure 2.7. Illustration of the output probability density functions of the opening operator: The solid line is the original input probability density function of the normal distribution; the dotted line is the output probability density function using a structuring element of 3 samples; the dashed line with short lines is the output probability density function using a structuring element of 4 samples; the dashed line with long lines is the output probability density function using a structuring element of 5 samples.

By separating x_i from rest of the samples, (2.2.8) can be formulated as:

$$y = \max\{\ x_i, z\ \}, \tag{2.2.9}$$

where

$$z = \min\ \{\max\{x_{i-n+1}, \ldots, x_{i-1}\}, \max\{\ x_{i-n+2}, \ldots, x_{i-1}, x_{i+1}\}, \ldots,$$

$$\max\{x_{i+1}, \ldots, x_{i+n-1}\}\ \}. \tag{2.2.10}$$

As in the derivation for the opening operator, a change is made of the index of the variables in (2.2.10).

$$z = \min\ \{\max\{x_1, x_2, \ldots, x_m\}, \max\{\ x_2, x_3, \ldots, x_{m+1}\}, \ldots,$$

$$\max\{x_{m+1}, x_{m+2}, \ldots, x_{2m}\}\ \}. \tag{2.2.11}$$

Proposition 2.2.5:

For $2m$ input samples, z can take on elements in the ordered sequence of the $2m$ elements with ranks from m to $2m-1$. That is, $z = x_{(r)}, m \leq r \leq 2m-1$.

The proof is similar to Proposition 2.2.1.

Proposition 2.2.6:

The probability of z taking on the rth element, $m \leq r \leq 2m-1$, in the ordered sequence of the $2m$ samples is:

$$P\{\ z = x_{(r)}\} = \frac{\dfrac{(m+1)!}{(r-m)!\ (2m-r-1)!}(r-1)!(2m-r)!}{(2m)!}, \quad m \leq r \leq 2m-1 \tag{2.2.12}$$

The proof of the proposition is similar to Proposition 2.2.2.

Proposition 2.2.7:

The probability distribution function of z is

$$F_z = P\{z \leq v\} = \sum_{r=m}^{2m-1} P\{z = x_{(r)}\}P\{x_{(r)} \leq v\}. \tag{2.2.13}$$

The probability distribution function $P\{x_{(r)} \leq v\}$ for an ordered sequence of i.i.d. random variables can be found in [40].

Proposition 2.2.8:

The output probability distribution function of a closing operator is:

$$F_y(v) = P\{\max(x_i, z) \leq v\} = F_x F_z.$$ (2.2.14)

Table 2.3 shows the output probability distribution functions of the closing operator using structuring elements of sizes ranging from 3 to 5 samples.

Given that the input is Gaussian distributed with zero mean and unit variance, Figure 2.8 illustrates the output probability density functions. The means and variances of the output distributions are shown in Table 2.4. Note that closing is also a biased operation. The output mean is always greater than the input mean. Again, the larger the structuring element, the greater the mean shift and the greater the variance reduction.

2.2.2 Two Dimensional Morphological Operators

The derivation of the output probability distribution functions of the opening and closing operators using two dimensional structuring elements is more complicated. One obvious complication is that the number of samples involved in the opening or closing operation depends not only on the size, but also the shape of the structuring element. For two structuring elements with the same number of samples but with different shapes, the number of samples involved in the operations can be very different. This fact is illustrated in Figure 2.9. It can be seen that for the structuring element k_1, eleven samples are involved in the operation, but only nine samples for the structuring element k_2. However, this situation does not mean that the derivation of the output probability distribution function for a two dimensional structuring elements is impossible. This fact can be demonstrated by the following example taken from[31]. In some cases the derivation is even easier than in the one dimensional case. The structuring element k, illustrated in

Table 2.3. Output probability distribution functions of the closing operator

Size of structuring element	Output Probability Distribution Function
3	$3 F_x^3 - 2F_x^4$
4	$4 F_x^4 - 3F_x^5$
5	$5 F_x^5 - 4F_x^6$

Table 2.4. Means and variances of the output distributions shown in Figure 2.8

Size of structuring element	Mean	Variance
3	0.479	0.495
4	0.629	0.411
5	0.746	0.358
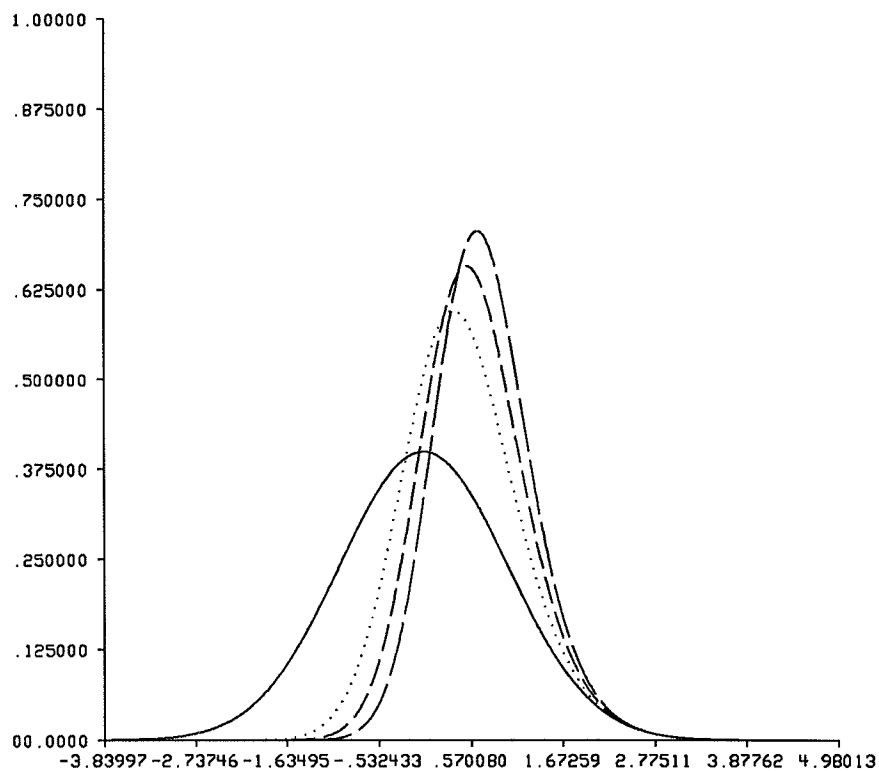
Figure 2.8.   Illustration of the output probability density functions of the closing operator: The solid line is the original input probability density function; the dotted line is the output probability density function using a structuring element of 3 samples; the dashed line with short lines is the output probability density function using a structuring element of 4 samples; the dashed line with long lines is the output probability density function using a structuring element of 5 samples.

k_1

(a)

k_2

(b)
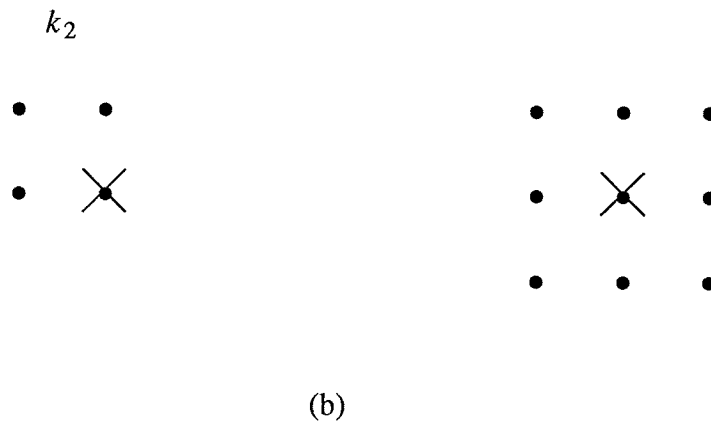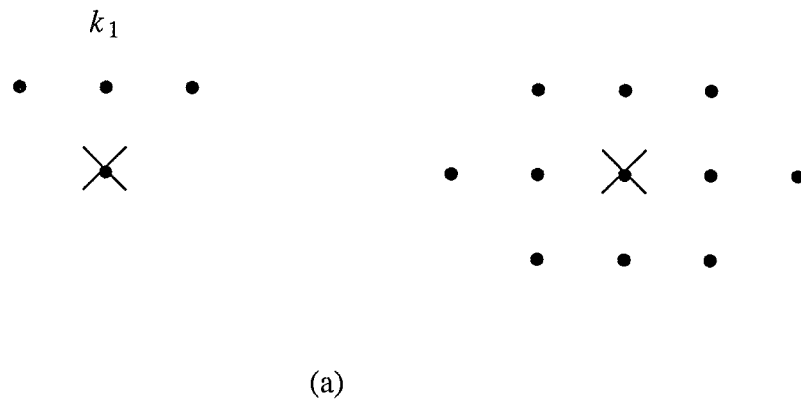
Figure 2.9. Structuring elements with the same number of samples but different patterns results in different numbers of pixels involved in the opening operation: (a) the structuring element k_1 and corresponding pixels involving in the operation; (b) the structuring element k_2 and corresponding pixels involved in the operation.

Figure 2.10, is defined as: {(-1,0) (0, 0), (0, -1)}. Suppose the opening operator using this structuring element is applied to the sample $x_{(0,0)}$ in an image consisting of i.i.d. random variables. Then the operation can be expressed as:

$$y = \max\{\min(x_{(-1,0)}, x_{(0,0)}, x_{(0,-1)}), \min(x_{(0,0)}, x_{(1,0)}, x_{(1,-1)}), \min(x_{(-1,1)}, x_{(0,1)}, x_{(0,0)})\}$$

$$= \min\{x_{(0,0)}, z\}.$$

where $z = \max\{\min(x_{(-1,0)}, x_{(0,-1)}), \min(x_{(1,0)}, x_{(1,-1)}), \min(x_{(-1,1)}, x_{(0,1)})\}$. Note that the results of the three min terms are still i.i.d. random variables since there is no sample correlation among them and every min term has two variables. The probability distribution function of z becomes:

$$F_z(v) = P\{z \le v\} = F_x^3 (2 - F_x)^3$$

Then the probability distribution function of y is:

$$F_y(v) = P\{\min\{x_{(0,0)}, z\} \le v\} = 1 - [1 - F_x][1 - F_z]$$

$$= F_x + 8F_x^3 - 20F_x^4 + 18F_x^5 - 7F_x^6 + F_x^7$$

Since the results obtained in this section are for the basic morphological operators, especially the opening and closing, they can be used as the foundation for other types of statistical analysis of morphological operations, such as the optimal design of the Generalized Morphological Filter [37, 38] that will be presented later.

2.3 Morphological Filters

A filter is used to extract from a signal those parts that are of interest to the user. The function of a filter can also be interpretated as a suppressing operation that removes the irrelevant parts from a signal. For example, a hi-pass filter extracts the high frequency components from a signal, or it can be said that it suppresses the low frequency components. In image enhancement, with the assumption that the image under study is contaminated by noise, the filter is used to recover the original image from the corrupted

•   •
(−1,1)   (0,1)

•   •   •   •   •
(−1,0)   (0,0)   (−1,0)   (0,0)   (1,0)

•   •   •
(0,−1)   (0,−1)   (1,−1)
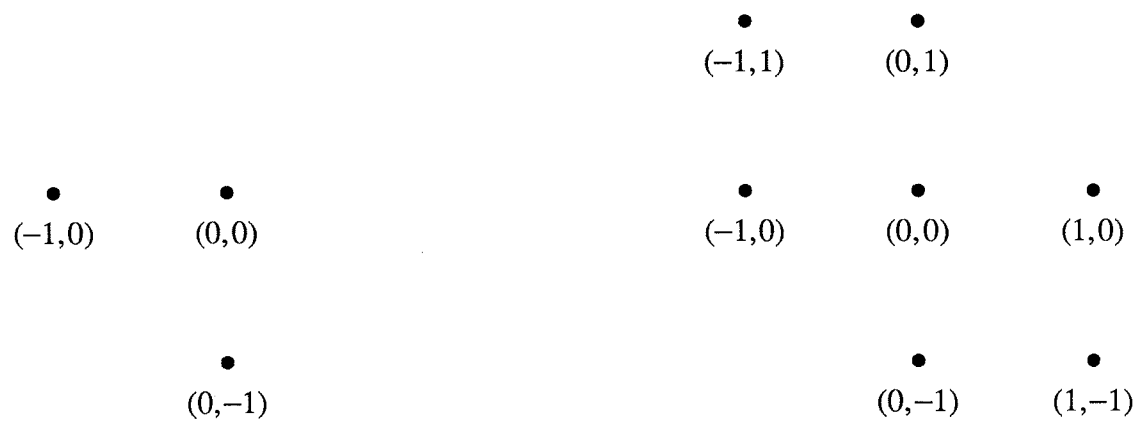
Figure 2.10.   An example of a two dimensional structuring element and the pixels involved in the opening operation.

data, or remove the noise from the image. With a known mathematical model of the original image, a Wiener filter can be used to suppress the additive noise. Some filters recover a signal based on a predefined criterion for the minimization of the difference between the original signal and the output of the filter.

Without exception, the morphological filter is also used to extract structural contents that are of interest to a user. Since mathematical morphology was introduced, morphological filters have gone through a tremendous period of development. During the early stages of its development, the morphological filter was mainly used in binary image processing. Later, by developing the relationships between set operations and algebraic operations, morphological filters were extended to gray scale image processing [11]. Sternberg used an alternating series of openings and closings of increasing size to efficiently clean noisy images [10]. Stevenson and Arce combined set operations and morphological operations to develop the 2D CO morphological filter which can remove impulsive noise and preserve fine details in an image [30]. In view of the fact that many kinds of morphological filters have been and will be developed, Serra proposed a formal definition of a morphological filter [3]. Base on the observation that since "*the world around us is not translucent; on the contrary, it is composed of opaque objects that hide one another*" [3], visual signals are not compounded linearly, hence the inclusion relationship is used as one prerequisite of morphological filters. Let ψ denote any morphological filter. For two gray scale images f and g, a morphological filter ψ satisfies the condition:

$$f \leq g \Rightarrow \psi(f) \leq \psi(g). \tag{2.3.1}$$

Another prerequisite for a filter to be a morphological filter is that the idempotent property must hold [3]. That is

$$\psi[\psi(f)] = \psi(f). \tag{2.3.2}$$

All of the above mentioned morphological filters satisfies these two prerequisites. In the

following, we will discuss these morphological filters in some detail.

2.3.1. Conventional Morphological Filters

Image enhancement is one of the areas that has seen the extensive application of morphological filters. Opening and closing operators are commonly used for extracting geometrical structures in an image. They are also used in image enhancement to suppress impulsive noise, due to their abilities of suppressing details in the image whose structures do not match the structuring element. Using a binary structuring element with a smooth boundary, a binary opening operator can smooth the boundary of a binary image by cutting narrow isthmuses and suppressing sharp caps and small islands. Using a gray scale structuring element with a smooth profile, a gray scale opening operator can clip sharp peaks to obtain a smooth profile of the image. A closing operator smooths an image in a different way, that is, blocking the narrow gulfs around the boundary of a binary image and filling narrow pits on the profile of a gray scale image. Since opening and closing operators smooth an image in different ways, they are almost always used together, usually in the form of a cascade. Applying an opening operator followed by a closing operator is usually referred to as an open-closing filter and applying a closing operator followed by an opening operator is referred to as a close-opening filter. A single structuring element is used in the conventional morphological filter. Figure 2.11 shows block diagrams of the two morphological filters.

Due to the bias problem discussed in the previous section, there can exist a large difference between the outputs of the open-closing and close-opening filters. Although successively applying a closing to the output of an opening operator or an opening operator to the output of a closing operator reduces the difference to some extent, the output of the close-opening filter is still larger than that of the open-closing filter. Figure 2.12 shows an example of this bias effect. Serra proved this property in[3]. One way to

(a)

(b)
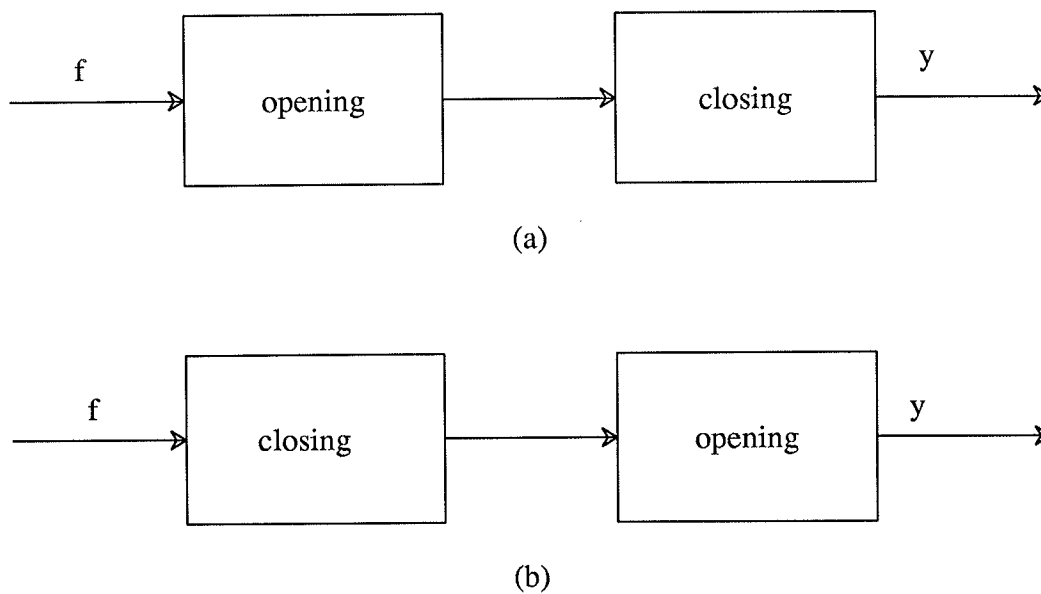
Figure 2.11.   (a) the open-closing filter; (b) the close-opening filter.
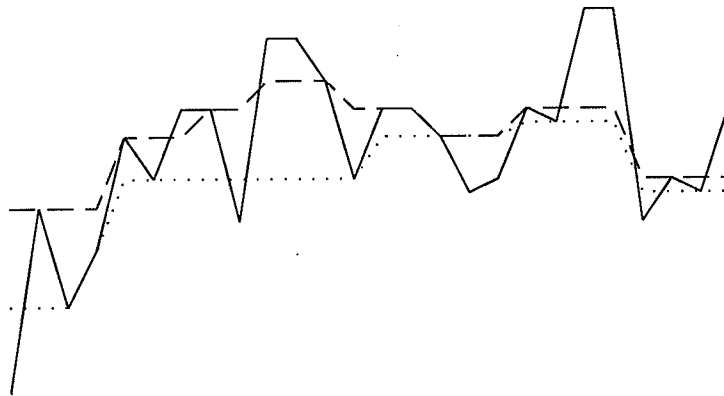
Figure 2.12.   Illustration of the bias problem. The structuring element used in this example is a line of three samples in length. The solid line represents the original data, the dotted line represents the result of the open-closing operation, and the dashed line represents the result of the close-opening operation.

reduce the bias effect is to average the outputs of the two filters. Figure 2.13 illustrates such a scheme.

Morphological filters can also be used to remove noise whose structure is known. Sternberg constructed a pair of structuring elements to remove the streaks appearing in gel images [9]. The two structuring elements were horizontal and vertical bars. The original gel image was opened by the two structuring elements, respectively. The results of the two openings were then subtracted from the original image so that the vertical and horizontal streaks were removed [9]. Specially designed structuring elements have been used to suppress impulsive noise and normalize the background level of EKG signals and to enhance infrared images [15, 17, 18].

When an image consists of large homogeneous regions and is corrupted by impulsive noise, a morphological filter can produce fairly good results using a single structuring element with a square or circular support region. If an image contains fine details, a morphological filter using a single structuring element is likely to suppress these fine details along with impulsive noise. Geometrical structure suppression can be improved by using a structuring element of small size, but the noise suppression ability of the filter is consequently weakened. Because of the idempotent property, an iterative approach cannot be used to compensate for the poor noise suppression caused by using a small structuring element. Another limit of the morphological filter is that it is very poor in suppressing non-impulsive noise.

2.3.2.Relations Between Morphological Filters and Order Statistic Filters

Order statistic filters are a class of nonlinear filters that have in the last decade achieved popularity in speech and image processing. A order statistic filter forms an ordered sequence from the input data spanned by a window. The ordering is based on their magnitudes. The output is selected from the ordered sequence according to a given
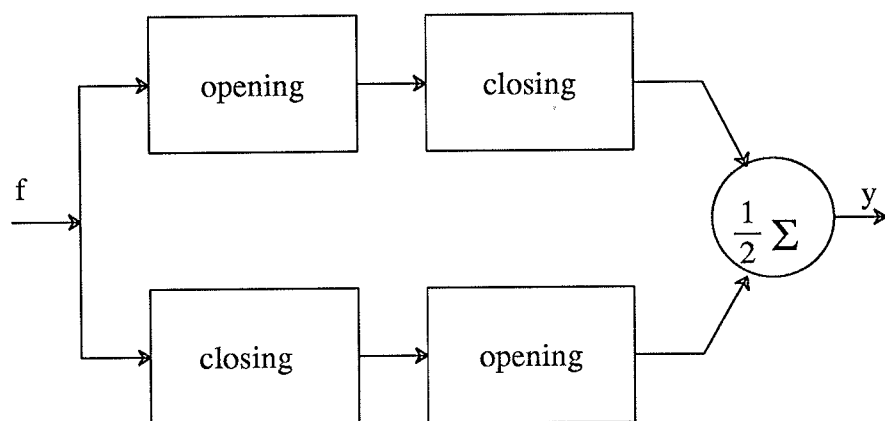
Figure 2.13.   One bias reduction scheme for a conventional morphological filter.

rank. The median filter is one of the most extensively studied order statistic filters [13, 40, 41]. Other order statistic filters include max and min filters [40, 42].

Properties of the order statistic filters that have contributed to their popularity include effective impulsive noise suppression and geometrical structure preservation [43, 44]. Median filters have an important property known as the root signal of the filter [45-47]. A root is a signal that is invariant under repeated applications of the filter [46, 47]. It has been shown that any finite signal will converge to a root after finite number of iterations of the median filter [46, 48].

Morphological filters are very closely related to order statistic filters. From the definitions of gray scale morphological operators, we can see that dilation and erosion are just max and min operations when a flat structuring element is used by the two operators. Serra also hinted about this relationship for 2-D hexagonally sampled signals between roots of the median and roots of the opening and closing [2]. Maragos did a quite extensive study of the relationships between order statistic filters and morphological filters [14, 49]. The results of his study include [14, 49]:

1) Any order-statistic filter can be exactly represented as a maximum of erosions, or as a minimum of dilations, both of which are given by a closed form not involving sortings.

2) Medians are bounded below by openings and above by closings.

3) A signal is a median root if and only if it is a root of both the opening and closing.

4) The open-closing and close-opening produce roots in a single pass.

A recent development in nonlinear filtering technique known as stack filters utilized the commutation of order statistic filters with thresholding [34]. This commutation is referred to as threshold decomposition [50]. It was mentioned in 2.1.2 that gray scale morphological operations also commute with thresholding. The development of the

stack filter has suggested a possible implementation of order statistic filtering techniques, that is, performing filtering on cross sections obtained by thresholding the signal at every gray level. Many of the results obtained for the stack filter may also be utilized in the study of morphological filters.

The close relationship between the order statistic filter and the morphological filter weaves the studies and applications of the two techniques together. In the following chapters, we will pursue the use of two techniques in order to improve the performance of the morphological filter.

CHAPTER 3

THE APPLICATION OF MATHEMATICAL MORPHOLOGY

IN AUTOMATIC INSPECTION OF FUEL INJECTION NOZZLES

3.1 Introduction

In this chapter, an application of mathematical morphology in image analysis is presented. It is a part of the ongoing atomization project in the Engineering Research Center of Purdue University. The goal of this project is to investigate the characteristics of the atomization process of fuel injectors. Previous work has shown that the spray process of the injector is affected by the nozzle geometry of the injector [51]. It is hoped that by incorporating information relative to the nozzle geometry will increase the understanding of the spray process of the injector.

We developed an inspection algorithm in which an image of the nozzle orifice is first captured, digitized, and analyzed using mathematical morphology. The fuel injector nozzle is located in the tip at one end of the fuel injector cup (see Figure 3.1). Fuel is pumped through a constellation of holes located in the nozzle. The shape of the cup as well as the location and size of the holes make it very hard to capture an image of the hole in the nozzle. Due to the small size of the nozzle, in the range of ten one thousandth of an inch, it is impossible to use mechanical means to accurately obtain a geometrical measurement of the nozzle. A microscope, therefore, has to be used to magnify the hole image. The magnification factor typically used in the study was 160. With a fixture built to hold and position the injector, light can be cast from the open end of the injector causing the hole to be lighted from the bottom as seen in Figure 3.1. Another technique is to directly light the cup from the top of the nozzle. We call the former back-lit and

the latter top-lit. The advantage of the back-lit approach is that the image is easier to process. However, the image of the hole can be distorted by metal chips that remain in the hole after it was drilled. The top-lit approach produces a hole image whose intensity distribution is not homogeneous. The lack of the homogeneity makes the processing task more difficult. The mounting fixture is placed under the microscope and a video camera is installed at the top of the microscope to capture the image. The output of the camera is digitized to 512x512 pixels. The image capture mechanism, a fuel injector cup, and back-lit and top-lit images are shown in Figure 3.1.

The analysis techniques using morphological operators will be presented in the following section along with the test results.

3.2 The Inspection Process

The inspection algorithm involves several stages including filtering, segmentation, binary image cleaning, area measurement, center location, and the discrepancy measurement. The output of the inspection algorithm can contain various parameters such as the effective area and the equivalent diameter of the hole under study. The discrepancy between the shapes of the real and ideal nozzles can also be obtained. A block diagram of the inspection algorithm is shown in Figure 3.2.

Filtering operations are first applied to the original image for image smoothing and feature enhancement. Different techniques were used for top-lit and back-lit images. The back-lit image usually consists of two main intensity values: the intensity value of the hole and the intensity value of the background. The hole generally has higher intensity values than the background. The goal of the filtering step for a back-lit image is to remove dubious spots within the hole image while keeping the original shape of the hole intact. A newly developed morphological filter which will be presented later in this thesis was used to smooth the back-lit image [52]. This filtering technique can
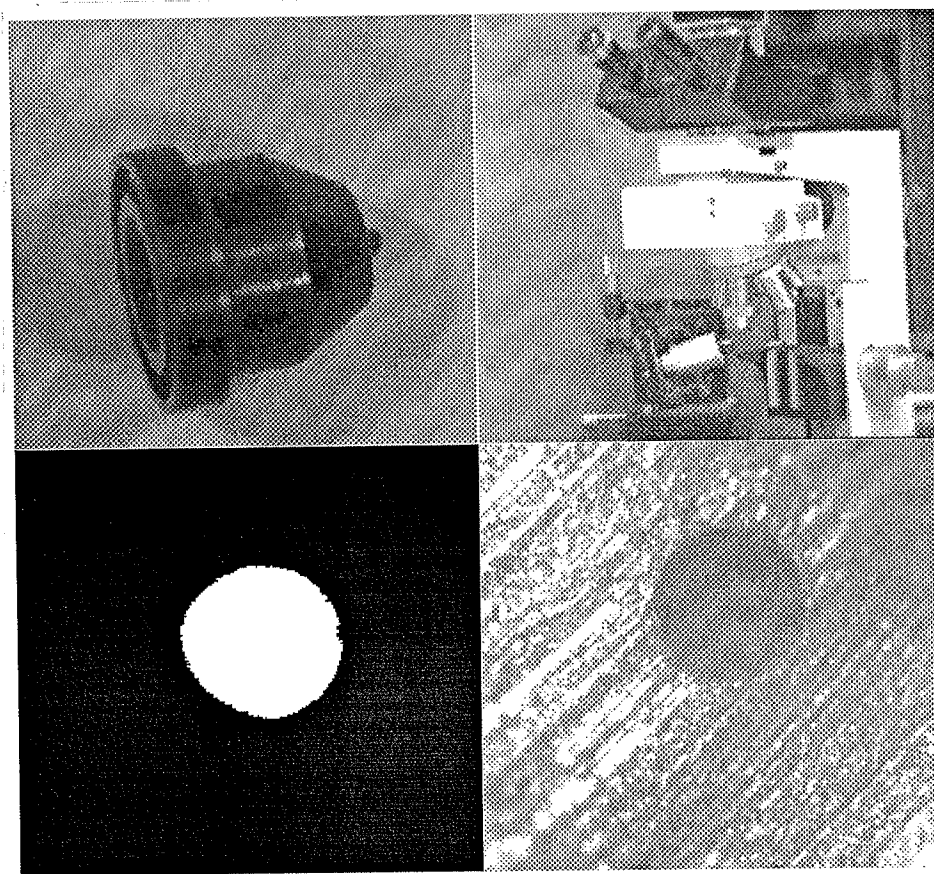
Figure 3.1. *Upper Left*: An injector cup; *Upper Right*: the fixture and microscope used for image acquisition; *Lower Left*: a back-lit hole image; *Lower Right*: a top-lit hole image.
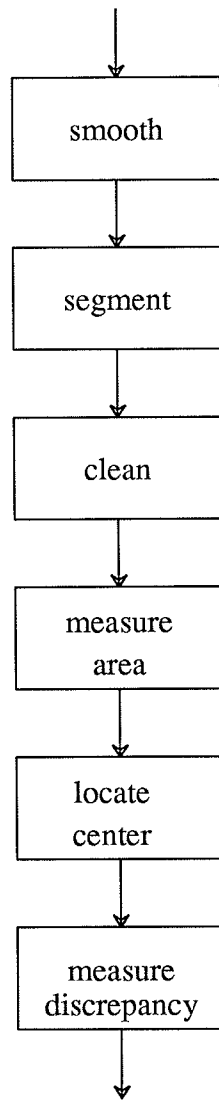
Figure 3.2. The block diagram of the inspection process.

effectively remove noisy spots and preserve the geometrical structure of the object shape in the image.

When the nozzle is top-lit, the image obtained is very different from the back-lit image. The hole of the top-lit image consists of a homogeneous region that has low intensity values. The background of the image has higher intensity values, but is very noisy due to the roughness of the magnified metal surface. The background consists of some regions that have stripe shapes of low intensity values close to the intensity values of the hole. Some of these stripe regions are also connected to the hole. Thresholding the image relative to the intensity values of the hole would definitely result in a distorted hole shape and a very noisy background. The purpose of the filtering step applied to the top-lit image is to suppress these stripes while preserving the shape of the hole. The filtering operation uses a closing operator with a round structuring element whose diameter is smaller than the size of the hole but greater than the width of low intensity stripes in the background. The purpose of such a selection of a structuring element is to remove dark stripes and retain the homogeneous hole region. The output image then contains a dark hole region with background having higher intensity values whose distribution is more homogeneous.

The next step is to extract the hole region from the image. As mentioned above, the back-lit image mainly consists of two groups of intensity values, and consequently has a bimodal gray scale histogram: one of the peak values in the histogram corresponds to the low intensity values of the background and and another one to the high intensity values of the hole. The thresholding segmentation technique developed in [53] was used in the segmentation process. In this technique, a median filter is first applied to the histogram and then the threshold selection algorithm in [42] is used in the thresholding process. The histogram of the filtered top-lit image does not have a well -defined bimodal shape. However, since the hole image consists of a region darker than the background after filtering, the first peak from the left in the histogram should be

formed by pixels within the hole. The threshold is then selected at the bottom, adjacent to the right side of the the first peak of the histogram.

In many cases, the thresholded binary image also contains some noisy spots. In order to obtain an image consisting of only the hole, a binary closing operator is applied to clean the image using a structuring element whose size is larger than the black spots scattered in the background.

Using the processed binary hole image, measurements of the outlet effective area, equivalent diameter, and circularity can be performed. The effective area can be obtained by counting the number of pixels contained in the hole image. The equivalent diameter is then obtained

The hole circularity measurement is based on the comparison between an ideal hole shape, a disk in this case, and the actual hole shape. One way to conduct the proper comparison is to find the best fit of the ideal hole shape with the actual hole image. There are a number of ways to find the best fit. In this project, our effort is focused on locating the center of the ideal hole shape that best fits the actual hole image. Again, a morphological operator is used for locating the center. A binary erosion operator is applied to the binary image using a structuring element consisting of the standard hole shape. In order to reduce the computation, the boundary of the disk is used as the structuring element. The boundary shall be referred to as the ring in the following discussion. The location of the center is chosen as the center of the largest ring inscribed in the hole image. The search for such a ring starts by using a ring the size of the expected diameter of the hole as the structuring element. If the output of the erosion operator is empty, the erosion operation is repeated using a ring of smaller size. The search continues in this manner until the output of the erosion is not empty. The center of the inscribed ring is then determined. Note that in this case the nonempty output of an erosion operator does not necessarily contain just a single center point due to the

irregularity of the actual hole shape. When multiple center points are obtained, the median point is selected as the center of the inscribed ring.

Based on the located center, the best fit disk is found when the "discrepancy" between the imaged hole and the standard disk is minimum. The discrepancy is defined as the total area of the nonoverlapped regions of the original hole image and the ideal hole. The regions can be extracted by using the exclusive OR operation on the two images.

An example of the entire process is shown in Figures 3.3. The original top-lit image is shown in Figure 3.3(a). Segments of the processed images containing the hole are shown in Figure 3.3(b).

This geometrical inspection technique shows that utilization of morphological operations in image analysis is effective in terms of the implementation and performance.
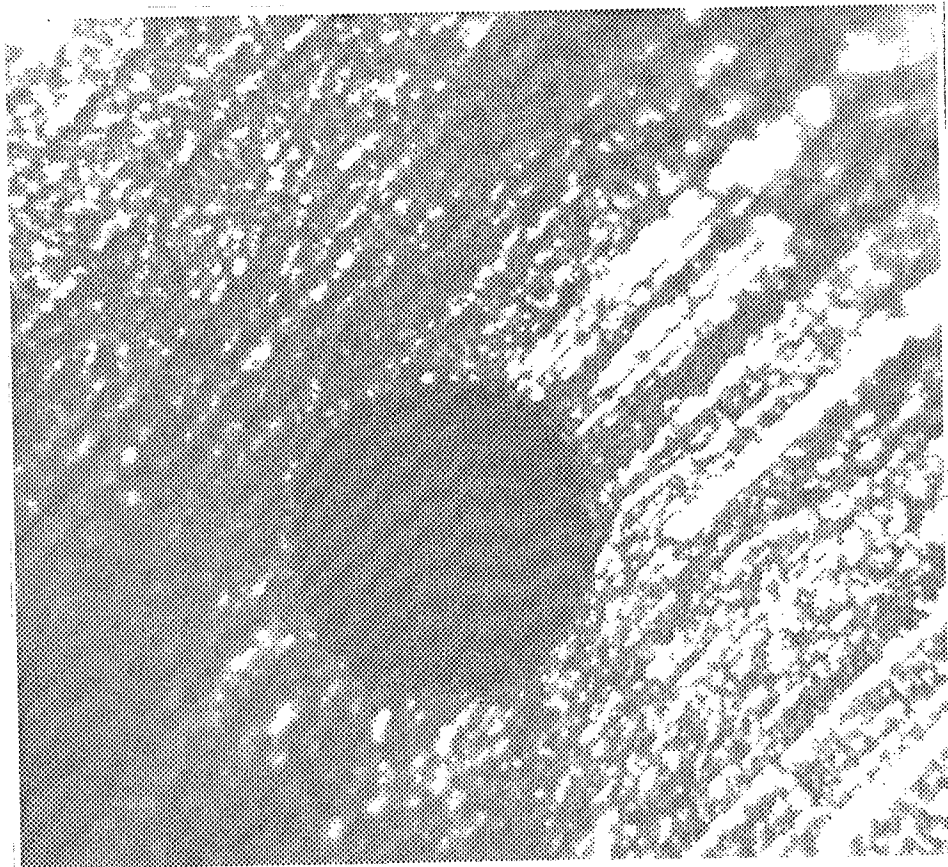
Figure 3.3 (a) The original top-lit hole image.
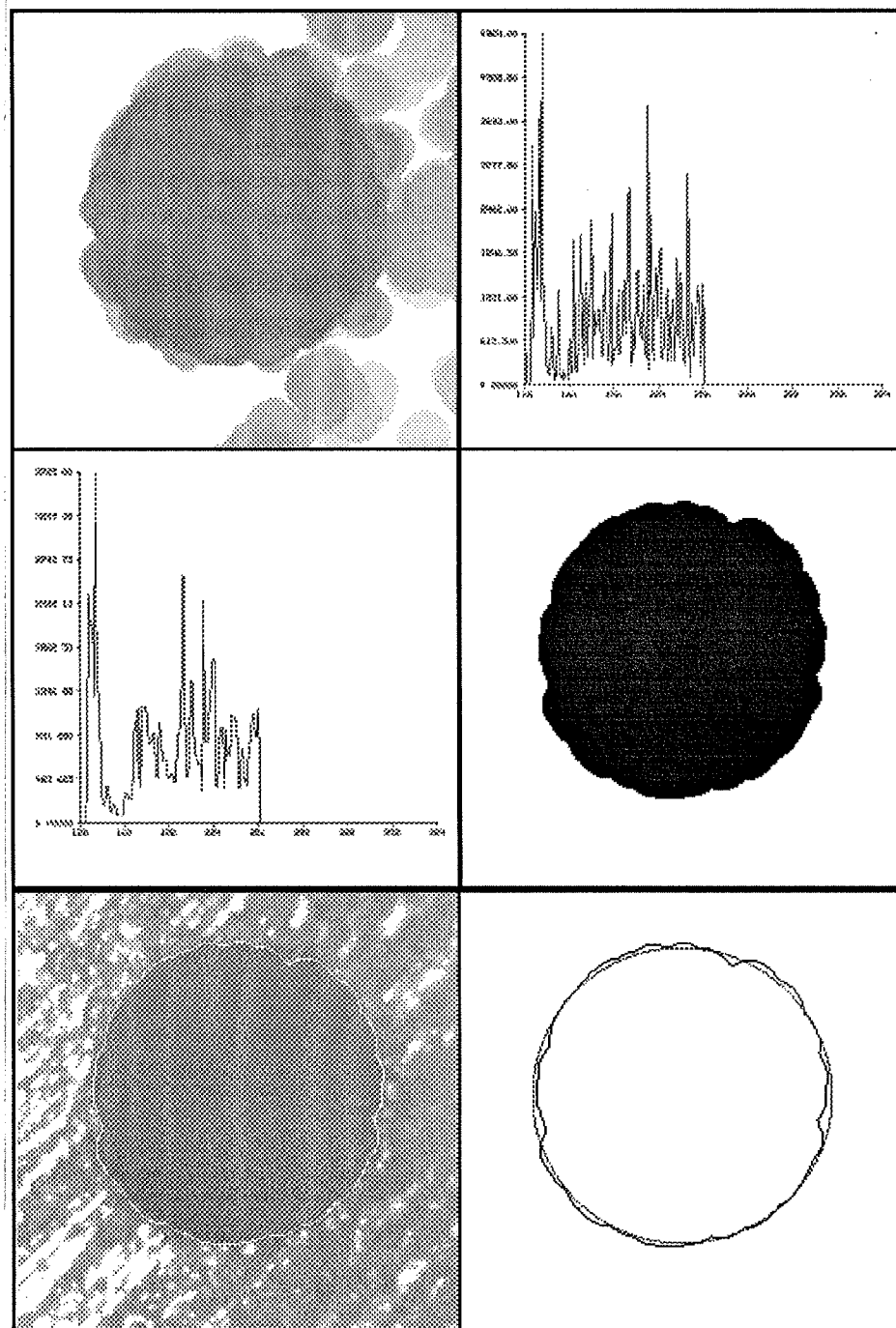
Figure 3.3 (continued) (b) *Upper Left*: the filtered top-lit image; *Upper Right*: the histogram of the filtered image; *Middle Left*: the histogram after the median filtering; *Middle Right*: the segmented image; *Bottom Left*: the overlap of the hole boundary in the segmented image and the hole in the original image; *Bottom Right*: the overlap of the segmented hole boundary and the ideal hole shape.

CHAPTER 4

THE GENERALIZED MORPHOLOGICAL FILTER

4.1 Introduction

Image enhancement is usually an initial step for further image analysis such as image segmentation, motion analysis, etc. Geometrical structures in an image play very important roles in these processes. For an example, one approach in motion analysis is to first extract geometrical features and then compute the velocity field of these features. Therefore, the performance of a filtering algorithm for image enhancement is judged not only by noise suppression effectiveness, but by the ability to preserve geometrical structure. It is always difficult for a filtering algorithm to meet both criteria. Many filtering algorithms used for noisy images assume homogeneity or stationarity. However, for real images, the homogeneity assumption only holds for small regions. Therefore, some filters always produce blurring effects, and consequently their performance is degraded despite their strong noise smoothing properties. Rank order filtering is one of the popular nonlinear filtering techniques that has been widely recognized to be capable of preserving geometrical features. The type of noise a rank order filter can effectively suppress is impulsive noise. For nonimpulsive noise, the performance of a rank order filter can be quite disappointing [44, 54].

Several approaches have been proposed so that the two above criteria can be properly balanced. Two techniques are often seen being used in the development of filtering algorithms to improve their performance. In order to improve geometrical structure preservation, multiple model approaches have been proposed to deal with the difficulty posed by inhomogeneity of real images. The basic idea of this approach is to

incorporate information for multiple geometrical features into the filtering algorithm. Multiple filters of the same type are usually used in this approach. They are applied to the input image in parallel and each of them is "sensitive" to one type of structure in the image. The outputs of the multiple filters are then processed according to a predefined criteria to better preserve geometrical structures. One of the criteria used is to select the output which best matches one of the geometrical structures. A typical example is the Multiple Model Kalman Filter [55, 56]. Five filters were used, one for the isotropic area, and four for edges. Five Kalman filters using the five models, respectively, were applied to the input image in parallel. The output of the Multiple Model Kalman Filter is selected from the outputs of five Kalman filters based on their *a priori* error variances [55]. Another example of the multiple model approach is the FIR-median hybrid filter [57]. In this filter, FIR filters were applied to the pixels located in several geometrical structures. The final result was selected as the median of the multiple outputs of the FIR filters. It is obvious that the improvement in geometrical feature preservation reported for the above two examples is obtained at the expense of increased complexity.

Another approach for performance improvement is the combination of linear and nonlinear operations. This approach is based on the desire to utilize the geometrical feature preservation capability of nonlinear filtering and the noise suppression capability of a linear filter. Although the above two examples can also be thought of as an application of this approach, another filter can be better used to illustrate the idea behind this approach. The example is the combination of ranking and linear operations, known as the order statistic filter (OSF) [44]. Another name for this filter is the L filter [58]. Rank order filtering has been recognized as being effective for a large number of applications [43, 59]. A special case of the rank order filter, the median filter has been shown to preserve geometrical structures such as edges or monotonic changes, while eliminating impulsive noise [46]. However, it has been noted that the performance of the median filter in suppressing nonimpulsive noise is not satisfactory [54]. A linear filter, on the

other hand, provides strong nonimpulsive noise suppression over a homogeneous region, but also introduces a smearing effect over areas with discontinuities. The OSF was introduced in order to make use of the merits of the rank order filter and the linear filter. The OSF can be formulated as the following. An input sequence $\{x_i, i = 1,2,,...,n\}$ is ordered as $\{x_i\} = \{x_{(1)}, x_{(2)}, \ldots, x_{(n)}\}$, such that $x_{(1)} \leq x_{(2)} \leq, \ldots, \leq x_{(n)}$. The output of the OSF is then the linear combination of the ordered samples, that is,

$$y = \sum_{i=1}^{n} \alpha_i x_{(i)}.$$

where the α_i's are real valued coefficients constrained by $\sum_{i=1}^{n} \alpha_i = 1$. By varying the values of the coefficients, many version of the OSF can be obtained. For example, the averaging filter, median filter, trimmed mean filter, etc., are all special cases of the OSF [44]. The optimal coefficients can also be derived based on the minimization of mean squared error [44].

As mentioned in Chapter 2, a simple morphological filter using a single structuring element is not suitable in many applications for suppressing noise. The Generalized Morphological Filter (GMF) introduced in the following section is developed to improve the performance of morphological filters. The two approaches mentioned above for performance improvement are used in the development. The multiple model idea is reflected by the use of multiple structuring elements in the GMF which represent different geometrical structures. The idea of combining linear and nonlinear operations is realized in the linear combination part of the GMF.

4.2. The Generalized Morphological Filter (GMF)

4.2.1 The Structure of the GMF

The Generalized Morphological Filter consists of a cascade of two stages. Each of the stages uses one type of morphological operator: either an opening or a closing [52].

The stage using closing operators is known as the CL stage and the stage using opening operators is known as the OL stage. Multiple structuring elements are used in each stage. The output of each stage is the linear combination of the ordered outputs of the multiple morphological operators. Figure 4.1 shows the structure of one configuration of the GMF.

In the CL stage, multiple closing operators using different structuring elements are applied to the input image in parallel. The output of the stage is the linear combination of the ordered outputs of the multiple closing operators. The operation of the CL stage, shown in Figure 4.2, can be formulated by the following. For an input image f and multiple structuring elements $\{k_1, k_2, \cdots, k_N\}$, the output of the stage is expressed as

$$y = \sum_{i=1}^{N} \alpha_i y_{(i)} , \qquad (4.2.1)$$

where $y_{(i)}$ are the ordered outputs of $f \bullet k_i$. The output sequence is ordered by $y_{(1)} \leq y_{(2)} \leq, \ldots, \leq y_{(N)}$. The α_i are real valued constants with the constraint that $\sum_{i=1}^{N} \alpha_i = 1$. The constraint is set in order not to introduce a brightness bias. The values of coefficients are determined by the application.

The OL stage, shown in Figure 4.3, can be formulated by the following. For an input image f and multiple structuring elements $\{k_1, k_2, \cdots, k_N\}$, the output of the stage is

$$y = \sum_{i=1}^{N} \beta_i y_{(i)} , \qquad (4.2.2)$$

where $y_{(i)}$ are the ordered outputs of $f \circ k_i$. The output sequence is ordered by $y_{(1)} \leq y_{(2)} \leq, \ldots, \leq y_{(N)}$. The β_i are also real valued constants with $\sum_{i=1}^{N} \beta_i = 1$.

With the above two stages, the GMF can be implemented in various ways. Figure 4.1 shows one implementation of the GMF. The order of the OL and CL stages in the
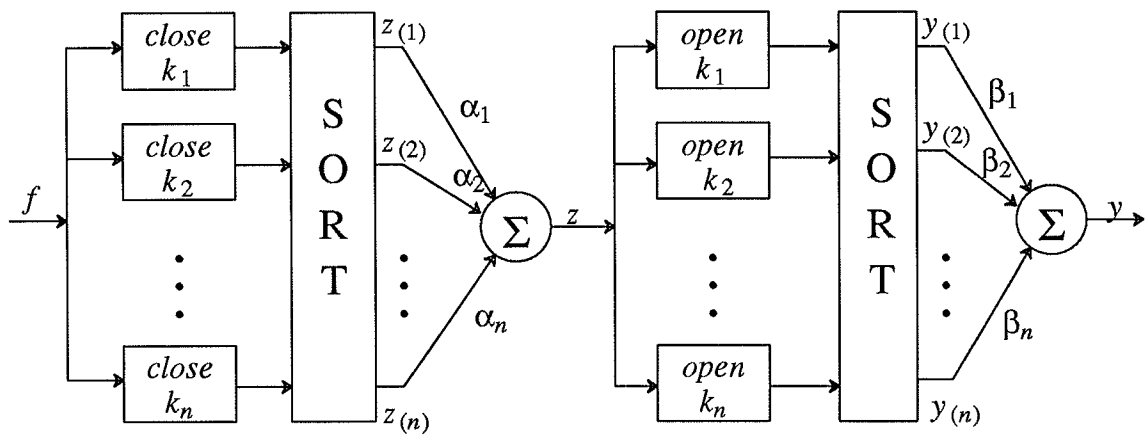
Figure 4.1.   One implementation of the Generalized Morphological Filter.
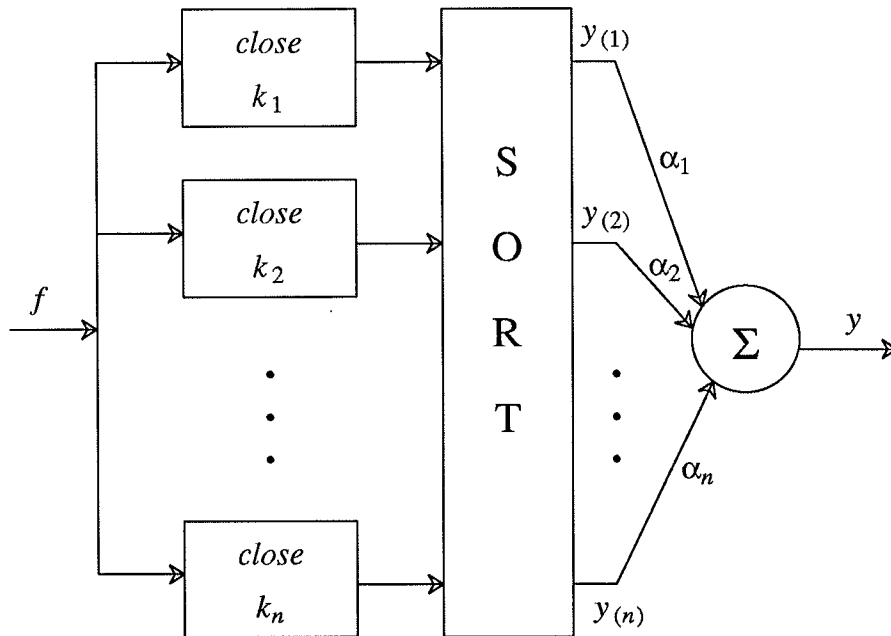
Figure 4.2.   The CL stage.
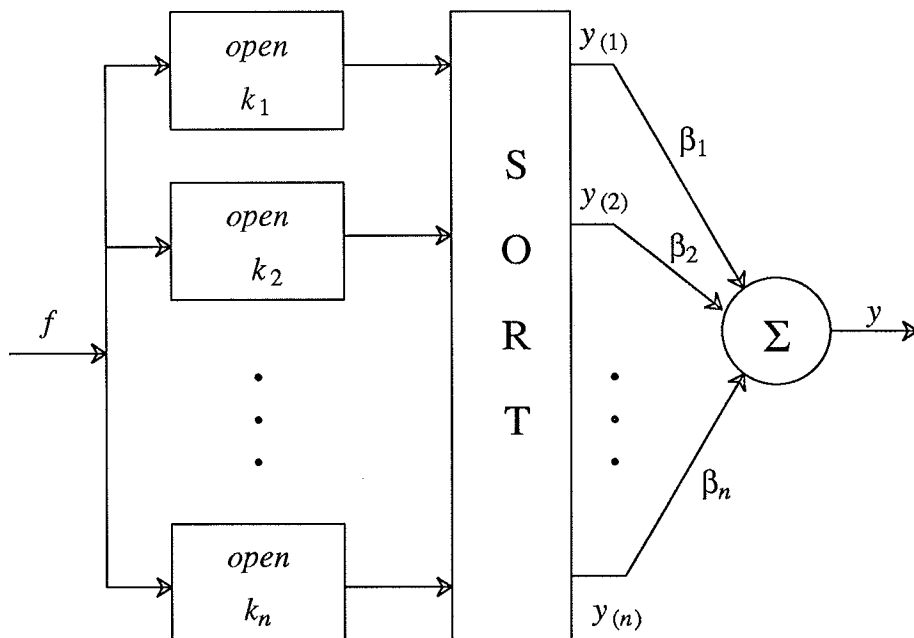
Figure 4.3.   The OL stage.

cascade can be altered to obtain other versions of the GMF. The GMF is described by the selection of the α's, β's, N, the set of structuring elements, and the order of the OL and CL stages.

4.2.2. Some Properties of the GMF

The followings are some interesting properties of the GMF. Some of them will be used in latter chapters.

Property 1.

The operation of the OL stage is antiextensive and the operation of the CL stage is extensive. That is, for an image f, we have (see Figure 4.1):

$$\sum_{i=1}^{N} \beta_i y_{(i)} \leq f \leq \sum_{i=1}^{N} \alpha_i z_{(i)}, \qquad (4.2.3)$$

where $y_{(i)}$ are the ordered outputs of $f \circ k_i$ and $z_{(i)}$ are the ordered outputs of $f \bullet k_i$.

The above properties can be easily proved by using the antiextensiveness and extensiveness properties of single opening and closing operators.

Proof: We first prove the antiextensive property of the OL stage. Let $f(p, q)$ be the gray level value of the pixel at location (p, q). Then when the GMF is applied to the pixel at location (p, q), from the antiextensive property of the opening operator (2.1.19), we have

$$y_i(p, q) \leq f(p, q) \quad \text{for} \quad i=1,2,\ldots,N.$$

Then, it is obvious that

$$\sum_{i=1}^{N} \beta_i y_{(i)} \leq \sum_{i=1}^{N} \beta_i f(p, q) = f(p, q) \sum_{i=1}^{N} \beta_i = f(p, q).$$

The last equality holds because the sum of the β_i's is one.

The extensive property of the CL stage can be similarly shown.

Because of their nonlinearity, the superposition property does not hold for morphological operations. However, when a morphological operator is applied to a sum of a signal and a constant, the output of the operator is equal to the sum of the outputs of the operator applied to the signal and the constant, respectively. The next property can be considered as the weak superposition property of the GMF.

Property 2.

Let $f = g + c$ where g is an image and c is a constant. Then for the OL and CL stages, we have:

$$y = \sum_{i=1}^{N} \beta_i \, y_{(i)} + c \quad \text{and} \quad z = \sum_{i=1}^{N} \alpha_i \, z_{(i)} + c, \tag{4.2.4}$$

where $y_{(i)}$ are the ordered outputs of $g \circ k_i$ and $z_{(i)}$ are the ordered outputs of $g \bullet k_i$.

Property 2 can be easily proved using the corresponding weak linearity property of a single morphological operator.

Proof: Consider the OL stage. Using (2.1.26) and noting that the constant c does not affect the ordering process, we obtain

$$y = \sum_{i=1}^{N} \beta_i \, (y_{(i)} + c) = \sum_{i=1}^{N} \beta_i \, y_{(i)} + c.$$

From Property 1, it can be seen that the GMF with different ordering of the morphological stages will produce different results. The output of the filter with a CL stage followed by an OL stage is always "brighter". This phenomenon, known as the bias effect, can be reduced by averaging the outputs of two filters as shown in Figure 4.4.

4.2.3. Variations of the GMF

As mentioned above, the values of the coefficients in the linear combination part of the filter are specified by the application. For example, if the image is corrupted with impulsive noise, we can obtain the max/min version of the GMF by specifying the coefficients by the following [30]:

$$\alpha_i = \begin{cases} 1, & i = 1, \\ 0, & otherwise; \end{cases} \quad and \quad \beta_i = \begin{cases} 1, & i = N, \\ 0, & otherwise. \end{cases} \tag{4.2.5}$$

It is more illustrative to formulate the operations of this version of the GMF using max and min operators. For the CL stage, the output is the minimum of the outputs of the closing operators, that is,

$$y = \min \{f \bullet k_1, f \bullet k_2, \ldots, f \bullet k_N \}. \tag{4.2.6}$$

The output of the OL stage is the maximum of the opening operators, that is,

$$y = \max \{f \circ k_1, f \circ k_2, \ldots, f \circ k_N \}. \tag{4.2.7}$$

Figure 4.5 illustrates the block diagram of this version. The purpose of such an arrangement of the GMF is to preserve any geometrical structure that matches at least one of the structuring elements. The max/min version of the GMF also has a binary counterpart. The equivalent binary expressions for the CL and OL stages of the max/min version of the GMF are:

$$Y = \bigcap_{i=0}^{N} F \bullet K_i; \quad and \quad Y = \bigcup_{i=0}^{N} F \circ K_i; \tag{4.2.8}$$

where Y and F are binary images and K_i are binary structuring elements. The max/min version of the GMF is also known as the 2D CO morphological filter [30]. Lay used the same concept in designing an algorithm to recognize anerisms in angiographs [60]. The max/min version has some interesting properties which are presented in the following chapter. Figure 4.6 shows an example of applying Equation 4.2.8 to a binary image
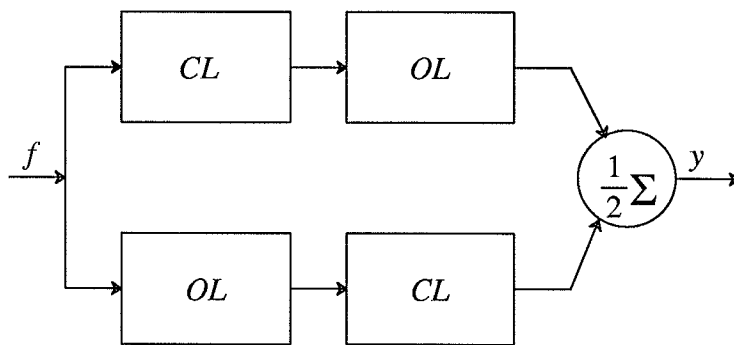
Figure 4.4.   Block diagram of one configuration of the GMF to reduce the bias effect.
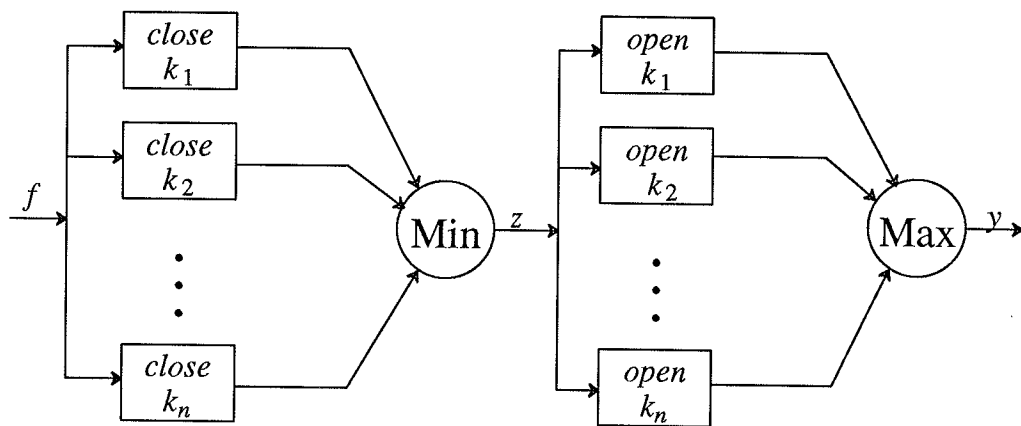
Figure 4.5.   Block diagram of the max/min version of the GMF.

using the four line structuring elements shown in Figure 4.7. An original binary image and a noisy version corrupted by impulsive noise are shown in Figure 4.6. Results of the max/min version of the GMF and the traditional morphological filter applied to the noisy image are also shown in Figure 4.6. A 3x3 square structuring element shown in Figure 4.7 is used by the traditional morphological filter. Comparing the output of the GMF with the traditional morphological filter, the GMF has superiorer geometrical structure preservation and noise suppression capability.

For an image corrupted by nonimpulsive noise, an averaging version of the GMF can be used. The averaging version of the filter is obtained by assigning the same value to all the coefficients [52]. The averaging versions of the OL and CL stages can be expressed, respectively, as:

$$y = \frac{1}{N} \sum_{i=1}^{N} f \bullet k_i; \quad \text{and} \quad y = \frac{1}{N} \sum_{i=1}^{N} f \circ k_i. \qquad (4.2.9)$$

Figure 4.8 illustrates one implementation of the averaging version of the GMF. Figure 4.9 shows an example of applying the averaging version of the GMF to an image corrupted by Gaussian noise. Four structuring elements shown in Figure 4.7 are used. In order to make a comparison, the result of the traditional morphological filter using a 3x3 square structuring element is also shown in Figure 4.9. Again, we can observe the significant improvement obtained by the GMF.

Later, we will derive an optimal design for the GMF using a set of special structuring elements.

4.3. Discussion of the Performance of the GMF

In order to achieve a better understanding of the GMF and provide some guidance in the design of the structuring elements, several aspects relevant to the performance of the filter are discussed in this section.
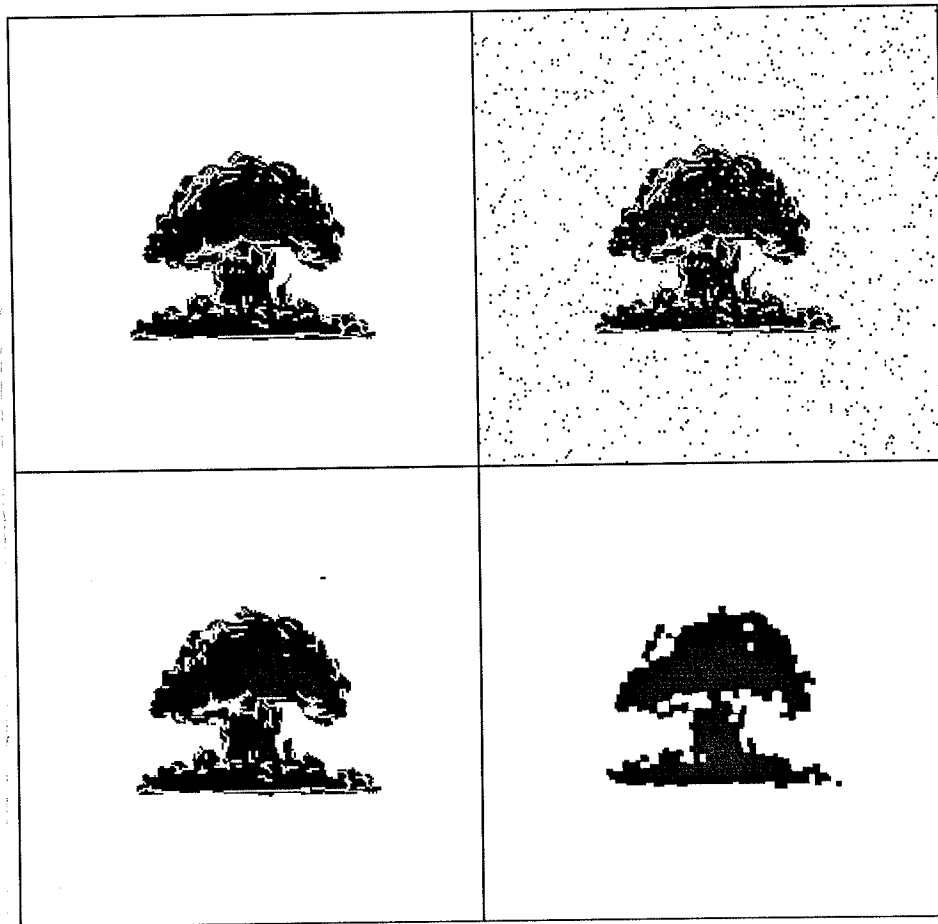
Figure 4.6. *Upper Left*: Original binary image; *Upper Right*: Impulsive noise corrupted image; *Bottom Left*: Output of the max/min version of the GMF using the structuring elements, k_i, i=1,...,4, shown in Figure 4.7; *Bottom Right*: Output of a traditional morphological filter using a single 3x3 square structuring element, k, shown in Figure 4.7.

k_1 $\quad$ k_2 $\quad$ k_3 $\quad$ k_4

k
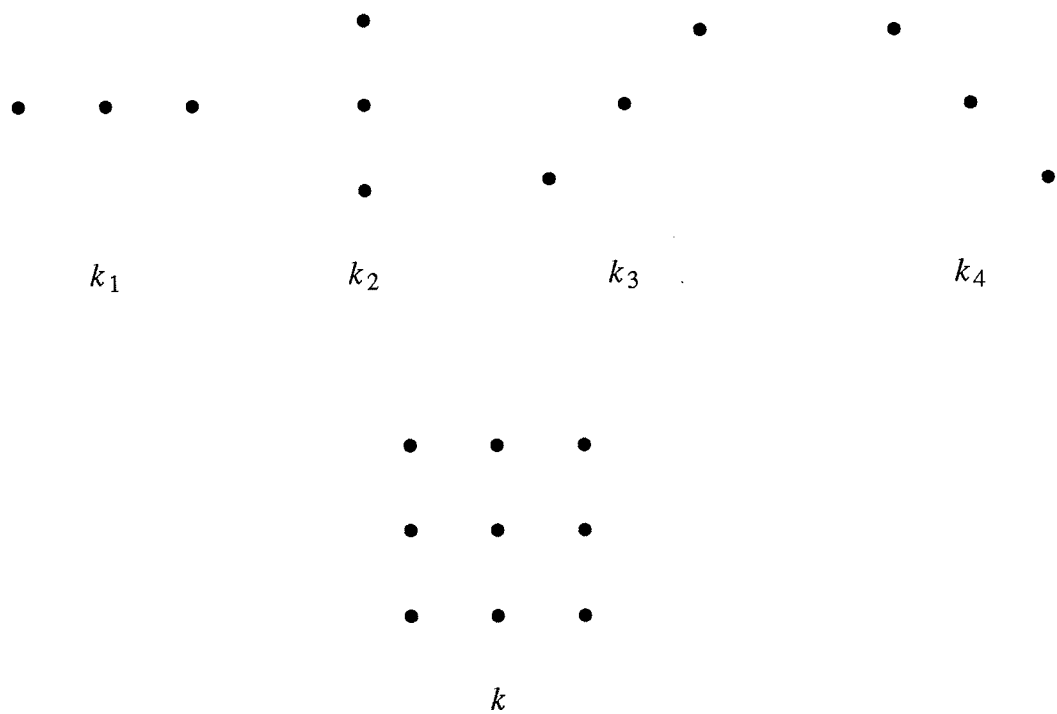
Figure 4.7.   Illustration of the structuring elements used to process the images in Figure 4.6.
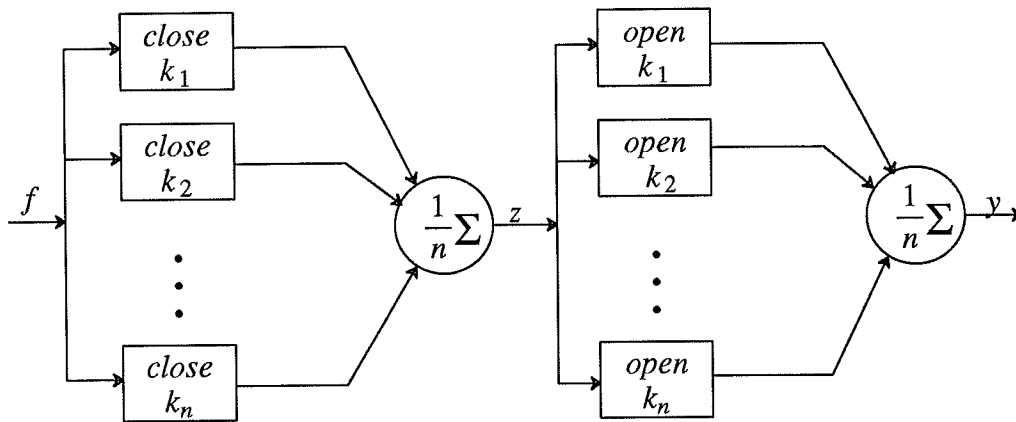
Figure 4.8. Block diagram of the averaging version of the GMF.
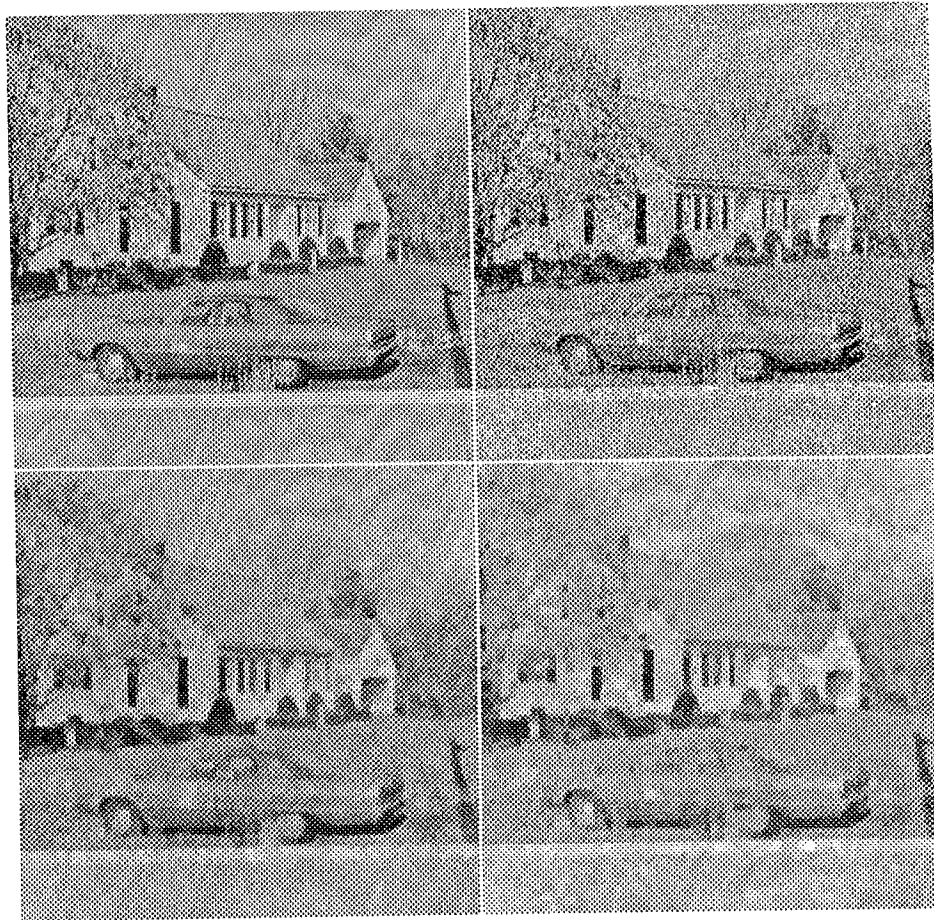
Figure 4.9. *Upper Left*: Original image; *Upper Right*: Gaussian noise corrupted image; *Bottom Left*: Output of the averaging version of the GMF using the structuring elements shown in Figure 4.7; *Bottom Right*: Output of a traditional morphological filter using a single 3x3 square structuring element shown in Figure 4.7.

4.3.1. Geometrical Structure Preservation of the GMF

As we discussed before, geometrical structure preservation is one of the most important criteria in the performance of a filter used in image enhancement. Several techniques proposed to improve the performance of filters used in image enhancement have been discussed in previous chapters. Efforts have also been made to use adaptive approaches in filtering algorithms to detect the presence or absence of edges in an image [54, 61]. The result of the edge detection determines the regions where the smoothing operation is performed. There are several schemes used in this approach. One scheme is to use a filter with strong geometrical preservation ability, such as a median filter, at pixels near edges, otherwise a filter with effective noise suppression, such as an averaging operation, is used at pixels in the homogeneous regions [54]. Another scheme is to select the pixels so that the smoothing operation will only be applied to pixels that belong to the same homogeneous region [62]. While the adaptive approaches result in a reduced smearing effect, they also increase computational complexity .

The above adaptation process inherently exists in the GMF. This feature of the GMF is due to the edge preservation nature of closing and opening operations. When a closing or opening operator is applied to an edge pixel location, the output of the operator will be on the same side of the edge pixel location if the region on that side contains the same geometrical structure as the structuring element. When the GMF is applied to an edge pixel location, the multiple morphological operators always produce outputs that are on the same side of the pixel location, provided that the region consists of geometrical structures represented by the structuring elements. Therefore, the GMF applied to an image that consists of homogeneous regions separated by intensity transitions has a reduced smearing effect since the linear operations in the GMF will be performed on pixels on the same side of an edge.

We know that the max/min version of the GMF has very strong geometrical feature preservation capability since any geometrical structure in the image that matches any one of the structuring elements will be preserved [30]. However, if the noise is nonimpulsive and linear operation has to be used for noise suppression, this strong preservation ability can be weakened. The condition mentioned above indicates that the smearing effect can be greatly reduced if the regions on both sides of an edge are compositions of the geometrical structures represented by the structuring elements. This smearing effect reduction does not apply to fine geometrical structures whose regions are too small to be decomposed into the structuring elements. Using structuring elements of small spatial support can alleviate this problem.

4.3.2 Noise Suppression Capability of the GMF

One attractive feature of the GMF is that it can be used to smooth noisy images corrupted by various types of noise. For example, impulsive noise can be effectively suppressed using the max/min version of the GMF and nonimpulsive noise can be suppressed using the averaging version of the GMF.

One problem in image enhancement is the existence of outliers which arise from heavy tailed noise distributions or are simply bad data points in the image acquisition process. In order to reduce the bias effect caused by the outliers, robust approaches have been developed to modify existing filtering algorithms so that outliers have much less influence. Another requirement is that the filter should be able to produce reasonably good results even when the outliers do not exist [63].

The above two concepts for robust filtering are well met by the GMF due to the use of morphological operators. In view of the fact that morphological operators, such opening and closing, eliminate outliers whose structures do not match the structuring elements, the multiple morphological operators in each stage of the GMF produce relatively outlier-free outputs and hence the linear operations will have reduced influence

from the outliers. Figure 4.10 shows two noisy images: one contaminated by composite of Gaussian noise and impulsive noise and one contaminated only by the same Gaussian noise. The results in the figure show that the performance of the averaging version of the GMF is not visibly degraded by the presence of impulsive noise.

The noise suppression ability of the Generalized Morphological Filter can also be evaluated by examining the noise variance reduction. This examination is based on the concept that a smoothing filter must reduce the variance of the input noise [64]. This was shown in Chapter 2 to be true for simple morphological operations. The variance reduction ability was examined by using an averaging version of the GMF with a set of test data generated by contaminating a constant gray level area with Gaussian noise of zero mean and various variances. The gray level value of the constant area was 125. The values of the noise standard deviation σ ranged from 10 to 100. The structuring elements shown in Figure 4.7 are used in this examination. The sample mean and variance of the output of the filter for each test were obtained using the following:

$$\mu = \frac{1}{M^2} \sum_{i=1}^{M} \sum_{j=1}^{M} y(i,j), \tag{4.3.1}$$

and

$$\sigma^2 = \frac{1}{M^2} \sum_{i=1}^{M} \sum_{j=1}^{M} (y(i,j) - \mu)^2. \tag{4.3.2}$$

where μ is the sample mean, σ^2 is the sample variance. M^2 is the total number of pixels in the image. The gray value at pixel location (i,j) of the smoothed image is denoted by $y(i,j)$. For the sake of comparison, averaging and median filters were also applied to the test data and the corresponding measurements were obtained. A 3x3 window was used for both the averaging and median filters. A plot the input standard deviation vs the standard deviation of the output of the GMF is shown in Figure 4.11. From the plot we can see that the averaging version of the GMF has better variance reduction capability when
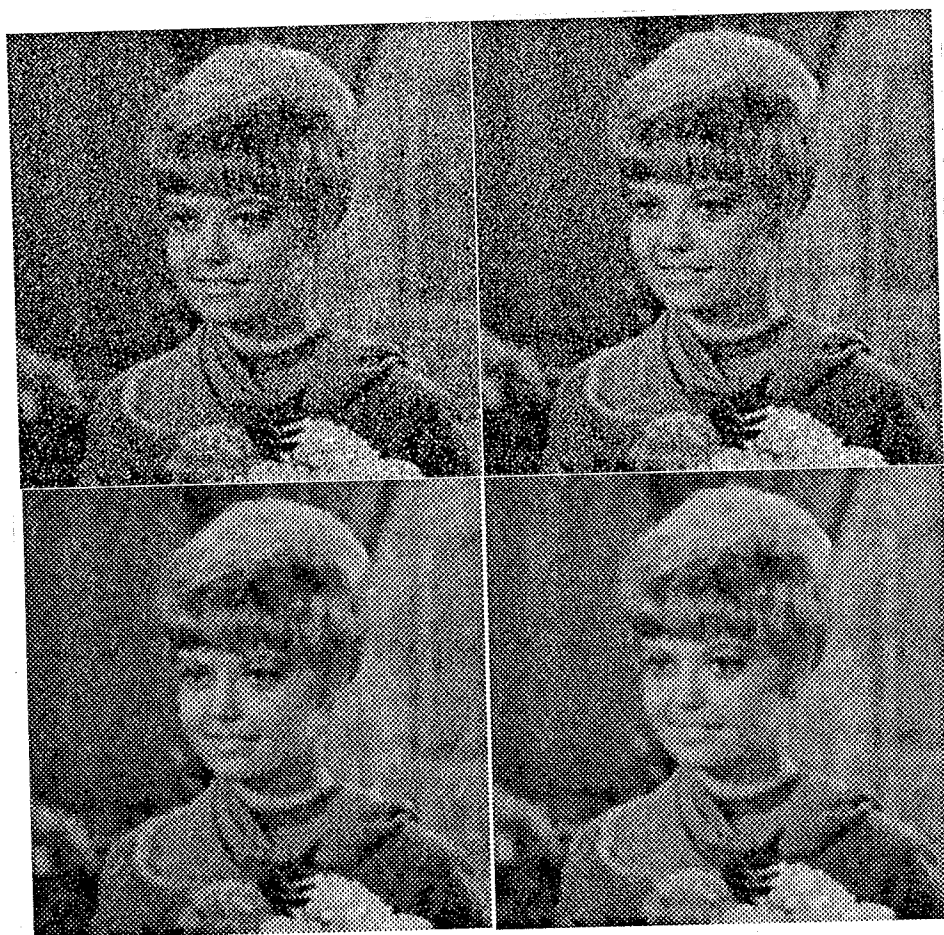
Figure 4.10.*Upper Left*: Noisy image contaminated by a composite of Gaussian noise and impulsive noise; *Upper Right*: Noisy image contaminated only by Gaussian noise; *Bottom Left*: Result of the averaging version of the GMF applied to the upper left image; *Bottom Right*: Result of the averaging version of the GMF applied to the upper right image.
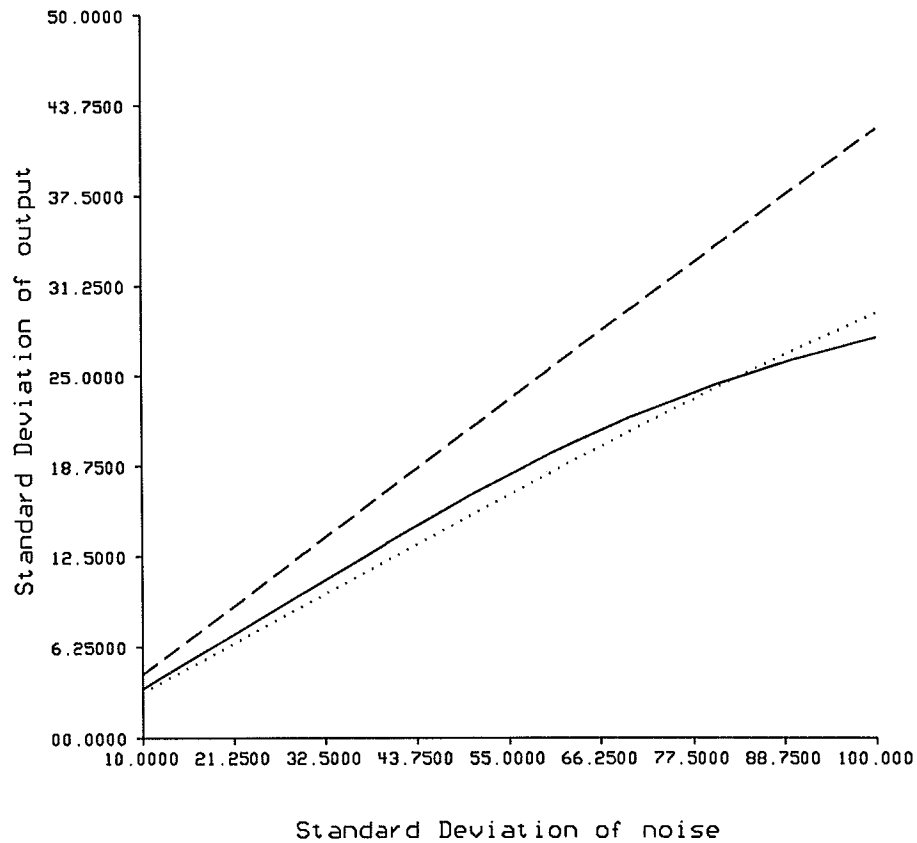
Figure 4.11.The standard deviation of the output of the GMF vs the standard deviation of the input. The dotted line represents the output of the GMF, the dashed line represents the output of the median filter, and the solid line represents the output of the mean filter.

the input standard derivation ranges from 10 to 80. However, the GMF performed poorer when the input variance is large. The intuitive reason for this is that when the input noise variance becomes large, some false geometrical structures are created and they may match some of the structuring elements in the GMF.

In order to examine both noise smoothing and feature preservation, another set of test images were generated. The original noise-free image consists of rings with various widths, ranging from 1 to 10 pixels. The same type of noise was used to contaminate the rings image. In this test, instead of estimating the sample variance, the mean squared error was estimated between the original image and the output of the GMF:

$$d_2 = \frac{1}{M^2} \sum_{i=1}^{M} \sum_{j=1}^{M} (g(i,j) - y(i,j))^2. \tag{4.3.3}$$

where $g(i,j)$ is the gray level value at pixel location (i,j) in the original noise-free image, and $y(i,j)$ is the gray level value at pixel location (i,j) in the smoothed image. A plot of the mean square error vs. the input noise standard deviation is shown in Figure 4.12. The plot shows that the GMF has better performance than the other two filters. The output image has visually sharper edges and better smoothing in the rings and the background. The limit of the geometrical feature preservation of the GMF is shown in the smoothed image, that is, the rings of small widths were smeared by the filter. The images in Figure 4.13 consists of the original noise-free image, one noisy image with noise variance 50 and the corresponding outputs of the filters.

A final test was performed using the filters on a set of noisy images whose original noise-free image is shown in Figure 4.14. The image was corrupted using the same types of noise as above. The mean squared error was also used to evaluate the performance of the GMF. Figure 4.15 shows a plot of the mean squared error vs the input noise standard deviation. Once again, the plot shows that the GMF achieved better performance.
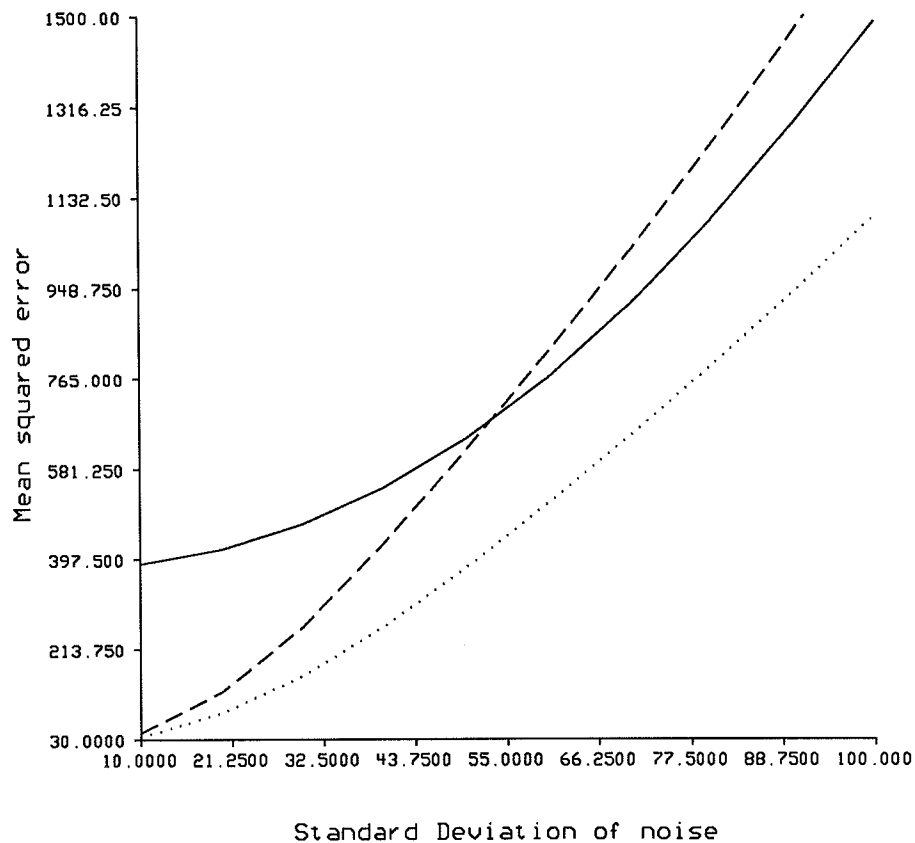
Figure 4.12. The mean squared error vs the standard deviation of the input noise for the rings image. The dotted line represents the output of the GMF, the dashed line represents the output of the median filter and the solid line represents the output of the mean filter.
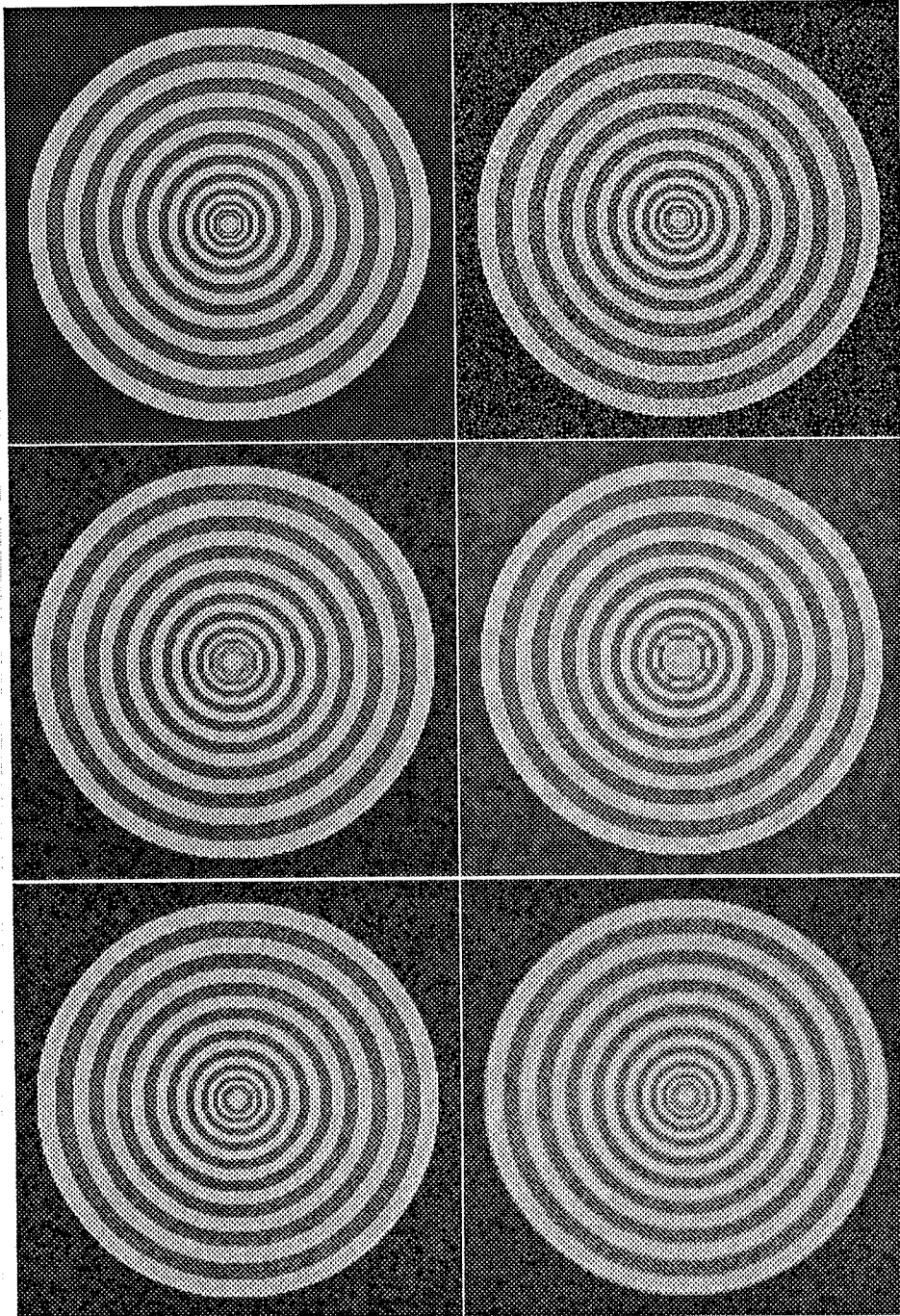
Figure 4.13.*Upper Left*: Original ring image; *Upper Right*: Noisy image; *Middle Left*: Output of the GMF; *Middle Right*: Output of a traditional morphological filter using a single structuring element; *Bottom Left*: Output of the median filter; *Bottom Right*: Output of the averaging filter.
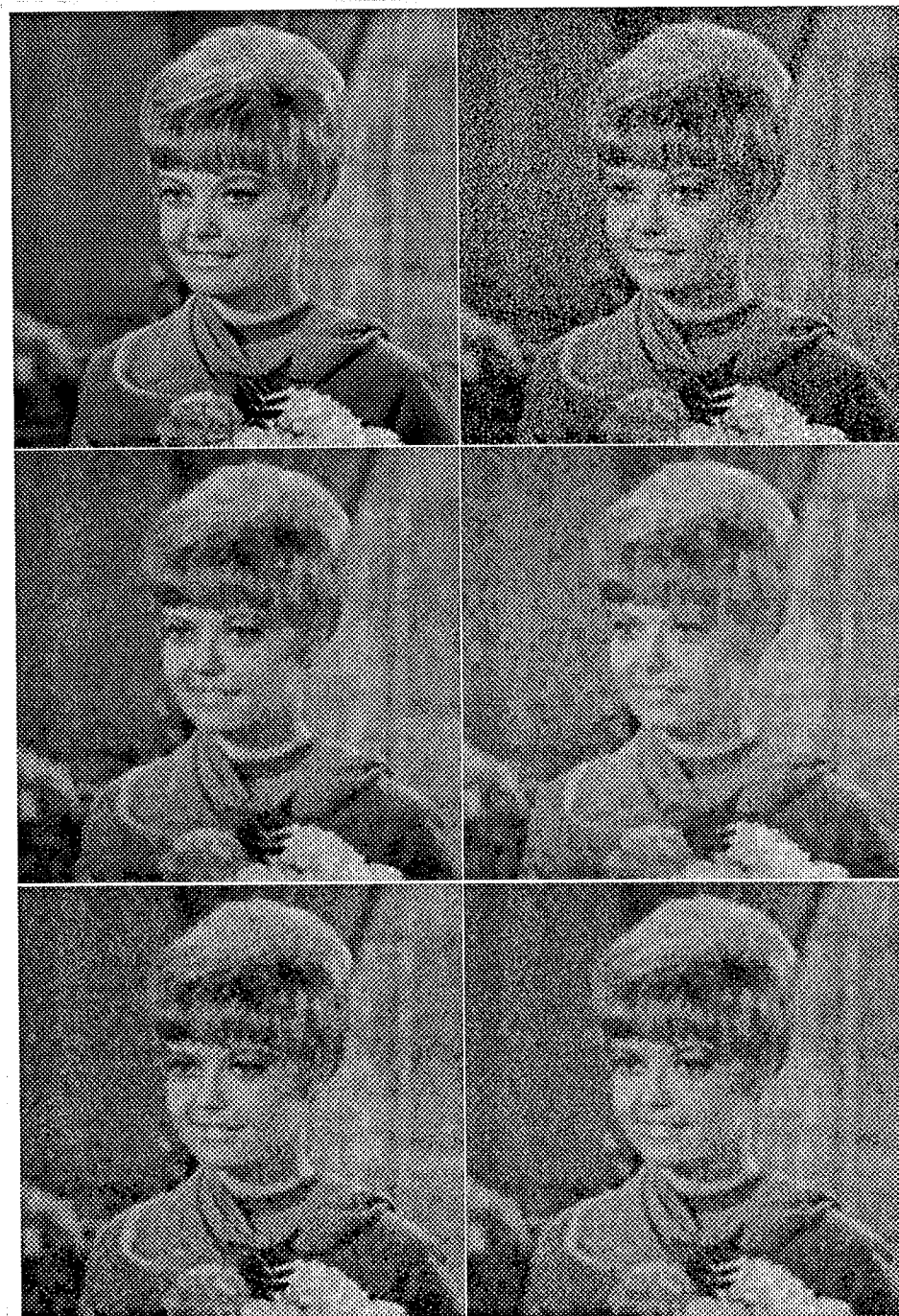
Figure 4.14.*Upper Left*: Original girl image; *Upper Right*: Noisy image; *Middle Left*: Output of the GMF; *Middle Right*: Output of a traditional morphological filter using a single structuring element; *Bottom Left*: Output of the median filter; *Bottom Right*: Output of the averaging filter.

4.3.3 Considerations in the selection of the multiple structuring elements

Selecting proper structuring elements is an essential step in designing the GMF since it greatly affects the noise suppression effectiveness and geometrical feature preservation. There is not yet a systematic approach for designing structuring elements. However, from the understanding of the morphological operations, we can obtain some intuitive ideas about how the structuring elements affect the performance of the GMF.

The parameters of a structuring element include the size and shape of the supporting area as well as the gray scale profile of the structuring element. The design of the gray scale profile of a structuring element is usually based on the application. For example, in some applications, images obtained from a known environment includes noise with a certain structure. The gray scale profile of the structuring element can then be designed so that it matches the structure of the noise [17, 18]. Flat structuring elements are commonly used if there is no a prior knowledge about the noise amplitude.

The high fidelity of the GMF is achieved if fine details can be maintained after the filtering process. Fine detail usually means geometrical structures of small sizes, such as thin lines, corners, etc. One way to preserve fine details is to use structuring elements of small sizes. The shapes of these structuring elements are designed so that they can form fine details in an image. For example, if the structuring elements are defined as four lines of three pixels long and directions of $0°$, $45°$, $90°$, and $135°$, as shown in Figure 4.7, then they can form lines with the four angles, and curves whose segments consists of the four lines. However, from a noise suppression point of view, structuring elements of large sizes are preferred in order to achieve better smoothing effect. So there is a conflict in choosing structuring elements for noise suppression and geometrical structure preservation. There are two approaches that can be used to alleviate this conflict. One way to resolve this conflict is to use more structuring elements for the large window size. Since a large window can be decomposed into more substructures, increasing the number of

Then for n images, we have

$$(\bigcup_{i=1}^{n} A_i) \circ K = [(\bigcup_{i=1}^{n-1} A_i) \cup A_n] \circ K \supseteq [(\bigcup_{i=1}^{n-1} A_i) \circ K] \cup (A_n \circ K)$$

$$\supseteq \bigcup_{i=1}^{n} (A_i \circ K),$$

The above proposition implies that the distributive property between the opening and set union does not exist. The geometrical interpretation of Proposition 5.1.1 can be described as the following: the union of several binary images may result in a larger image in which some geometrical patterns, that are not contained in the original images, may be created. Since an opened image is basically the collection of the same patterns, represented by the structuring element and distributed in the original image [2], we may obtain a larger collection from the image which is formed by set union. Therefore the above containment relationship is established. An example of this property is shown in Figure 5.1.

The following proposition describes the relationship between interchanging the order of set intersection and opening.

Proposition 5.1.2:

For a finite number of binary images $A_1, A_2, ..., A_n$, the following relation holds:

$$(\bigcap_{i=1}^{n} A_i) \circ K \subseteq \bigcap_{i=1}^{n} (A_i \circ K). \tag{5.1.2}$$

The proof of this proposition is similar to the proof of Proposition 5.1.1. Proposition 5.1.2 indicates that the distributive property between the opening and set intersection does not exist. The geometrical explanation of the proposition is that since the geometrical patterns extracted from the image formed by the set intersection are also contained in every opened image obtained from the original images which form the
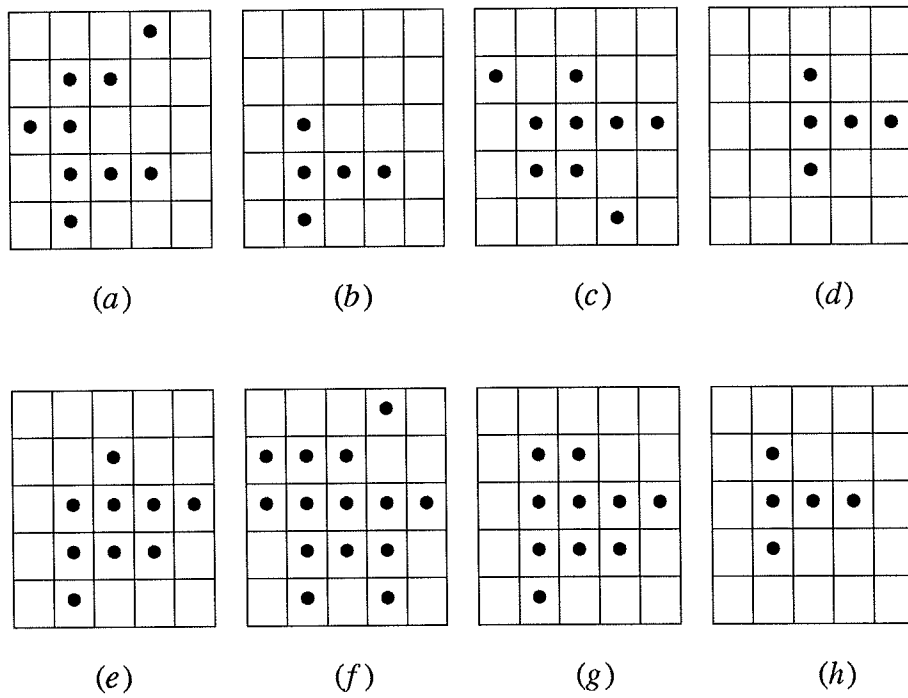
Figure 5.1.　(a) image A; (b) opening of A by K: $A \circ K$; (c) image B; (d) opening of B by K: $B \circ K$; (e) the union of $A \circ K$ and $B \circ K$: $(A \circ K) \cup (B \circ K)$; (f) the union of A and B: $A \cup B$; (g) opening of $A \cup B$ by K: $(A \cup B) \circ K$; (h) the structuring element K.

intersection, the intersection of the opened images will contain the result of the opening operator applied to the image formed by the intersection. The example in Figure 5.2 illustrates the above property.

Interchanging the order of the closing and set operations also possesses similar properties. The next two propositions provide properties for interchanging set operations, such as set union and intersection, and the closing operation when applied to a finite number of images using the same structuring element.

Proposition 5.1.3:

For a finite number of binary images $A_1, A_2, ..., A_n$, the following relation holds:

$$(\bigcup_{i=1}^{n} A_i) \bullet K \supseteq \bigcup_{i=1}^{n} (A_i \bullet K). \tag{5.1.3}$$

Proof:

The relation is proved using induction. First we prove that the relation holds for two images. From (2.1.7c) and (2.1.8d), we can obtain the following result:

$$(A_1 \cup A_2) \bullet K = [(A_1 \cup A_2) \oplus K] \ominus K = [(A_1 \oplus K) \cup (A_2 \oplus K)] \ominus K$$

$$\supseteq (A_1 \oplus K) \ominus K] \cup [(A_2 \oplus K) \ominus K] = (A_1 \bullet K) \cup (A_2 \bullet K).$$

Assume that the relation holds for n-1 images, that is:

$$(\bigcup_{i=1}^{n-1} A_i) \bullet K \supseteq \bigcup_{i=1}^{n-1} (A_i \bullet K).$$

Then for n images, we have

$$(\bigcup_{i=1}^{n} A_i) \bullet K = [(\bigcup_{i=1}^{n-1} A_i) \cup A_n] \bullet K \supseteq [(\bigcup_{i=1}^{n-1} A_i) \bullet K] \cup (A_n \bullet K)$$

$$\supseteq \bigcup_{i=1}^{n} (A_i \bullet K),$$
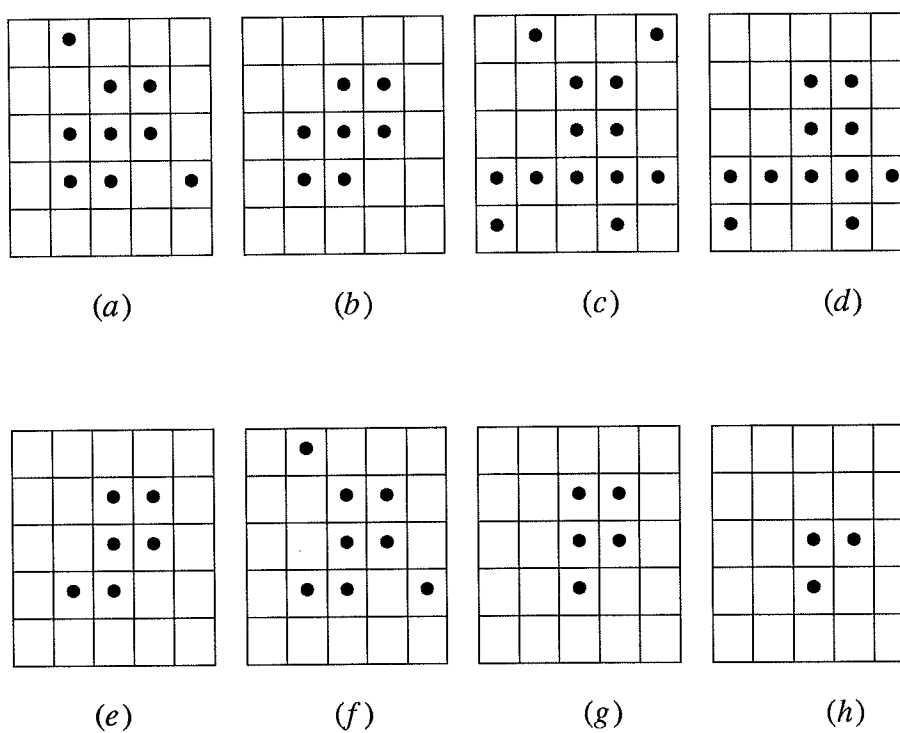
Figure 5.2. (a) image A; (b) opening of A by K: $A \circ K$; (c) image B; (d) opening of B by K: $B \circ K$; (e) the intersection of $A \circ K$ and $B \circ K$: $(A \circ K) \cap (B \circ K)$; (f) the intersection of A and B: $A \cap B$; (g) opening of $A \cap B$ by K: $(A \cap B) \circ K$; (h) the structuring element K.

As mentioned in Chapter 2, closing is a dual operation to opening. It operates as the opening on the background of the image. The closed image can also be considered as the collection of points that are contained in all the translates of the structuring element whose intersections with the image are not empty (that "hit" the image) [2]. Since the set union produces a larger set, it is true that the new image may be hit by a greater number of translated structuring elements. Therefore, the result from the closing of the new image contains all the points that results from closing the original images, respectively. An example of this property is shown in Figure 5.3.

Proposition 5.1.4:

For a finite number of binary images $A_1, A_2,..., A_n$, interchanging set intersection and the closing operation results in the following relation:

$$(\bigcap_{i=1}^{n} A_i) \bullet K \subseteq \bigcap_{i=1}^{n} (A_i \bullet K). \qquad (5.1.4)$$

The proof of this proposition is similar to the proof of Proposition 5.1.3. Since the intersection of several images contains the common elements of these images, the translated structuring elements that hit the intersection will definitely hit the original images. Therefore, the collection of points contained in all the translated structuring elements that hit the intersection of the images will be contained in each closed image obtained from the original images. So the above containment relationship is justified. The example in Figure 5.4 illustrates this property.

One of the salient features of the opening operation is the idempotent property. Since we are dealing with the opening operation using multiple structuring elements, it is natural to ask whether the idempotent property exists for such an operation and if it does under what conditions does the property hold. The following proposition states that the idempotent property does exist for opening operations using multiple structuring elements, and the property holds for the union of the results of these opening operations.
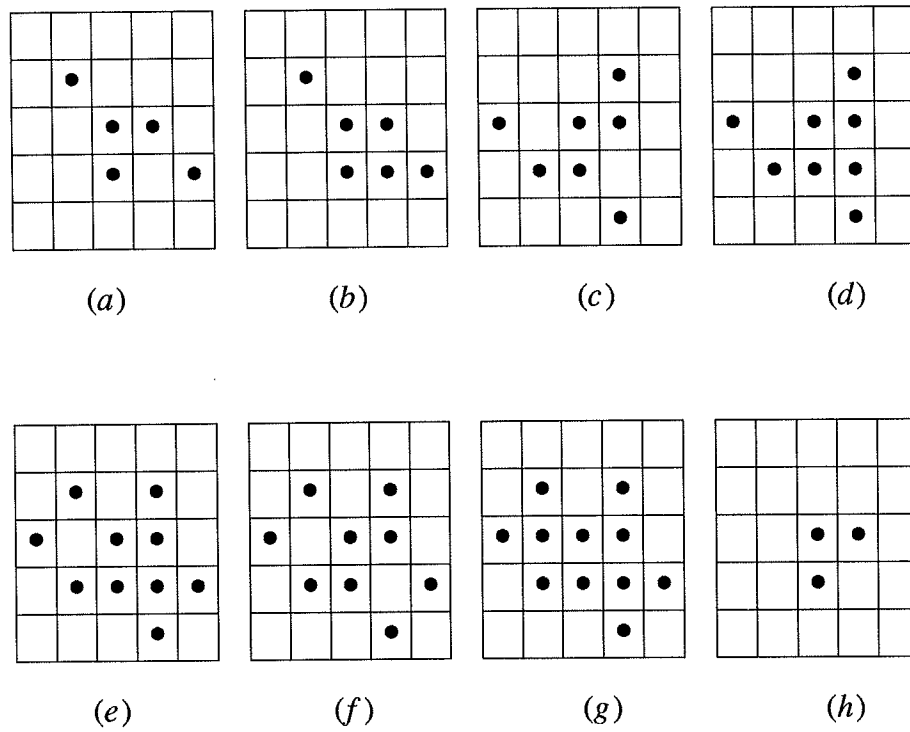
Figure 5.3. (a) image A; (b) closing of A by K: $A \bullet K$; (c) image B; (d) closing of B by K: $B \bullet K$; (e) the union of $A \bullet K$ and $B \bullet K$: $(A \bullet K) \cup (B \bullet K)$; (f) the union of A and B: $A \cup B$; (g) closing of $A \cup B$ by K: $(A \cup B) \bullet K$; (h) the structuring element K.
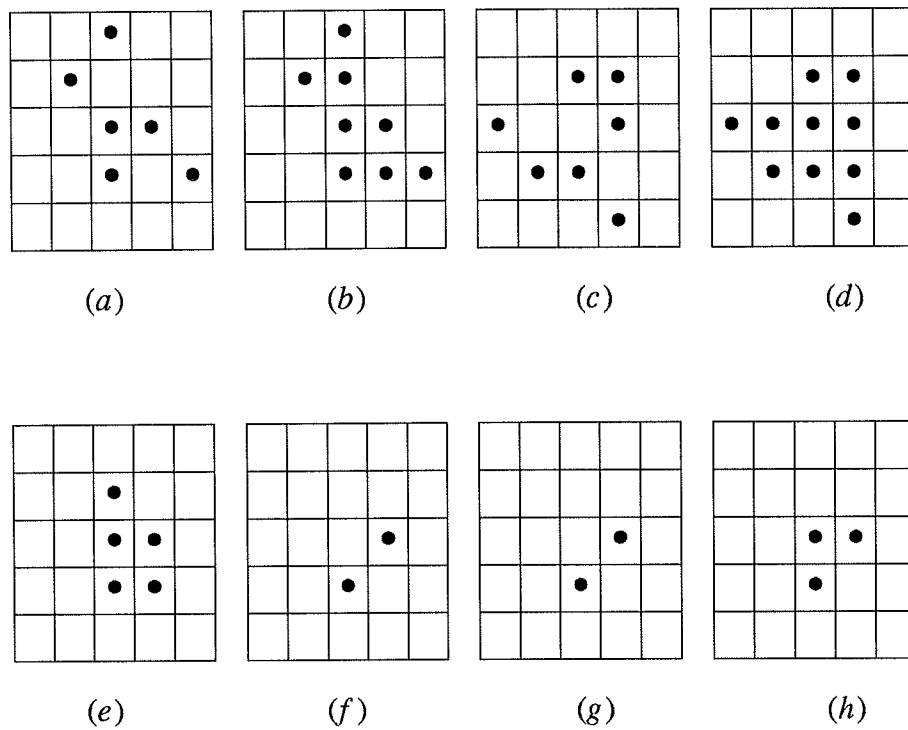
Figure 5.4. (a) image A; (b) closing of A by K: $A \bullet K$; (c) image B; (d) closing of B by K: $B \bullet K$; (e) the intersection of $A \bullet K$ and $B \bullet K$: $(A \bullet K) \cap (B \bullet K)$; (f) the intersection of A and B: $A \cap B$; (g) closing of $A \cap B$ by K: $(A \cap B) \bullet K$; (h) the structuring element K.

This is actually the binary version of the OL stage in the max/min version of the GMF.

Proposition 5.1.5:

For a finite number of binary structuring elements $K_1, K_2, ..., K_n$,

$$\text{let} \quad A_n = \bigcup_{i=1}^{n} (A \circ K_i).$$

$$\text{Then} \quad A_n = \bigcup_{i=1}^{n} (A_n \circ K_i). \qquad\qquad (5.1.5)$$

Proof:

The relation is obtained by induction. First we prove that the relation holds for two images.

Let $B_1 = A \circ K_1$, $B_2 = A \circ K_2$. From Proposition 5.1.1, we have the following relation:

$$(B_1 \cup B_2) \circ K_1 \supseteq (B_1 \circ K_1) \cup (B_2 \circ K_1)$$

$$= (A \circ K_1) \cup [(A \circ K_2) \circ K_1];$$

and

$$(B_1 \cup B_2) \circ K_2 \supseteq (B_1 \circ K_2) \cup (B_2 \circ K_2)$$

$$= [(A \circ K_1) \circ K_2] \cup (A \circ K_2).$$

Taking unions on both sides of the above two expressions, we obtain the following containment relation:

$$(A_2 \circ K_1) \cup (A_2 \circ K_2) \supseteq (A \circ K_1) \cup (A \circ K_2),$$

since $[(A \circ K_1) \circ K_2] \cup (A \circ K_1) = (A \circ K_1)$;

and $[(A \circ K_2) \circ K_1] \cup (A \circ K_2) = (A \circ K_2)$.

Due to the antiextensive property of the opening described from (5.1.1), we obtain the following two relationships:

$$(B_1 \cup B_2) \circ K_1 \subseteq (B_1 \cup B_2),$$

and

$$(B_1 \cup B_2) \circ K_2 \subseteq (B_1 \cup B_2).$$

Taking unions on both sides of the above two expressions, we have

$$(A_2 \circ K_1) \cup (A_2 \circ K_2) \subseteq (A \circ K_1) \cup (A \circ K_2).$$

So the property for $n = 2$ is proved. Assume that the property holds for n-1 structuring elements, that is:

$$\text{let} \quad A_{n-1} = \bigcup_{i=1}^{n-1} (A \circ K_i),$$

$$\text{then} \quad A_{n-1} = \bigcup_{i=1}^{n-1} (A_{n-1} \circ K_i).$$

Now for n structuring elements, we can arrange the equation by the following:

$$\bigcup_{i=1}^{n} (A_n \circ K_i) = \bigcup_{i=1}^{n-1} \{ [A_{n-1} \cup (A \circ K_n)] \circ K_i \} \cup [A_{n-1} \cup (A \circ K_n) \circ K_n].$$

The following relations are derived:

$$\bigcup_{i=1}^{n-1} \{ [A_{n-1} \cup (A \circ K_n)] \circ K_i \} \supseteq \bigcup_{i=1}^{n-1} \{ (A_{n-1} \circ K_i) \cup [(A \circ K_n) \circ K_i] \}$$

$$= A_{n-1} \cup \{ \bigcup_{i=1}^{n-1} [(A \circ K_n) \circ K_i] \} \; ;$$

and

$$[A_{n-1} \cup (A \circ K_n)] \circ K_n \supseteq (A_{n-1} \circ K_n) \cup (A \circ K_n).$$

Taking the union of the above two expressions, we obtain:

$$\bigcup_{i=1}^{n} (A_n \circ K_i) \supseteq A_{n-1} \cup (A \circ K_n).$$

From the antiextensive property of opening, the following relations are obtained:

$$\bigcup_{i=1}^{n-1} \{ [A_{n-1} \cup (A \circ K_n)] \circ K_i \} \subseteq A_{n-1} \cup (A \circ K_n);$$

and

$$[A_{n-1} \cup (A \circ K_n)] \circ K_n \subseteq A_{n-1} \cup (A \circ K_n).$$

Taking the union of the above two expressions, we obtain:

$$\bigcup_{i=1}^{n} (A_n \circ K_i) \subseteq A_{n-1} \cup (A \circ K_n).$$

The proposition is proved.

The result of opening an image by one structuring element is the union of the same geometrical patterns represented by the structuring element and distributed in the original image [2]. Similarly, the result of the operation in Proposition 5.1.5 is then the union of the geometrical patterns, represented by a finite number of the given structuring elements and distributed in the original image. Therefore, once the patterns are sorted out of the original image, repeating the same operation will not obtain new information and the operation is hence idempotent. Figure 5.5 shows an example of this property.

The idempotent property for the binary version of the CL stage follows by duality. That is, the intersection of results of the closing operation using multiple structuring elements is idempotent. This property is described by Proposition 5.1.6.

Proposition 5.1.6:

For a finite number of binary structuring elements $K_1, K_2, ..., K_n$,

$$\text{let} \quad A_n = \bigcap_{i=1}^{n} (A \bullet K_i).$$

$$\text{Then} \quad A_n = \bigcap_{i=1}^{n} (A_n \bullet K_i). \tag{5.1.6}$$

The proof of this proposition is similar to the previous proposition.

The result of closing an image by a structuring element is the union of the same geometrical patterns represented by the structuring element and contained in the background of the original image [2]. The result of the operation in Proposition 5.1.6 is then
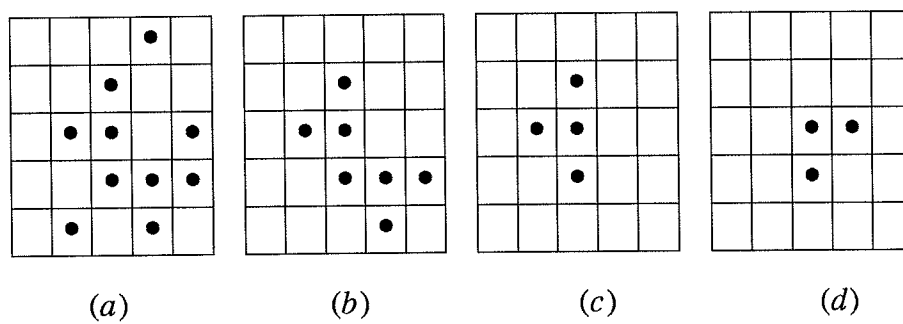
Figure 5.5. (a) image A; (b) $(A \circ K_1) \cup (A \circ K_2)$; (c) structuring element K_1; (d) structuring element K_2.

the union of geometrical patterns represented by a finite number of the given elements and distributed in the original background. Hence iteration of the same operation will not change the first result. Figure 5.6 presents an example of the above property.

We have shown that the binary version of the OL and CL stages are idempotent. Since the GMF consists of cascades of OL and CL stages, the question is whether the GMF as a whole possesses the idempotent property. The answer is yes and the following two propositions shows the idempotent property of two configurations of the GMF with OL and CL stages cascaded in different orders. Using Propositions 5.1.5 and 5.1.6, the proofs of the propositions are quite straightforward.

Proposition 5.1.7:

$$\text{Let } A_{K^n} = \bigcup_{i=1}^{n}(A \circ K_i), \quad A^{K^n} = \bigcap_{i=1}^{n}(A \circ K_i), \text{ and } B = (A_{K^n})^{K^n}.$$

$$\text{Then } B = (B_{K^n})^{K^n}. \tag{5.1.7}$$

Proof:

$$B = B^{K^n} \supseteq (B_{K^n})^{K^n} = \{[(A_{K^n})^{K^n}]_{K^n}\}^{K^n} \supseteq [(A_{K^n})_{K^n}]^{K^n} = (A_{K^n})^{K^n} = B.$$

Proposition 5.1.8:

$$\text{Let } A_{K^n} = \bigcup_{i=1}^{n}(A \circ K_i), \quad A^{K^n} = \bigcap_{i=1}^{n}(A \circ K_i), \text{ and } B = (A^{K^n})_{K^n}.$$

$$\text{Then } B = (B^{K^n})_{K^n}. \tag{5.1.8}$$

Proof:

$$B = B_{K^n} \subseteq (B^{K^n})_{K^n} = \{[(A^{K^n})_{K^n}]^{K^n}\}_{K^n} \subseteq [(A^{K^n})^{K^n}]_{K^n} = (A^{K^n})_{K^n} = B.$$

Note that, the above properties are different than structuring element decomposition, in which a structuring element is decomposed into two or more sub-structuring elements [32]. The purpose of such an arrangement is to reduce computational complexity or to meet special hardware requirements. The result, using the decomposition
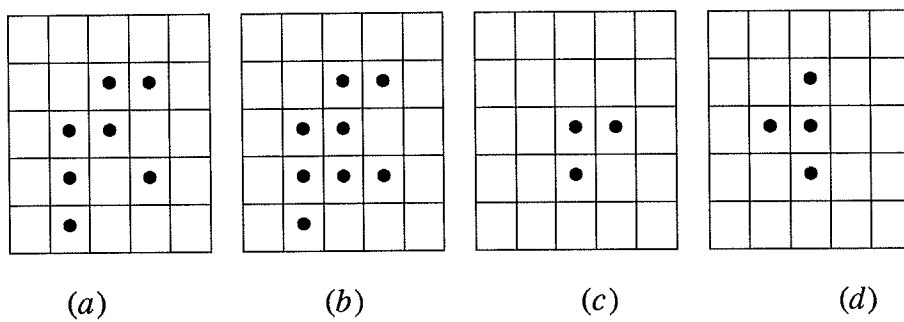
Figure 5.6.   (a) image A; (b) $(A \bullet K_1) \cap (A \bullet K_2)$; (c) structuring element K_1 ; (d) structuring element K_2 .

technique, is based only on the one pattern represented by the undecomposed structuring element. The operations in Propositions 5.1.5, 5.1.6, 5.1.7, and 5.1.8 will extract different patterns from an image or the background of an image. The final result is the collection of at least one of the patterns represented by the structuring elements.

5.2 Properties of Gray Scale Morphological Operators Using Multiple Structuring Elements

In this section, similar properties of gray scale morphological operators are derived. With the concept of the umbra of an image, the geometrical interpretation of the following properties for gray scale morphological operations can be made similar to the ones in the previous section. Let f and $\{ f_1, f_2, \ldots, f_n \}$ be gray scale images and k and $\{ k_1, k_2, \ldots, k_n \}$ be gray scale structuring elements.

Propositions 5.2.1 and 5.2.2 state that the distributive property does not exist between opening and the max or min. Interchanging the order of the operations of opening and max or min will produce the results shown in the following:

Proposition 5.2.1:

For a finite number of images $f_1, f_2, \ldots, f_n$, the following relation holds:

$$\max_{i \in (1,\ldots,n)} (f_i \circ k) \leq \max_{i \in (1,\ldots,n)} (f_i) \circ k. \tag{5.2.1}$$

Proof:

The proof is obtained by induction. For $n = 2$ the following relationship is obtained from (12) and (10):

$$max\ [(f_1 \ominus k) \oplus k,\ (f_2 \ominus k) \oplus k] = max\ [(f_1 \ominus k),\ (f_2 \ominus k)] \oplus k$$

$$\leq max\ (f_1, f_2) \circ k.$$

Assume that the relation holds for n-1 images, that is

$$\max_{i \in (1,...,n-1)} (f_i \circ k) \leq \max_{i \in (1,...,n-1)} (f_i) \circ k.$$

Then for n images, we have

$$\max_{i \in (1, \ldots, n)} = \max [\max_{i \in (1, \ldots, n-1)} (f_i \circ k), f_n \circ k]$$

$$\leq \max [\max_{i \in (1, \ldots, n-1)} (f_i) \circ k, f_n \circ k]$$

$$\leq \max_{i \in (1, \ldots, n)} (f_i) \circ k.$$

Proposition 5.2.2:

For a finite number of images $f_1, f_2, \ldots, f_n$, the following relation holds:

$$\min_{i \in (1,...,n)} (f_i \circ k) \geq \min_{i \in (1,...,n)} (f_i) \circ k. \qquad (5.2.2)$$

The proof is similar to the previous one.

Analogous to Propositions 5.2.3 and 5.2.4, the following two propositions state properties that results from the closing and the "max" or the closing and the min operations.

Proposition 5.2.3:

For a finite number of images $f_1, f_2, \ldots, f_n$, the following relation holds:

$$\max_{i \in (1,...,n)} (f_i \bullet k) \leq \max_{i \in (1,...,n)} (f_i) \bullet k. \qquad (5.2.3)$$

Proof:

For $n = 2$ the following relationship is obtained from (12) and (10):

$$\max [(f_1 \oplus k) \ominus k, (f_2 \oplus k) \ominus k] \leq \max [(f_1 \oplus k), (f_2 \oplus k)] \ominus k$$

$$= \max (f_1, f_2) \bullet k.$$

Assume that the relation holds for n-1 images, that is

$$\max_{i \in (1,...,n-1)} (f_i \bullet k) \leq \max_{i \in (1,...,n-1)} (f_i) \bullet k.$$

Then for n images, we have

$$\max_{i \in (1, \ldots, n)} = \max \left[\max_{i \in (1, \ldots, n-1)} (f_i \bullet k), f_n \bullet k \right]$$

$$\leq \max \left[\max_{i \in (1, \ldots, n-1)} (f_i) \bullet k, f_n \bullet k \right]$$

$$\leq \max_{i \in (1, \ldots, n)} (f_i) \bullet k .$$

Proposition 5.2.4:

For a finite number of images $f_1, f_2, \ldots, f_n$, the following relation holds:

$$\min_{i \in (1, \ldots, n)} (f_i \bullet k) \geq \min_{i \in (1, \ldots, n)} (f_i) \bullet k. \tag{5.2.4}$$

The proof is similar to the previous proposition.

The following proposition describes the idempotent property relative to the operation which selects the maximum of the results of opening operations using multiple structuring elements. This is the operation that consists of the OL stage of the max/min version of the GMF.

Proposition 5.2.5:

For a finite number of structuring elements,

$$\text{let } f_n = \max_{i \in (1, \ldots, n)} (f \circ k_i) .$$

$$\text{Then } f_n = \max_{i \in (1, \ldots, n)} (f_n \circ k_i) . \tag{5.2.5}$$

Proof:

First the case for $n = 2$ is considered: Let $g_1 = (f \circ k_1)$ and $g_2 = (f \circ k_2)$. From Proposition 9, we obtain the following two inequalities:

$$\max (g_1, g_2) \circ k_1 \geq \max(g_1 \circ k_1, g_2 \circ k_1),$$

and

$$\max(g_1, g_2) \circ k_2 \geq \max(g_1 \circ k_2, g_2 \circ k_2),$$

From these two inequalities, we can easily obtain the following relationship:

$$\max(\max(g_1, g_2) \circ k_1, \max(g_1, g_2) \circ k_2)$$

$$\geq \max[\max(g_1 \circ k_1, g_2 \circ k_1), \max(g_1 \circ k_2, g_2 \circ k_2)]$$

$$= \max[f \circ k_1, (f \circ k_2) \circ k_1, (f \circ k_1) \circ k_2, f \circ k_2]$$

$$= \max(f \circ k_1, f \circ k_2).$$

Due to the antiextensive property of the opening from (8), we have the following two inequalities:

$$\max(g_1, g_2) \circ k_1 \leq \max(g_1, g_2)$$

and

$$\max(g_1, g_2) \circ k_2 \leq \max(g_1, g_2).$$

From the above two inequalities, the following relationship can be established:

$$\max(\max(g_1, g_2) \circ k_1, \max(g_1, g_2) \circ k_2)$$

$$\leq \max(g_1, g_2) = \max(f \circ k_1, f \circ k_2).$$

Assume that the relation holds for n-1 structuring elements, that is

$$\text{let } f_{n-1} = \max_{i \in (1, \ldots, n-1)} (f \circ k_i).$$

$$\text{Then } f_{n-1} = \max_{i \in (1, \ldots, n-1)} (f_{n-1} \circ k_i).$$

Now for the n structuring elements, we have

$$\max_{i \in (1, \ldots, n)} (f_n \circ k_i) = \max\left[\max_{i \in (1, \ldots, n-1)} (f_n \circ k_i), f_n \circ k_n \right]$$

$$= \max\left\{ \max_{i \in (1, \ldots, n-1)} [\max(f_{n-1}, f \circ k_n) \circ k_i], \max(f_{n-1}, f \circ k_n) \circ k_n \right\}.$$

The following relations are derived:

Proposition 5.2.6:

For a finite number of structuring elements,

$$\text{let } f_n = \min_{i \in (1, \ldots, n)} (f \bullet k_i).$$

$$\text{Then } f_n = \min_{i \in (1, \ldots, n)} (f_n \bullet k_i). \tag{5.2.6}$$

The proof is similar to the previous proposition.

This operation can also be visualized in the following way: the structuring elements are floating freely above the surface of the function f, and any downward part of the surface will be filled in if none of these structuring elements fits above the surface. So at least one of the given structuring element will fit above the resulting surface. Consequently, the repeated application of the operation on the resulting surface will not change.

The next two properties state the idempotent property for the max/min version of the GMF consisting of cascades of OL and CL stages in different orders. In other words, the consecutive applications of operations in Propositions 5.2.5 and 5.2.6 are idempotent.

Proposition 5.2.7:

$$\text{Let } f_{k^n} = \max_{i \in (1, \ldots, n)} (f \circ k_i), \quad f^{k^n} = \min_{i \in (1, \ldots, n)} (f \circ k_i), \quad \text{and} \quad g = (f_{k^n})^{k^n}.$$

$$\text{Then } g = (g_{k^n})^{k^n}. \tag{5.2.7}$$

Proof:

$$g = g^{k^n} \geq (g_{k^n})^{k^n} = \{[(f_{k^n})^{k^n}]_{k^n}\}^{k^n} \geq [(f_{k^n})_{k^n}]^{k^n} = (f_{k^n})^{k^n} = g.$$

Proposition 5.2.8:

$$\text{Let } f_{k^n} = \max_{i \in (1, \ldots, n)} (f \circ k_i), \quad f^{k^n} = \min_{i \in (1, \ldots, n)} (f \circ k_i), \quad \text{and} \quad g = (f^{k^n})_{k^n}.$$

$$\text{Then } g = (g^{k^n})_{k^n}. \tag{5.2.8}$$

$$\max_{i \in (1,\ldots,n-1)} [\max(f_{n-1}, f \circ k_n) \circ k_i] \geq \max_{i \in (1,\ldots,n-1)} \{\max [f_{n-1} \circ k_i, (f \circ k_n) \circ k_i]\} \ ;$$

and

$$\max (f_{n-1}, f \circ k_n) \circ k_n \geq \max [(f_{n-1} \circ k_n), (f \circ k_n)] \ .$$

Combining the above two expressions, we obtain:

$$\max_{i \in (1,\ldots,n)} (f_n \circ k_i) \geq \max [f_{n-1}, (f \circ k_n)] \ .$$

From the antiextensive property of opening, the following relations are obtained:

$$\max_{i \in (1,\ldots,n-1)} [\max(f_{n-1}, f \circ k_n) \circ k_i] \leq max [f_{n-1} \circ k_i, (f \circ k_n) \circ k_i] \ ;$$

and

$$\max (f_{n-1}, f \circ k_n) \circ k_n \leq \max [f_{n-1}, (f \circ k_n)] \ .$$

Combining the above two expressions, we obtain:

$$\max_{i \in (1,\ldots,n)} (f_n \circ k_i) \leq \max [f_{n-1}, (f \circ k_n)] \ .$$

The property is proved.

The operation in the proposition can be visualized in the following way: given that the structuring elements are floating freely under the surface of an image, after the operation, any part of the surface will be removed if none of these structuring elements fits under the surface. The resulting surface underneath will then consists of geometrical structures represented by the given structuring elements. That is, at least one of the structuring elements will fit under the resulting surface. Therefore, the resulting surface will be invariant under repeated application of the operation.

The idempotent property of the CL stage of the max/min version of the GMF is described in Proposition 5.2.6. That is, selecting the minimum of the results of closing operations using multiple structuring elements is an idempotent operation.

Proof:

$$g = g_{k^n} \leq (g^{k^n})_{k^n} = \{[(f^{k^n})_{k^n}]^{k^n}\}_{k^n} \leq [(f^{k^n})^{k^n}]_{k^n} = (f^{k^n})_{k^n} = g \; .$$

So we have proved that the max/min version of the GMF has the idempotent property.

5.3. Root Signal Structures of the GMF

One of the important features of the median filter is its root signal structure. The appealing characteristic of this root signal structure is its invariability against repeated application of the filter [46]. Opening and closing operators have an even stronger invariant property. The idempotent properties of the opening and closing operators indicates that the root structure of the two operators can be obtained through one application of the operators. The relationship between root structures of the median filter and morphological operators using flat structuring elements were discussed in [14]. Maragos, et al., established upper and lower bounds on the root signal of the median filter relative to the opening and closing, respectively [14]. In the above two subsections, we showed that the idempotent property exists for the max/min version of the GMF. In this section, we will investigate the root signal structure of the GMF.

As a morphological filter, a root signal structure also exists for the GMF. But since the linear operation is involved, the idempotent property does not hold in general for the GMF. The root signal structure of the GMF depends on the set of structuring elements and can be described as the composition of structures represented by the structuring elements. From the descriptions of the two stages of the GMF, it is noted that invariability holds if the outputs of the multiple morphological operators in each stage have the same value as the input at every pixel location since the sum of the coefficients in the linear operation part of the GMF is one. This situation exists when the input consists of geometrical structures from which the substructures represented by the structuring

elements exists at every pixel location.

The root signal structure can be better illustrated using the threshold decomposition concept [50]. We will only consider flat structuring elements here. The result can easily be extended to gray level structuring elements. Suppose the gray level values of the pixels in the image range from 0 to M. Let Ψ denotes the morphological operation and Π_t thresholding at gray level t. Then the threshold decomposition concept can be expressed as:

$$\Psi(f) = \sum_{t=0}^{M} \Psi[\Pi_t(f)].$$
$$(5.3.1)$$

For the sake of simplicity, the averaging version of the OL stage will be used. The corresponding expression for the averaging version of the OL stage is

$$y(x) = \frac{1}{N} \sum_{i=1}^{N} f \circ k_i(x) = \frac{1}{N} \sum_{i=1}^{N} \sum_{t=0}^{M} \Pi_t(f) \circ k_i(x).$$

$$= \sum_{t=1}^{M} \frac{1}{N} \sum_{i=0}^{N} \Pi_t(f) \circ k_i(x).$$
$$(5.3.2)$$

A similar expression can be derived for the general case as well as the CL stage. It can be seen from the above expression that if, at each cross-section and each pixel location, the multiple opening operators produce the same outputs as the input, then the output of the stage at each cross-section will not differ from the input. This condition requires that at a pixel location there exist geometrical structures represented by the structuring elements. If a region consists of all such pixels, then the region is invariant under repeated applications of the GMF. Consequently an image consisting of such regions will be invariant to the applications of the GMF.

We will use an example to illustrate a binary root signal structure. The structuring elements in Figure 4.7 are used which consist of four lines, each three pixels long. The corresponding root signal structure, shown in Figure 5.7, is a hexagon each side of

which is three pixels long. Note that at every pixel location, there are four connecting lines lying within the hexagon. In order to further illustrate the situation, the hexagon is shown in Figure 5.8 with some pixel locations within the hexagon being marked with an "x" and at each location the four lines are shown. It is apparent then that the four opening operators using the four line structuring elements at every pixel location in the hexagon will produce outputs with the same value as the input signal. Correspondingly the hexagon remains unchanged under repeated application of the GMF. The structure shown in Figure 5.7 can be considered as the minimal or base root signal structure with respect to the structuring elements. It is obvious that any collection of such base structures is still a root signal structure.

We can conclude that an image is the root signal of the GMF if all its cross-sections are the root signals of the GMF. Such an image can be referred to as the root image. More specifically, an root image contains plateaus that have the same shapes as their cross-sections. The transient regions connecting these plateaus have cross-sections that are the collection of the base root signal structures. Figure 5.9 shows a segment of an image which is the root signal of the averaging version of the GMF.

It should be noted that the above argument shows that a root signal exists for the GMF but we have not addressed the issue whether the GMF will reach this root signal in a finite number of iterations.

```
0    0    0    0    0    0    0    0    0

0    0    0    1    1    1    0    0    0

0    0    1    1    1    1    1    0    0

0    1    1    1    1    1    1    1    0

0    1    1    1    1    1    1    1    0

0    1    1    1    1    1    1    1    0

0    0    1    1    1    1    1    0    0

0    0    0    1    1    1    0    0    0

0    0    0    0    0    0    0    0    0
```

Figure 5.7.   An example of a binary root signal structure of the GMF.
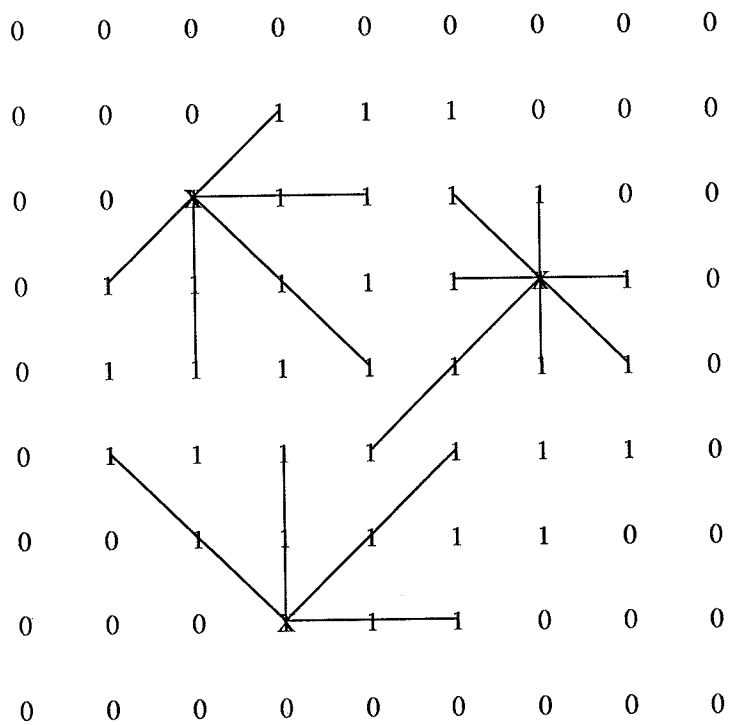
Figure 5.8.   The structuring elements and binary root signal structure combined.

0	0	0	1	13	45	46	46	48	48	50	51
0	0	11	22	66	66	66	55	50	50	50	51
0	20	54	70	70	70	70	66	55	50	50	50
20	54	70	70	70	70	70	70	66	55	50	50
54	70	70	70	70	70	70	70	70	62	52	50
54	70	70	70	70	70	70	70	70	62	57	52
54	70	70	70	70	70	70	70	70	62	57	52
54	58	70	70	70	70	70	70	57	57	57	52
55	55	58	70	70	70	70	62	57	57	52	52
55	55	55	58	58	58	57	57	57	52	52	52
55	55	55	55	55	52	50	52	52	52	52	52
55	55	55	54	52	49	47	49	52	52	52	52
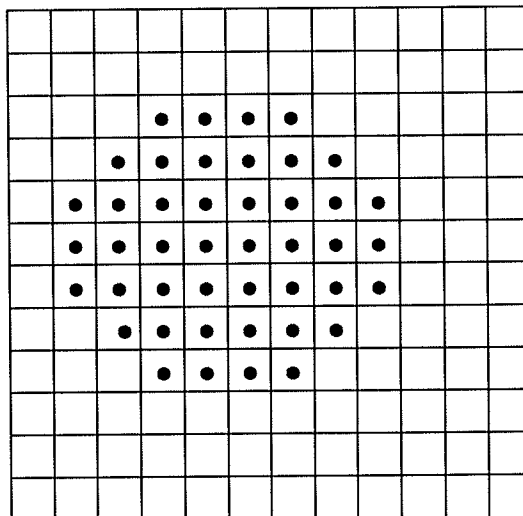
Threshold at 70
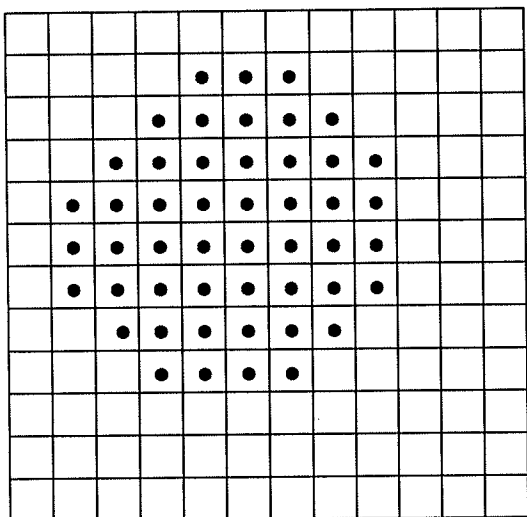
Threshold at 66
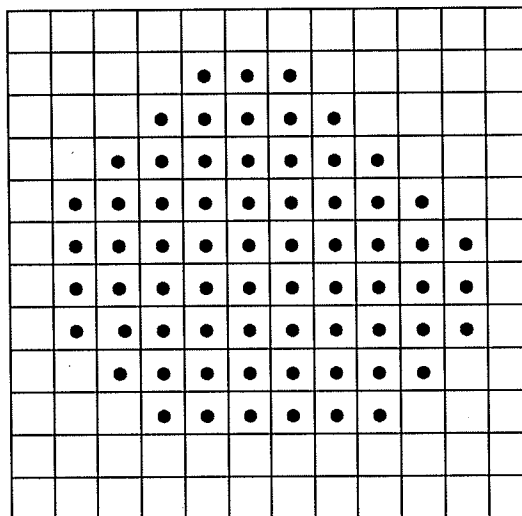
Threshold at 57

Figure 5.9. An example of a gray scale root signal structure of the averaging version of the GMF and cross-sections of the signal at various gray scale levels.

CHAPTER 6

COMPUTATION OF OPTIMAL COEFFICIENTS OF THE GMF

We showed in Chapter 3 that by assigning different values to the coefficients in the linear operation part of the GMF results in different versions of the GMF that can be used to deal with different types of noise. The design of the max/min version of the GMF is based on the characteristics of impulsive noise. The averaging version of the GMF is used for smoothing noise with an unknown input probability distribution.

Because of the nonlinearity of the morphological operations as well as the the high correlation in the pixels caused by the morphological operations and the multiple structuring elements, it is very difficult to derive at each stage a general closed form for the output pixel probability distribution function in terms of the input probability distribution function. In this chapter, we will derive a optimal set of coefficients for the GMF using a set of special structuring elements. Although these structuring elements are specially constructed, they can be used in many practical applications. They are line structuring elements that intersect at only one pixel location. Figure 6.1 illustrates four such structuring elements of 5 pixels in length.

6.1 Mean-Squared Error Minimization

In this subsection, optimal coefficients are obtained using mean squared error minization for the OL stage. This can similarly be derived for the CL stage. We first assume that the input image can be modeled as a constant region contaminated by zero-mean noise. Each pixel $f_{i,j}$ in the input image to an OL stage then has the following form:

$$f_{i,j} = c + x_{i,j}, \tag{6.1.1}$$
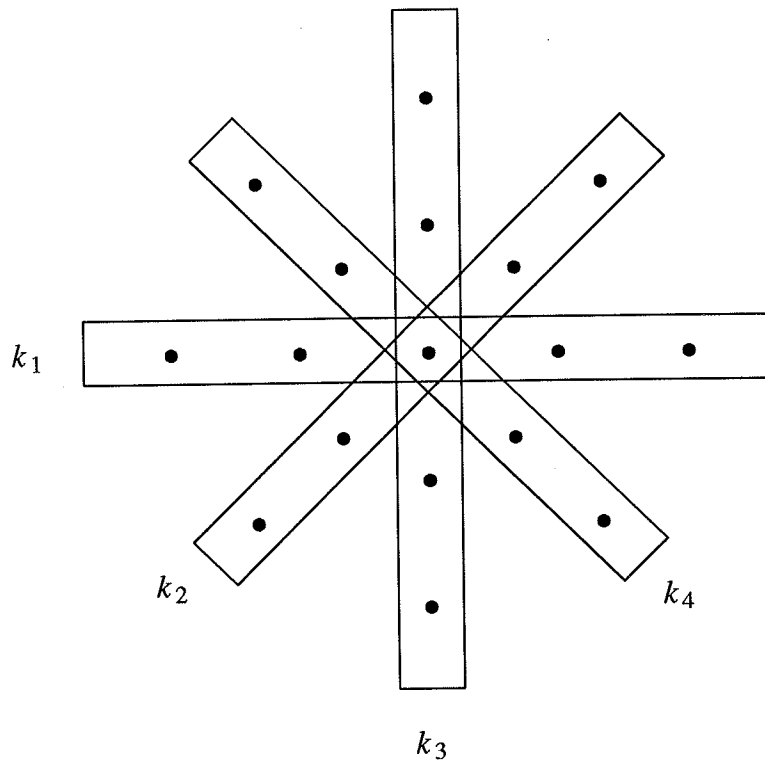
Figure 6.1.   The illustration of four line structuring elements.

where $x_{i,j}$ are zero-mean independent, identically distributed random variables and c is a constant. The mean-squared error can be formed by the following:

$$e^2 = E[(y-c)^2];$$ (6.1.2)

where y is the output of the OL stage.

The above expression for the mean squared error can be simplified by applying Property 2 in Chapter 5:

$$y - c = \sum_{i=1}^{4} \beta_i(y_{(i)}+c) - c = \sum_{i=1}^{4} \beta_i y_{(i)},$$ (6.1.3)

where $y_{(i)}$ is the ordered sequence of $y_i = x \circ k_i$ and $\sum_{i=1}^{4}\beta_i = 1$ [‡]. Now the mean squared error can be expressed as:

$$e^2 = E[(\sum_{i=1}^{4} \beta_i y_{(i)})^2].$$ (6.1.4)

Expanding the above equation, we obtain:

$$e^2 = \sum_{i=1}^{4}\sum_{j=1}^{4} \beta_i\beta_j R_{i,j},$$ (6.1.5)

where $R_{i,j} = E[y_{(i)}y_{(j)}]$. Equation (6.1.5) can be expressed in matrix form:

$$e^2 = \beta^t R \beta,$$ (6.1.6)

where the constant column vector $\beta = \{\beta_1, \beta_2, \beta_3, \beta_4\}^t$, and R is the 4x4 correlation matrix with elements $R_{i,j}$ which are the cross correlations of $y_{(i)}$ and $y_{(j)}$.

The problem of minimizing e^2 subject to the constraint $\sum_{i=1}^{4} \beta i = 1$ can be addressed using a Lagrange multiplier. The Lagrangian function is given by

---

[‡] Note: The notation has changed slightly. y_i is the output of the ith opening operation when the noise only is the input.

$$F(\beta, \lambda) = \beta^t R \beta + \lambda(1 - I^t \beta), \tag{6.1.7}$$

where I is the column unit vector whose elements are 1's and λ is the Lagrange multiplier.

Taking the derivative with respect to β and setting it equal to zero result in:

$$2R\beta - \lambda I = 0. \tag{6.1.8}$$

Using the constraint that $I^t \beta = 1$ we obtain

$$\lambda = 2/[I^t R^{-1} I]. \tag{6.1.9}$$

The optimal coefficients are obtained after substituting λ into (6.1.8), that is,

$$\beta = R^{-1} I / [I^t R^{-1} I]. \tag{6.1.10}$$

In order to obtain the optimal coefficients, it is necessary to compute (or estimate) the elements of the correlation matrix R. The difficulty of doing such a computation comes from the fact that y_i's are correlated so that it is difficult to derive the joint probability distribution function of $y_{(i)}$ and $y_{(j)}$. However, for the special case of the GMF using the structuring elements shown in Figure 6.1, the joint probability distribution function can be derived.

6.2. Computation of the Correlation Matrix R

Note that the structuring elements in Figure 6.1 intersect at one pixel which is denoted as $x_{i,j}$. The opening operation using one structuring element in Figure 6.1 can be arranged so that $x_{i,j}$ is separated from the rest of the pixels involved in the operation. Such a separation allows the derivation of the joint probability distribution function of $y_{(r)}$ and $y_{(s)}$. In order to simplify the notation, we change $x_{i,j}$ to x_i.

For one line structuring element k_r ($1 \le r \le 4$) of m pixels long, the output of the opening operator can be expressed in the following form:

$$y_r = \max \ \{\min\{x_{i-m+1}, \ldots, x_i\}, \ \min\{x_{i-m+2}, \ldots, x_i, x_{i+1}\}, \ldots,$$

$$\min\{x_i, \ldots, x_{i+m-1}\} \ \}. \tag{6.2.1}$$

Note that since x_i appears in every min term, it can be separated from the rest of the terms in the following manner:

$$y_r = \min\{ \ x_i, \ z_r \ \}, \tag{6.2.2}$$

where

$$z_r = \max \ \{\min\{x_{i-m+1}, \ldots, x_{i-1}\}, \ \min\{ \ x_{i-m+2}, \ldots, x_{i-1}, x_{i+1}\}, \ldots,$$

$$\min\{x_{i+1}, \ldots, x_{i+m-1}\} \ \}. \tag{6.2.3}$$

The probability distribution functions of z_r $(1 \leq r \leq 4)$ can be obtained in terms of the probability distribution function of x. The derivation for the probability distribution functions of z_r is presented in Appendix. Let $F_z(v)$ denote the probability distribution function of z_r, that is,

$$F_z(v) = \Pr\{ \ z_r \leq v \ \}. \tag{6.2.4}$$

From the above, it is obvious that x_i is independent of z_r. Then based on (6.2.2), the probability distribution function of y_r can be derived. Let $F_y(v)$ denote the probability distribution function of y_r.

$$F_y(v) = \Pr\{ \ \min\{x_i, z_r\} \leq v\} = 1 - [1 - F_x][1 - F_z]. \tag{6.2.5}$$

The above derivations for the probability distribution functions of z_r and y_r are applicable to every one of the four line structuring elements because they have the same length.

Since there is no pixel correlation among the z_r's, they are still i.i.d. random variables. The probability distribution functions of the rth order statistic $z_{(r)}$ $(1 \leq r \leq 4)$ can then obtained as in [40]:

$$F_{z_{(r)}}(v) = \Pr\{z_{(r)} \leq v\} = \sum_{i=r}^{4} \binom{4}{i} F_z^{\ i}(v)[1 - F_z(v)]^{4-i}, \qquad 1 \leq r \leq 4. \tag{6.2.6}$$

The joint probability distribution function $F_{z_{(r)}z_{(s)}}(v, w)$ of $z_{(r)}$ and $z_{(s)}$ $(1 \leq r < s \leq 4)$ for $v < w$ is [40]:

$$F_{z_{(r)}z_{(s)}}(v, w) = \sum_{i=r}^{4} \sum_{j=max(0,s-i)}^{4-i} \frac{4!}{i!j!(4-i-j)!}$$

$$\cdot F_z^{\,i}(v)[F_z(w) - F_z(v)]^j [1 - F_z(w)]^{4-i-j}. \qquad (6.2.7)$$

For $v \geq w$ the inequality $z_{(s)} \leq w$ implies $z_{(r)} \leq v$, so that

$$F_{z_{(r)}z_{(s)}}(v, w) = F_{z_{(s)}}(w). \qquad (6.2.8)$$

The joint probability density function of $z_{(r)}$ and $z_{(s)}$ for $1 \leq r < s \leq 4$ is [40]:

$$f_{z_{(r)}z_{(s)}}(v, w) = \frac{4!}{(r-1)!(s-r-1)!(4-s)!} F_z^{r-1}(v) f_z(v)$$

$$[F_z(w) - F_z(v)]^{s-r-1} f_z(w)[1 - F_z(w)]^{4-s}. \qquad (6.2.9)$$

Since x_i is the common variable in every y_r, the rth ordered statistic $y_{(r)}$ can be expressed as a function of x_i and the rth order statistic $z_{(r)}$:

$$y_{(r)} = \min\{x_i, z_{(r)}\}. \qquad (6.2.10)$$

The probability distribution function of $y_{(r)}$ is then obtained:

$$F_{y_{(r)}}(v) = Pr\{y_{(r)} \leq v\} = Pr\{\min(x_i, z_{(r)}) \leq v\}$$

$$= 1 - [1 - F_x(v)][1 - F_{z_{(r)}}(v)]. \qquad (6.2.11)$$

The probability density function of $y_{(r)}$ is obtained by taking derivative of $F_{y_{(r)}}$:

$$f_{y_{(r)}}(v) = f_x(v)[1 - F_{z_{(r)}}(v)] + [1 - F_x(v)]f_{z_{(r)}}(v). \qquad (6.2.12)$$

The joint probability distribution function of $y_{(r)}$ and $y_{(s)}$ $(1 \leq r < s \leq 4)$ can be obtained as the following:

$$F_{y_{(r)}y_{(s)}}(v, w) = Pr\{y_{(r)} \leq v, y_{(s)} \leq w\}$$

$$= Pr\{\min(x_i, z_{(r)}) \leq v, \min(x_i, z_{(s)}) \leq w\}. \qquad (6.2.13)$$

For $v \geq w$, the joint probability distribution function is just a function of w, that is,

$$F_{y_{(r)}y_{(s)}}(v,\ w) = \Pr\{y_{(s)} \leq w,\ y_{(r)} \leq v\} = \Pr\{\ \min(x_i,\ z_{(s)}) \leq w\}. \qquad (6.2.14)$$

In the derivation of the joint probability distribution function for $v < w$, the law of total probability is used in order to separate x_i from the $z_{(r)}$'s.

$$F_{y_{(r)}y_{(s)}}(v,w) = \Pr\{\ \min(x_i,\ z_{(r)}) \leq v,\ \min(x_i,\ z_{(s)}) \leq w\}$$

$$= \Pr\{\ \min(x_i,\ z_{(r)}) \leq v,\ \min(x_i,\ z_{(s)}) \leq w \mid x_i \leq v\}\ \Pr\{\ x_i \leq v\}$$

$$+ \Pr\{\ \min(x_i,\ z_{(r)}) \leq v,\ \min(x_i,\ z_{(s)}) \leq w \mid v < x_i \leq w\}\ \Pr\{\ v < x_i \leq w\}$$

$$+ \Pr\{\ \min(x_i,\ z_{(r)}) \leq v,\ \min(x_i,\ z_{(s)}) \leq w \mid x_i > w\}\ \Pr\{\ x_i > w\} \qquad (6.2.15)$$

or

$$F_{y_{(r)}y_{(s)}}(v,\ w) = \Pr\{\ \min(x_i,\ z_{(r)}) \leq v,\ \min(x_i,\ z_{(s)}) \leq w\}$$

$$= \Pr\{\ x_i \leq v\} + \Pr\{\ z_{(r)}) \leq v\}\ \Pr\{\ v < x_i \leq w\} + \Pr\{\ z_{(r)}) \leq v,\ z_{(s)} \leq w\}\ \Pr\{\ x_i > w\}$$

$$= F_x(v) + F_{z_{(r)}}(v)[F_x(w) - F_x(v)] + F_{z_{(r)}z_{(s)}}(v,\ w)[1 - F_x(w)]. \qquad (6.2.16)$$

The joint probability density function can be obtained by taking partial derivatives with respect to v and w:

$$f_{y_{(r)}y_{(s)}}(v,\ w) = f_{z_{(r)}}(v)f_x(w) + f_{z_{(r)}z_{(s)}}(v,\ w)[1 - F_x(w)]$$

$$- f_x(w) \int_{-\infty}^{w} f_{z_{(r)}z_{(s)}}(v,\ t)dt. \qquad (6.2.17)$$

With the marginal and joint probability density functions (6.2.12) and (6.2.17) of $y_{(r)}$ and $y_{(s)}$, the elements of the correlation matrix can easily be obtained by the following:

$$R_{r,r} = \int_{-\infty}^{\infty} v^2 f_{y_{(r)}}(v)dv. \qquad (6.2.18)$$

and

$$R_{r,s} = \iint_{-\infty}^{\infty} vw f_{y_{(r)}y_{(s)}}(v,\ w)dvdw \qquad (6.2.19)$$

Since the closing is the dual operation of opening, a similar derivation can be made for the correlation matrix of the CL stage. We will omit the detailed derivation and present the probability distribution and density functions for the CL stage. Using the line structuring element k_r of m samples long, the closing operation applied to the pixel x_i can be expressed by the following:

$$y_r = \max\{x_i, z_r\},\tag{6.2.20}$$

where

$$z_r = \min\{\max\{x_{i-m+1}, \ldots, x_{i-1}\}, \max\{x_{i-m+2}, \ldots, x_{i-1}, x_{i+1}\}, \ldots,$$

$$\max\{x_{i+1}, \ldots, x_{i+m-1}\}\}.\tag{6.2.21}$$

The derivation of the probability distribution function F_z of z_r is similar to the Appendix. The probability distribution function of y_r is obtained as:

$$F_y(v) = \Pr\{\max(x_i, z_r) \leq v\} = F_x(v)F_z(v).\tag{6.2.22}$$

Consequently, the probability distribution function for the ordered statistics $y_{(r)}$ is:

$$F_{y_{(r)}}(v) = \Pr\{y_{(r)} \leq v\} = \Pr\{\max(x_i, z_{(r)}) \leq v\} = F_x(v)F_{z_{(r)}}(v).\tag{6.2.23}$$

The probability density function of $y_{(r)}$ is obtained by taking derivative of $F_{y_{(r)}}(v)$:

$$f_{y_{(r)}}(v) = f_x(v)F_{z_{(r)}}(v)a + F_x(v)f_{z_{(r)}}(v).\tag{6.2.24}$$

The joint probability distribution function for $y_{(r)}$ and $y_{(s)}$ for $r < s$ and $v < w$ is given by:

$$F_{y_{(r)}y_{(s)}}(v, w) = \Pr\{\max(x_i, z_{(r)}) \leq v, \max(x_i, z_{(s)}) \leq w\}$$

$$= \Pr\{z_{(r)}) \leq v, z_{(s)} \leq w\}\Pr\{x_i \leq v\} + \Pr\{z_{(s)} \leq v\}\Pr\{v < x_i \leq w\}$$

$$= F_{z_{(r)}z_{(s)}}(v, w)F_x(v) + F_{z_{(s)}}(w)[F_x(w) - F_x(v)].\tag{6.2.25}$$

The corresponding joint density function for $y_{(r)}$ and $y_{(s)}$ is

$$f_{y_{(r)}y_{(s)}}(v,\ w) = f_{z_{(r)}z_{(s)}}(v,\ w)F_x(v) + f_x(v)\int_{-\infty}^{v} f_{z_{(r)}z_{(s)}}(t,\ w)dt - f_x(v)f_{z_{(s)}}(w). \qquad (6.2.26)$$

Next section is devoted to experiments in obtaining the optimal coefficients for various distribution functions. The coefficients obtained are then used in the GMF applied to various test images.

6.3 Example of Optimal Coefficients of the GMF

In this section, we will obtain optimal coefficients for various noise distributions and structuring elements of lengths ranging from 3 to 5 samples. Due to the complexity of the probability distribution and density functions, the computations of the optimal coefficients are performed numerically. Several input distribution functions are used; they include normal, uniform, and Laplacian distributions. Tables 6.1 and 6.2 show the optimal coefficients of the OL and CL stages for the three distribution functions. The optimal coefficients for the normal distribution using structuring elements of various sizes are shown in Tables 6.3 and 6.4.

From these coefficients, we can make several interesting observations. First, note that the values of the coefficients clearly shows the tendency for better geometrical preservation. The values of the coefficients agree with the nature of the opening and closing operators in this regard. Opening operators always locate the structures beneath and closest to the profile of the image. In order to preserve geometrical structures in an image, it is necessary to choose the opening operator outputs that have higher magnitudes. The values of the optimal coefficients for the OL stage meets this requirement: the higher ranked outputs of the opening operators have larger weights. Since a closing operator locates the structures above and closest to the profile of the image, it is desirable to choose the closing operator outputs with lower magnitudes. This requirement is also met by noting that the optimal coefficients for the CL stage have larger values for

Table 6.1. Optimal Coefficients for the OL Stage for Different Input Distributions

Using A Structuring Element of 3 Samples

Distribution	Optimal Coefficients $(\beta_1, \beta_2, \beta_3, \beta_4)$
Normal	(0.1128, 0.2818, 0.2931, 0.3123)
Laplacian	(0.1259, 0.2793, 0.2934, 0.3015)
Uniform	(0.1061, 0.2822, 0.2895, 0.3221)

Table 6.2. Optimal Coefficients for the CL Stage for Different Input Distributions

Using A Structuring Element of 3 Samples

Distribution	Optimal Coefficients $(\alpha_1, \alpha_2, \alpha_3, \alpha_4)$
Normal	(0.3445, 0.3714, 0.2988, -0.0147)
Laplacian	(0.3316, 0.3532, 0.2876, 0.0276)
Uniform	(0.3509, 0.3810, 0.3124, -0.0444)

Table 6.3. Optimal Coefficients for the OL Stage for the Normal Distribution
Using Different Size Structuring Elements

Size of Structuring Element	Optimal Coefficients (β_1, β_2, β_3, β_4)
3	(0.1128, 0.2818, 0.2931, 0.3123)
4	(-0.0395, 0.3081, 0.3195, 0.4119)
5	(-0.1857, 0.3555, 0.3288, 0.5014)

Table 6.4. Optimal Coefficients for the CL Stage for the Normal Distribution
Using Different Size Structuring Elements

Size of Structuring Element	Optimal Coefficients (α_1, α_2, α_3, α_4)
3	(0.3445, 0.3714, 0.2988, -0.0147)
4	(0.5059, 0.3610, 0.2373, -0.1041)
5	(0.5547, 0.3940, 0.2188, -0.1675)

the lower ranked outputs of the closing operators. The max/min version of the GMF is actually the extreme case.

The second interesting observation is that the values of the optimal coefficients suggest a majority rule in choosing the outputs of the morphological operators. Three coefficients of the OL stage for the three largest outputs of the opening operators have large values; the coefficient for the smallest output of the opening operator has either a much smaller value or even a negative value. That means that the smallest output of the opening operators has very little influence on the output of the OL stage. The optimal coefficients of the CL stage show the same characteristics except in the opposite direction. The majority rule enhances the geometrical structure preservation ability of the GMF. Note that although the averaging version of the GMF can preserve edges, it tends to blur sharp corners using the four line structuring elements since corners usually consists of three lines instead of four [67]. By using optimal coefficients, the geometrical preservation ability of the GMF can be extended to sharp corners.

For structuring elements of different lengths, the values of the coefficients also show the emphasis on geometrical structure preservation. When a larger structuring element is used, the opening operator is likely to produce a result whose value is less than the result produced by the opening operator using a smaller structuring element. This actually implies the deletion of small geometrical structures in the original image. More weight is then assigned to the highest output of the operators to enhance the geometrical structure preservation in this situation. A similar observation can be made for the closing operators except that more weight is assigned to the smallest output.

We applied various filters to a test image in order to make some comparisons. The filters we used include median, averaging, the traditional morphological filter, and the optimal GMF. The test image is corrupted by a composite of impulsive and Gaussian noise. For the median, averaging, and traditional morphological filters, a 3x3 window is

used. For the optimal GMF, four line structuring elements of 3 samples shown in Figure 4.7 are used. The images are shown in Figure 6.2. It is clearly shown that the optimal GMF has superior performance. Comparing with the averaging filter, the GMF is more robust with respect to impulsive noise, and has better geometrical structure preservation. Comparing with the median filter, the GMF is more effective in suppressing nonimpulsive noise with strong geometrical structure preservation.
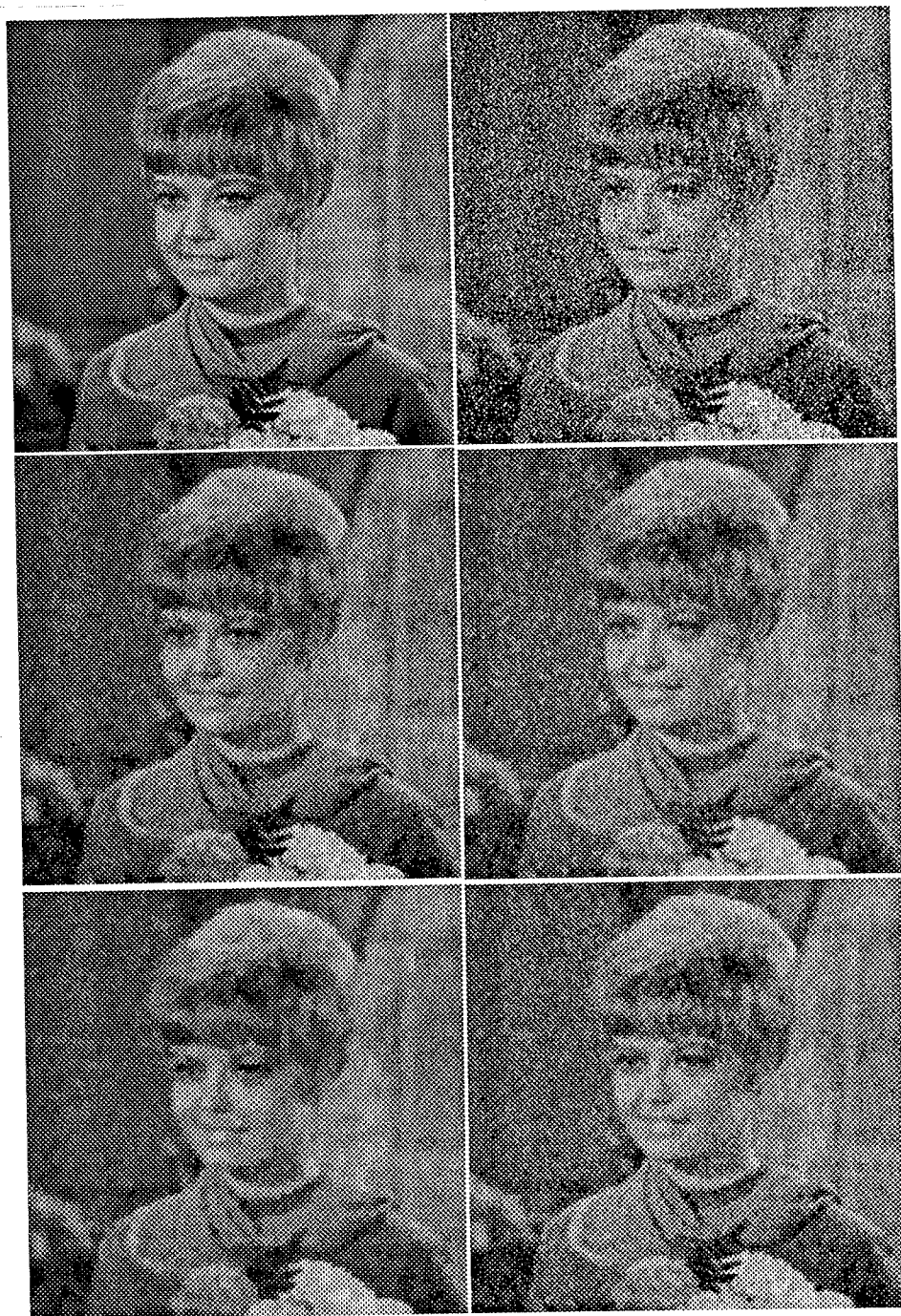
Figure 6.2. *Upper Left*: Original image; *Upper Right*: noisy image corrupted by a composite of impulsive and Gaussian noise; *Middle Left*: Output of the averaging operation; *Middle Right*: Output of the median filter; *Bottom Left*: Output of the traditional morphological filter using a single structuring element shown in Figure 4.7; *Bottom Right*: Output of the optimal GMF using four line structuring elements shown in Figure 4.7.

CHAPTER 7

CONCLUSIONS AND RECOMMENDATIONS

In this thesis, we developed a new morphological filter structure known as the General Morphological Filter (GMF). The GMF utilizes multiple structuring elements which can be used to represent various geometrical structures contained in an image. The substantial improvement in the performance of this type of filter when compared with traditional filters was shown. The new filter enhances the geometrical structure preservation and noise suppression abilities of morphological filters.

In addition to the development of the syntactical properties, we developed an optimal design of the GMF based on the minimum mean square error criterion. In this design, the optimal coefficients of the GMF are obtained for a set of special structuring elements. This design has practical applications in that the results of the optimal design provide valuable insight into the general design of the GMF. The strong geometrical structure preservation capability of the GMF is demonstrated by the resulting optimal coefficient values. The distribution of the values of the resulting optimal coefficients also suggests a majority rule in processing the sorted outputs of the multiple morphological operators. In this thesis, we also derived output probability distribution functions of gray scale opening and closing operators.

Further work on the GMF should include a systematic study of the properties of the GMF root signals. In particular the convergence rate of the root signal needs to be investigated. A statistical analysis of morphological operations for correlated signals could greatly advance the further understanding of morphological operations and the design of the GMF. Extension of these results to two dimensional is greatly needed.

Another open research problem is the systematic design of the structuring elements. Finally, the use of the GMF for multispectral data is being investigated.

LIST OF REFERENCES

LIST OF REFERENCES

[1]   H.C. Andrews and B.R. Hunt, *Digital Image Restoration*. Englewood Cliffs, New Jersey: Prentice-Hall, Inc., 1982.

[2]   J. Serra, *Image Analysis and Mathematical Morphology*. New York: Academic Press, 1982.

[3]   J. Serra, *Image Analysis and Mathematical Morphology, Volume 2: Theoretical Advances*. New York: Academic Press, 1988.

[4]   P.A. Maragos and R.W. Schafer, "Morphological systems for multidimentional signal processing," *Proceedings of the IEEE*, vol. 78, no. 4, pp. 690-710, April 1990.

[5]   G. Matheron, *Random Sets and Integral Geometriy*. New York: J. Wiley and Sons, 1975.

[6]   V. Goetcherian, "From binary to gray scale level tone image processing using fuzzy logic concepts," *Pattern Recognition*, vol. 12, pp. 7-15, 1980.

[7]   K. Preston, Jr., "Ξ-Filters," *IEEE Transactions on Acoustics, Speech, and Signal Processing*, vol. ASSP-31, no. 12, pp. 861-876, August 1983.

[8]   S.R. Sternberg, "Cellular computers and biomedical image processing," *Proceedings of US-France Biomedical Image Processing*, pp. 294-319, 1982.

[9]   S.R. Sternberg, "Biomedical image processing," *IEEE Computer*, vol. 16, pp. 22-34, January 1983.

[10] S.R. Sternberg, "Grayscale morphology," *Computer Vision, Graphics, and Image Processing*, vol. 35, no. 3, pp. 333-355, September 1986.

[11] S.R. Sternberg, "Parallel architecture for image processing," *Proceedings of 3rd Int. IEEE Compac*, pp. 294-319, Chicago, 1979.

[12] R.M. Haralick, S.R. Sternberg, and X. Zhuang, "Image analysis using mathematical morphology," *IEEE Transactions on Pattern Analysis and Machine Intelligence*, vol. PAMI-9, no. 4, pp. 532-550, July 1987.

[13] I. Pitas and A.N. Venetsanopoulos, *Nonlinear Digital Filters, Principles and Applications*. Norwell, Massachusetts: Kluwer Academic, 1990.

[14] P.A. Maragos and R.W. Schafer, "Morphological filters-Part II: their relations to median, order-statistic, and stack filters," *IEEE Transactions on Acoustics, Speech, and Signal Processing*, vol. ASSP-35, no. 8, pp. 1170-1184, August 1987.

[15] J. Song, R.L. Stevenson and E.J. Delp, "The use of mathematical morphology in image enhancement," *Proceedings of the 32nd Midwest Symposium on Circuits and Systems*, pp. 67-70, Urbana-champaign, IL, August 1989.

[16] M.M. Skolnick, "Application of morphological transformations to the analysis of two-dimensional electrophoretic gels of biological materials," *Computer Vision, Graphics, and Image Processing*, vol. 35, no. 3, pp. 306-331, September 1986.

[17] C.H. Chu and E.J. Delp, "Impulsive noise suppression and background normalization of electrocardiogram signals using morphological operations," *IEEE Transactions on Biomedical Engineering*, vol. 36, no. 2, pp. 262-273, February 1989.

[18] C.H. Wright, E.J. Delp, and N.C. Gallagher, "Nonlinear target enhancement for the hostile nuclear environment," *IEEE Transactions on Aerospace and Electronic Systems*, vol. 26, no. 1, pp. 122-145, January 1990.

[19] F. Safa and G. Flouzat, "Speckle removal on radar imagery based on mathematical morphology," *Signal Processing*, vol. 16, no. 4, pp. 319-333, April 1989.

[20] T.R. Crimmins and W.M. Brown, "Image algebra and automatic shape recognition," *IEEE Transactions on Aerospace and Electronic Systems*, vol. AES-21, no. 1, pp. 60-69, January 1985.

[21] D. Sinha and C.R. Giardina, "Discrete black and white object recognition via morphological functions," *IEEE Transactions on Pattern Analysis and Machine Intelligence*, vol. PAMI-12, no. 3, pp. 275-293, March 1990.

[22] P.A. Maragos, "Morphological correlation and mean absolute error criteria," *Proceedings of IEEE ICASSP-89*, Glasgow, Scotland, May 1989.

[23] J.S.J. Lee, R.M. Haralick, and L.G. Shapiro, "Morphological edge detection," *IEEE Journal of Robotics and Automation*, vol. RA-3, no. 2, pp. 142-156, April 1987.

[24] R.J. Feehs and G.R. Arce, "Multidimensional morphological edge detection," *Proceedings of the SPIE Visual Computing and Image Processing II*, pp. 285-292, October 27, 1987.

[25] J.W. Klingler, Jr., C.L. Vaughan, T.D. Fraker, Jr., and L.T. Andrews, "Segmentation of echocardiographic images using mathematical morphology," *IEEE Transactions on Biomedical Engineering*, vol. BME-35, no. 11, pp. 925-934, Novermber 1988.

[26]   P.A. Maragos and R.W. Schafer, ''Morphological skeleton representation and coding of binary images,'' *IEEE Transactions on Acoustics, Speech, and Signal Processing*, vol. ASSP-34, no. 5, pp. 1228-1244, October 1986.

[27]   J. Goutsias and D. Schonfeld, ''Image coding via morphological transformations: a general theory,'' *Proceedings of the IEEE Computer Society Conference on Computer Vision and Pattern Recognition*, pp. 178-183, June, 1989.

[28]   S.A. Rajala, H.A. Peterson, and E.J. Delp, ''Use of mathematical morphology for encoding graytone images,'' *Proceedings of IEEE Internation Symposium on Circuits and Systems*, pp. 2807-2811, Espoo, Finland, June, 1988.

[29]   R.M. Haralick, X. Zhuang, C. Lin, and J.S.J. Lee, ''The digital morphological sampling theorem,'' *IEEE Transactions on Acoustics, Speech, and Signal Processing*, vol. ASSP-37, no. 12, pp. 2067-2090, December 1989.

[30]   R.L. Stevenson and G.R. Arce, ''Morphological filters: statistics and further syntactic properties,'' *IEEE Transactions on Circuits and Systems*, vol. CAS-34, no. 11, pp. 1292-1305, November 1987.

[31]   L. Koskinen, J. Astola, and Yrjo Neuvo, ''Statistical properties of discrete morphological filters,'' *Proceedings of 1990 IEEE International Symposium on Circuits and Systems*, pp. 1219-1222, New Orleans, LA, May 1990.

[32]   X. Zhuang and R.M. Haralick, ''Morphological structuring element decomposition,'' *Computer Vision, Graphics, and Image Processing*, vol. 35, no. 3, pp. 370-382, September 1986.

[33]   P.A. Maragos and R.W. Schafer, ''Morphological filters-Part I: their set-theoretic analysis and relations to linear shift-invariant filters,'' *IEEE Transactions on Acoustics, Speech, and Signal Processing*, vol. ASSP-35, no. 8, pp. 1153-1169, August 1987.

[34]   P.D. Wendt, E.J. Coyle, and N.C. Gallagher, ''Stack filters,'' *IEEE Transactions on Acoustics, Speech, and Signal Processing*, vol. ASSP-34, no. 4, pp. 898-911, August 1986.

[35]   F.Y.-C. Shih and O.R. Mitchell, ''Threshold decomposition of gray-scale morphology into binary morphology,'' *IEEE Transactions on Pattern Analysis and Machine Intelligence*, vol. PAMI-11, no. 1, pp. 31-42, January 1989.

[36]   J. Song and E.J. Delp, ''A study of the generalized morphological filter,'' to appear in *Circuits, Systems, and Signal Processing*.

[37]   J. Song and E.J. Delp, ''The general morphological filter: a new class of morphological filters with multiple structuring elements,'' to appear in *Mathematical Morphology: Theory and Application* edited by R.M. Haralick, Springer-Verlag, New York, 1991.

[38] J. Song and E.J. Delp, "The generalized morphological filter," *Proceedings of the 23rd Asilomar Conference on Signals, Systems, and Computers*, pp. 147-151, Asilomar, CA, October 1989.

[39] J. Song and E.J. Delp, "Statistical analysis of mophological operators," *Presendted at the the 1991 Hopkins Conference on Information sciences and Systems*, Baltimore, Maryland, March 20-21, 1991.

[40] H.A. David, *Order Statistics*. New York: Wiley, 1981.

[41] J.W. Tukey, "Nonlinear (Nonsuperposable) methods for smoothing data," *Cong. Rec. 1974 EASCON* , p. 673.

[42] A. Rosenfeld and A.C. Kak, *Digital Picture Processing*. New York: Academic Press, 1982.

[43] N.S. Jayant, "Average and median-based smoothing techniques for improving digital speech quality in the presence of transmission errors," *IEEE Transactions on Communications*, vol. COM-24, no. 8, pp. 1043-1045, Spet. 1976.

[44] A.C. Bovik, T.S. Huang, and D.C. Munson, Jr., "A generalization of median filtering using linear combinations of order statistics," *IEEE Transactions on Acoustics, Speech, and Signal Processing*, vol. ASSP-31, no. 6, pp. 1342-1350, December 1983.

[45] S.G. Tyan, "Median filtering: deterministic properties," in*Two-Dimensional Digital Signal Processing II: Transforms and Median Filters* (T.S. Huang, ed.), springer Verlag, 1981.

[46] N.C. Gallagher and G.L. Wise, "A theoretical analysis of the properties of median filters," *IEEE Transactions on Acoustics, Speech, and Signal Processing*, vol. ASSP-29, no. 6, pp. 1136-1141, December 1981.

[47] J.P. Fitch, E.J. Coyle, and N.C. Gallagher, "Root properties and convergence rates of median filters," *IEEE Transactions on Acoustics, Speech, and Signal Processing*, vol. ASSP-33, no. 1, pp. 230-239, February 1985.

[48] T.A. Nodes and N.C. Gallagher, "The output distribution of median type filters," *IEEE Transactions on Communications*, vol. COM-32, no. 5, pp. 532-541, May 1984.

[49] P.A. Maragos and R.W. Schafer, "A unification of linear, median, order statistics, and morphological filters under mathematical morphology," *Proceedings of the 1985 IEEE International Conference on Acoustics, Speech, and Signal Processing*, Tampa, FL, March 1985.

[50] J.P. Fitch, E.J. Coyle, and N.C. Gallagher, "Threshold decomposition of multidimensional ranked order operations," *IEEE Transactions on Circuits and Systems*,

vol. CAS-32, pp. 445-450, May 1985.

[51] A.H. Lefebvre, D.W. Senser, H.E. Snyder, N.E. Kosinski, A.E. Mithchell, and M.R. Supple, "Basic studies on paint spray characteristics," *CIDMAX Annual Report*, pp. 234-238, Engineering Research Center, Purdue University, 1986.

[52] J. Song and E.J. Delp, "A generalization of morphological filters using multiple structuring elements," *Proceedings of the 1989 IEEE International Symposium on Circuits and Systems*, pp. 991-994, Portland, OR, May 1989.

[53] A. Farag and E.J. Delp, "Some experiments with histogram-based segmentation," *Proceedings of the Fourth Annual Conference on Intelligent Systems and Machines*, pp. 251-256, Rochester, Michigan, April 1986.

[54] A. Restrepo and A.C. Bovik, "Adaptive trimmed mean filters for image restoration," *IEEE Transactions on Acoustics, Speech, and Signal Processing*, vol. ASSP-36, no. 8, pp. 1326-1337, August 1988.

[55] R. Mediavilla, H. Kaufman, M. Tekalp, and J. W. Woods, "Multiple models for nonstationary image estimation," *Proceedings of the 6th IFAC Symposium on Identification and System Parameter Estimation*, pp. 1467-1471, June 1982.

[56] S. Dravida, J. W. Woods, and W. C. Shen, "A comparison of image filtering algorithms," *Proceedings of the 1984 IEEE International Conference on Acoustics, Speech, and Signal Processing*, pp. 23.3.1-23.3.4, March 1984.

[57] A. Nieminen, P. Heinonen, and Y. Neuvo, "A new class of detail-preserving filters for image processing," *IEEE Transactions on Pattern Analysis and Machine Intelligence*, vol. PAMI-9, no. 1, pp. 74-90, January 1987.

[58] J.S.J. Lee, R.M. Haralick, and L.G. Shapiro, "Morphological edge detection," *Proceedings of the 1986 IEEE International Conference on Pattern Recognition*, pp. 369-373, October 1986.

[59] L.R. Rabiner, M.R. Sambur, and C.E. Schmidt, "Applications of a nonlinear smoothing algorithm to speech processing," *IEEE Transactions on Acoustics, Speech, and Signal Processing*, vol. ASSP-23, no. 8, pp. 552-557, December 1975.

[60] B. Lay, *Analyse automatique des images angiofluorographiques du cours de la retinopat hie diabetique*. Ecole des Mines, Paris: Thesis Doct.Ing., 1983.

[61] L.S. Davis and A. Rosenfeld, "Noise cleaning by iterated local averaging," *IEEE Transactions on Systems, Man and Cybernetics*, vol. SMC-8, no. 9, pp. 705-710, September 1978.

[62] D.C.C. Wang, A.H. Vagnucci, and C.C. Li, "Gradient inverse weighted smoothing scheme and the evaluation of its performance," *Computer Graphics and Image Processing*, vol. 15, pp. 167-181, 1981.

[63] R.V. Hogg, "An introduction to robust estimation," *in Robustness in Statistics*, edited by R. L. Launer and G. N. Wilkinson, New York, Academic Press, 1979.

[64] G.A. Mastin, "Adaptive filters for digital image noise smoothing: an evaluation," *Computer Vision, Graphics and Image Processing*, vol. 31, pp. 103-120, 1985.

[65] J. Song and E.J. Delp, "An analysis of a multiple model morphological filter," *Proceedings of the Twenty-Fifth Annual Allerton Conference on Communication, Control and Computing*, pp. 775-784, Allerton, IL, October, 1987.

[66] J. Song and E.J. Delp, "The analysis of morphological filters with multiple structuring elements," *Computer Vision, Graphics and Image Processing*, vol. 50, pp. 308-328, June 1990.

[67] J. Song and E.J. Delp, "A study of morphological operators with multiple structuring elements," *Proceedings of the Electronic Imaging West 90 Conference*, pp. 314-320, Pasadena, CA, February 1990.

APPENDIX

APPENDIX

The proof of the numerator of (2.2.5) is presented in this appendix. To be complete, the problem is restated. We have an operation involving an ordering process and $2m$ samples:

$$z = \max \{\min\{x_1, x_2, \ldots, x_m\}, \min\{x_2, x_3, \ldots, x_{m+1}\}, \ldots,$$

$$\min\{x_{m+1}, x_{m+2}, \ldots, x_{2m}\} \}. \tag{A.1}$$

The number of permutations of the ordered sequence $\{x_{(1)} \le x_{(2)} \le, \ldots, \le x_{(r)} \le, \ldots, \le x_{(2m)}\}$ such that $z = x_{(r)}$ is:

$$\frac{(m+1)!}{(r-2)! \, (m-r+1)!} (r-1)!(2m-r)!. \tag{A.2}$$

The range of r is determined in Proposition 1 of Section III.

Proof:

The $2m$ elements of the ordered sequence can be divided into three groups: Group 1 contains only one element, $x_{(r)}$; Group 2 contains the $r-1$ elements whose ranks are less than r; and Group 3 consists of the rest of the elements in the ordered sequence that have ranks greater than r. Assume that $x_{(r)}$ is located at position i, that is $x_i = x_{(r)}$. It is obvious that when the location of $x_{(r)}$ is fixed and the positions for the other two groups are set, then there are $(r-1)!$ permutations for the $r-1$ elements in Group 2 and $(2m-r)!$ permutations for the $2m-r$ elements in Group 3. We need to find how many possible ways for Groups 2 and 3 such that $z = x_{(r)}$.

There are two necessary conditions for $z = x_{(r)}$.

Condition 1: $x_{(r)} = \min\{x_{i-j}, \ldots, x_i, \ldots, x_{i+k}\}$, $j+k=m-1$, and $0 \le j, k \le m-1$.

In other words, $x_{(r)}$ must be the minimum of its $m-1$ neighbors. This situation implies that there is at least one neighborhood of $x_{(r)}$ that has $m-1$ elements with ranks greater

than r.

Condition 2: $x_{(r)} \geq \min\{x_j, \ldots, x_{j+m-1}\}$, $\forall\, j \in [1, m+1]$.

This condition suggests that in the sequence $\{x_i; 1 \leq i \leq 2m\}$ there exists no neighborhoods consisting of m elements the rank of whose minimum element is greater than r. Our analysis will be based on the above two conditions.

We separate this problem into 3 different cases. Let us consider the first case in which $r = 2$. There is only one element whose rank is less than 2, that is, $x_{(1)}$. We have assumed that $x_{(2)}$ is located at position i. The range of i is now restricted in the interval $[1, m]$. It is easy to see that the result for i in the interval $[m+1, 2m]$ is the same as in the interval $[1, m]$.

Suppose $x_{(1)}$ is located at the position k. In order for $z = x_{(2)}$, it is necessary that $m + 1 \leq k$ and $k - i \leq m$. So we have $m + 1 \leq k \leq m + i$ with $1 \leq i \leq m$. This situation is illustrated in Figure A.1.
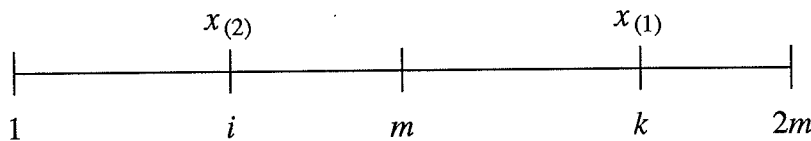

Figure A.1. Illustration of the situation when $r=2$.

Then the number of possibilities such that $z = x_{(2)}$ in the range of $1 \leq i \leq m$ is the sum of the k's for all possible i's. By noting the relationship between i and k, we can have the following:

$$\sum_{k=1}^{m} k = \frac{(m+1)m}{2}.$$

The total number for both ranges of i is $m(m + 1)$.

The next case is that r is greater than 3 and $x_{(r)}$ is not located at positions 1 and $2m$, that is, $3 \leq r$ and $2 \leq i \leq 2m - 1$. Suppose $x_{(s)}$ and $x_{(t)}$ are located at positions $j-1$ and $k+1$ with s, $t < r$ and $2 \leq j < i < k \leq 2m$. And all the elements in the intervals $[j, i-1]$ and $[i+1, k]$ have ranks greater than r. This situation is illustrated in Figure A.2.
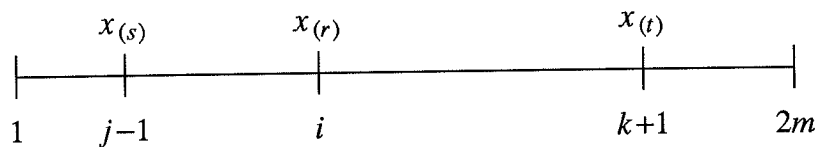

Figure A.2.   Illustration of the situation when $2 < r$ and $1 < j \leq i \leq k < 2m$.

We obtain the following conditions for $z = x_{(r)}$:

$$0 \leq i - j \leq m - 1; \quad k - i \leq m - 1; \quad m - 1 \leq k - j \leq 2m - r$$

In this case the range of j is $2 \leq j \leq m$. The range of k is determined by:

$$m + j - 1 \leq k \leq \min(2m - r + j, 2m - 1).$$

The number of possible intervals $[j, k]$ is $2m - (k - j + 1)$. There are $\begin{bmatrix} 2m - (k - j + 3) \\ r - 3 \end{bmatrix}$ ways to arrange the $r - 3$ elements whose ranks are less than r. So the total numbers of the combinations for $z = x_{(r)}$ in this case is:

$$\sum_{j=2}^{m} \sum_{k=m+j-1}^{\min(2m-r+j, 2m-1)} \left[(2m - k + j - 1) \begin{bmatrix} 2m - (k - j + 3) \\ r - 3 \end{bmatrix} \right]$$

The above summation can be divided into the following two cases:

$$I_1 = \sum_{j=2}^{r-1} \sum_{k=m+j-1}^{2m-r+j} \left[(2m-k+j-1) \left[\binom{2m-k+j-3)}{r-3} \right] \right]$$

and

$$I_2 = \sum_{j=r}^{m} \sum_{k=m+j-1}^{2m-1} \left[(2m-k+j-1) \left[\binom{2m-k+j-3}{r-3} \right] \right]$$

Letting $d = 2m - k + j - 3$, we have

$$I_1 = \sum_{j=2}^{r-1} \sum_{d=r-3}^{m-2} (d+2) \left[\binom{d}{r-3} \right] = \sum_{d=r-3}^{m-2} (r-2)(d+2) \left[\binom{d}{r-3} \right];$$

and

$$I_2 = \sum_{j=2}^{m} \sum_{d=j-2}^{m-2} (d+2) \left[\binom{d}{r-3} \right]$$

From $d \geq j-2$, we have $j \leq d+2$. Exchanging the two summations, we obtain:

$$I_2 = \sum_{d=r-2}^{m-2} \sum_{j=r}^{d+2} (d+2) \left[\binom{d}{r-3} \right] = \sum_{d=r-2}^{m-2} (d-r+3)(d+2) \left[\binom{d}{r-3} \right]$$

Note that changing the lower limit $r - 2$ of d to $r - 3$ will not change the summation I_2.

Thus combining I_1 and I_2 results in

$$I_1 + I_2 = \sum_{d=r-3}^{m-2} (d+2)(d+1) \left[\binom{d}{r-3} \right]$$

$$= \frac{1}{(r-3)!} \sum_{d=r-3}^{m-2} (d+2)(d+1) \cdots (k-r+4).$$

Letting $j = d - r + 4$, we have

$$I_1 + I_2 = \sum_{j=1}^{m-r+2} j(j+1) \cdots (j+r-2)$$

Noting that:

$$\sum_{j=1}^{n} j(j+1)\cdots(j+k) = \frac{1}{k+2}\frac{(n+k+1)!}{(n-1)!}$$ (A.3)

Using this, the final result is

$$I_1 + I_2 = \frac{1}{(r-3)!}\frac{1}{r}\frac{(m+1)!}{(m-r+1)!}.$$

The last case is similar to the previous one except that it has two instances regarding the location of the interval $[j, k]$. In the first instance, the interval is located at the left end of the interval $[1, 2m]$, that is, $j = 1$. The second instance is that $[j, k]$ is located at the right end of $[1, 2m]$, that is, $k = 2m$. It is easy to see that the result for $j = 1$ is the same as $k = 2m$. So we will just consider the case in which $k = 1$. Suppose that all the neighboring elements of $x_{(r)}$ in the interval $[1, k]$ are in Group 3. An element $x_{(s)}$ in Group 2 is located at $k + 1$, that is, $s < r$. This is illustrated in Figure A.3.
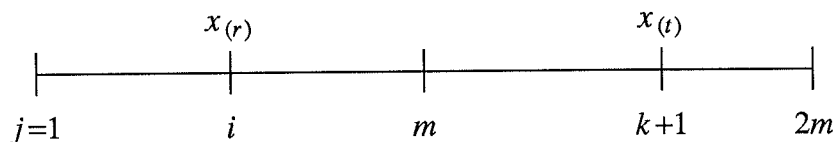

Figure A.3.   Illustration of the situation when $2 < r$ and $j = 1$.

Then we have $r - 2 \leq 2m - (k + 1)$ and $m \leq k$ in order for $z = x_{(r)}$. Using the same analysis as in the case 2, we obtain the number of combinations:

$$I_3 = \sum_{k=m}^{2m-r+1}(2m-k)\begin{bmatrix}2m-k-1\\r-2\end{bmatrix}.$$

Letting $d = 2m - k - 1$, we obtain

$$I_3 = \sum_{d=r-2}^{m-1} (d+1) \begin{bmatrix} d \\ r-2 \end{bmatrix}$$

Letting $j = d - r + 3$ and using the result in (A.3):

$$I_3 = \frac{1}{(r-2)!} \sum_{j=1}^{m-r+2} j(j+1)\cdots(j+r-2) = \frac{1}{(r-2)!} \frac{1}{r} \frac{(m+1)!}{(m-r+1)!}.$$

The final result for this case is

$$I_3 = 2\frac{1}{(r-2)!} \frac{1}{r} \frac{(m+1)!}{(m-r+1)!}.$$

Now we can obtain the total number of combinations in which $z = x_{(r)}$, $3 \le r \le m + 1$, by combining the results from the last two cases. That is:

$$I_1 + I_2 + I_3 = \frac{1}{(r-3)!} \frac{1}{r} \frac{(m+1)!}{(m-r+1)!} + 2\frac{1}{(r-2)!} \frac{1}{r} \frac{(m+1)!}{(m-r+1)!}$$

$$= \frac{1}{(r-3)!} \frac{1}{r} \frac{(m+1)!}{(m-r+1)!} \left[1 + \frac{2}{(r-2)} \right]$$

$$= \frac{(m+1)!}{(r-2)!(m-r+1)!} \tag{A.4}$$

Note that the result obtained for $r = 2$ is just a special case of the result in (A.4). Hence, the result in (A.4) can be used for all the cases. Then it is very easy to obtain the total number of permutations in which $z = x_{(r)}$, $2 \le r \le m + 1$:

$$\frac{(m+1)!}{(r-2)!(m-r+1)!}(r-1)!(2m-r)!$$

The derivation of the numerator in (5) is complete.

VITA

VITA

Jisheng Song received the Bachelor of Science in Electrical Engineering from He Hai University in Nanjing, China, in 1982. In 1985, he received the Master of Science in Electrical Engineering from Purdue University in West Lafayette, Indiana. He worked at He Hai University as an assistant lecturer for a year involved in supervising the System and Control Laboratory and tutoring students in control and computer engineering courses. Mr. Song's research interests include image processing, computer vision, computer graphics, and artificial intelligence.